August 2016

Representative Volume Element (RVE) Finite-Element Analysis (FEA) of Al Metal-matrix Composites

Yuzhe Cao
University of Wisconsin-Milwaukee

REPRESENTATIVE VOLUME ELEMENT (RVE) FINITE-ELEMENT ANALYSIS (FEA) OF AL METAL-MATRIX COMPOSITES

by

Yuzhe Cao

A Thesis Submitted in

Partial Fulfillment of the

Requirements for the Degree of

Master of Science

in Engineering

at

The University of Wisconsin-Milwaukee

August 2016

ABSTRACT
REPRESENTATIVE VOLUME ELEMENT (RVE) FINITE-ELEMENT ANALYSIS (FEA) OF AL METAL-MATRIX COMPOSITES

by

Yuzhe Cao

The University of Wisconsin-Milwaukee, 2016
Under the Supervision of Professor Chang-Soo Kim

Metal matrix composites reinforced by particles (a.k.a particle reinforced metal matrix composites, PRMMCs) could be suitable for a large number of applications with their enhanced mechanical properties. These composites generally consist of a base metal filled with hard/strong particles of which physical and mechanical properties very different from those of the matrix. These particles are intended to improve the properties of the base material including wear resistance, damping properties, and mechanical strength. Aluminum (Al) and its alloys have attracted most attention as base metal in these metal matrix composites due to their light weight and inexpensive nature. As for the reinforcements, aluminum Oxide (Al_2O_3) is one of the most commonly used ceramic particles. This study is aimed at developing a finite-element analysis (FEA) computational model to predict the bulk mechanical behavior of Al_2O_3 particle reinforced Al-based metal matrix composites. In our work, the representative volume element (RVE) models of hierarchical composites have also been created to predict the stress-strain behavior of Mg-Al-Al_2O_3 hierarchical composites. RVE models have been developed to predict the mechanical properties of different PRMMCs assuming that ceramic particles are fractured during the plastic deformation of the whole composite.

From the results, it was found that the particle volume fraction plays a critical role determining various mechanical properties such as Young's modulus. However, the developed RVE model showed that the particle size and the particle distributions have little effects on the mechanical properties of PRMMCs, which could be considered as the limitation of the current study. For the hierarchical composites, the numerical and experimental results were reasonably in a good agreement.

TABLE OF CONTENTS

LIST OF FIGURES

LIST OF TABLES

Chapter 1. Introduction

1. Overview

Metal-matrix composites (MMC) are often used in automotive, electronics, aerospace, and defense industries, due to their high resistance to fire, moisture and radiation, in addition to high electrical and thermal conductivities [1]. Using conventional materials, it is difficult to make progress in multiple structural applications, however, the increasing use of MMC's make the improvement in multiple structural functions possible. For instance, it is claimed that, by adding hard particles into the matrix material, the strength of particle-reinforced metal-matrix composites (PRMMC) can be significantly improved without reducing their desired ductility [2].

In MMCs, a metal is often combined with another nonmetallic phase to produce a new material. This kind of composites includes many different materials that can be distinguished i) due to their base metal types, such as Cu, Al, or Ti, ii) due to the reinforcement phase types, such as fibers, particles and whiskers, or iii) due to their manufacturing process, such as power metallurgy, diffusion bonding, infiltration and stir casting.

The main reasons why MMC's are highly attractive can be summarized as follows:

- First, the design of composites makes it possible for some properties to go beyond the boundaries drawn by the basic attributes of more traditional materials. It is known that lightweight metals are not as stiff or rigid, however. Incorporating ceramics into these lightweight metal matrices can make the composite not only light, but also tougher and stronger.
- Second, synthesizing a composite is the only way to introduce a large volume fraction of oxides or carbides into most desired metals. Different from Fe, typical lightweight metals

including liquid Al, Mg, and Cu have almost no solubility for carbon. The only way to successfully incorporate carbides into these metals is through the use of composites.

These basic considerations have driven a lot of research on MMCs, which began several decades ago, and reached a high level of intensity in the late 1980s and early 1990s. Significant interest continues today in a wider array of more distinct directions and with less visibly. The yearly number of articles published on MMC's, and related subjects, has increased a lot during the past decade. The topic of MMCs is wide-ranging. There are mainly two more formal directions. The first direction concerns the invention of new intriguing and promising MMCs, such as bulk metallic glass composites, and microcellular metals. The other direction concerns the application of the MMCs. For instance, recent research has found that these materials can be wonderful used for the exploration of the physics or the micromechanics of some composite materials.

According to the specific characteristics (i.e., types) of the incorporated reinforcement, MMCs are generally distinguished as: particle-reinforced, short fiber- or whisker-reinforced, continuous fiber, or layered MMCs. Particle-reinforced metals have a very low aspect ratio. The aspect ratio of the reinforcement is an important quantity, because the degree of load transfer from the matrix to the reinforcement could be directly proportional to the reinforcement aspect ratio. Thus, continuous particles typically provide the highest degree of load transfer, due to their inherent high aspect ratio [2]. In the current thesis, we focus on the particulate-reinforced MMCs (PRMMCs) because they are relatively inexpensive and have high potential for commercial applications, owing to their promising properties suitable for a large number of functional and structural applications. Constraint imposed by the ceramic reinforcements on matrix plastic deformation induces large tensile hydrostatic stresses in the matrix. This enhances the load carried

by the reinforcements and hence the composite flow stress but also triggers the early development of internal damage in the form of particle fracture, interface decohesion, and/or matrix void growth. [2]

For the metal-matrix, the use of Al has been widely explored. Particulate-reinforced Al matrix composites have several advantages including low cost and ease of fabrication; they are generally isotropic, as well as both high stiffness-to-density and strength-to-weight ratios [3]. Meanwhile, Mg and its alloys are also broadly used in the fabrication of MMCs as they are light in weight, economically viable, amenable for production by various processing techniques and possess high specific strength and good corrosion resistance. The ceramic particles generally include SiC, Al_2O_3, TiB_2, and B_4C. Ceramics can exhibit high strength and elastic moduli, resulting in materials that show high wear and fatigue resistances that make them ideal choices as the reinforcements in particulate-reinforced Al matrix composites. It is widely recognized that the mechanical properties of MMCs are controlled by the size and volume fraction of the reinforcements, as well as the nature of the matrix reinforcements interface bonding strength.

In this thesis, we also pay attention to the mechanical performance of hierarchical composites. Alongside the astonishing advantages that mentioned above, Mg possesses some limitations such as low elastic modulus, rapid loss of strength with increasing temperature and poor creep resistance. Numerous efforts have been made so far to improve these restrictions by addition of various types of reinforcements (Y_2O_3 [4], Al_2O_3 [5], SiC [6, 7], Ti [8, 9], TiC [10] and CNT [11]). Motivated by the significant enhancements in the mechanical response of Mg achieved through protean types of nano-scaled reinforcement, Meisam K. Habibi et al. [12] found: if the stiff elastic inclusions are judiciously integrated into a compatible softer, sub-micron metallic reinforcement, the degrees of freedom in such a design provide an exciting route to engineering

the behavior of Mg composites. Such a hierarchical Mg microstructure indeed exhibits excellent mechanical properties derived from superposition of the deformation mechanisms active at small length scales.

Different from traditional PRMMCs, hierarchical composites include a reinforcing constituent that is a composite in itself, so there are two constituent phases, where one phase at a finer scale. We always define the reinforcing constituent as level-I and the whole hierarchical composite as level-II.[12] To be specific, we developed a composite (alternatively referred to as a level II composite) with monolithic Mg as the matrix, reinforced by another level I composite comprising a pure aluminum (Al) matrix in which are embedded Al_2O_3 particles. The level II composite was obtained by adding a small volume fraction of the level I composite to Mg.

Compared with the monolithic pure Mg, the hierarchical composites exhibited significant simultaneous enhancement of strengthening, hardening and failure strain, and also non-monotonic mechanical performance as a function of level I volume fraction. [12]

2. Finite-Element Analysis (FEA)

In the current work, we concentrate on the prediction of mechanical properties of PRMMCs using finite-element analysis (FEA) computational technique. FEA is a widely-used numerical technique, where all the complexities of the problems, like varying shape, boundary conditions, and loads could be maintained as they are in a real situation. However, the obtained solutions are approximate. Due to its diversity and flexibility as an analysis tool, it is receiving much attention in engineering. The extensive improvements in computer hardware technology and reduction in cost of computers, have boosted the feasibility of this method. A number of popular FEA packages are now available commercially. Some of the popular packages include: STAAD-PRO, GT-

STRUDEL, NASTRAN, NISA, ABAQUS, and ANSYS. Using these packages one can analyze the physic-mechanical behaviors of complex structures, which is not possible in an analytical way.

FEA originated as a method of stress analysis in the design of aircrafts [13]. It started as an extension of the matrix method of structural analysis. These days, this method is used not only for the analysis in solid mechanics, but also in the analysis of fluid flow, heat transfer, electric and magnetic fields, and many more. Civil engineers use this FEA approach extensively for the analysis of beams, space frames, plates, shells, folded plates, foundations, rock mechanics problems, and seepage analysis of fluid through porous media [13]. Both static and dynamic problems can be handled by finite element analysis. This method is used extensively for the analysis and design of ships, aircrafts, space crafts, electric motors and heat engines.

In engineering problems, there are typically several unknowns. If these unknowns are found, the behavior of the entire structure can be predicted. The basic unknowns or the field variables that are encountered in the engineering problems, might be the displacements in solid mechanics, the velocities in fluid mechanics, the electric and magnetic potentials in electrical engineering, or the temperatures in heat flow problems. In a continuum, the number of these unknowns could be infinite. The finite-element procedure reduces such unknowns to a finite number by dividing the solution region into small parts called elements and by expressing the unknown field variables in terms of assumed approximating functions (interpolating functions/shape functions) within each element [13]. The approximating functions are defined in terms of field variables of specified points called nodes or nodal points. Thus, in FEA, the unknowns are treated as the field variables of the nodal points. These field variables at any point can be found by using interpolation functions by using adequate FEA algorithm.

3. Motivations

As addressed, we will focus on the prediction of mechanical properties of Al-based PRMMCs. It is known that mechanical properties of Al-based PRMMCs are determined by numerous factors including the types and the volume fractions of reinforcements, grain size of metal-matrix, the types and amounts of alloying elements in the metal-matrix, processing methods, and post-processing treatments, etc.

PRMMCs have great values and potentials in automotive, aerospace and consumer goods industries, but traditional experimental investigations always cost a lot. Thus, FEA has a great potential in predicting the performance of PRMMCs. In the past decades, thousands of FEA analyses have been carried out by a number of researchers by considering matrix and reinforcement properties and their respective volume fractions. However, previous research always have limitations. Firstly, most of the previous research has focused on the 2D finite element modeling. Then, previous researches that compare FEA with experimental results only focused on the comparison between the general stress-strain curves without considering detailed particle failure mechanisms. What's more, some of the previous particle damage models either didn't or has limitation in simulating the stress-strain relationships of ceramic reinforcements. In this study, we are providing a new way to address the tension stress applied on the ceramic particle. Close to the real experiments, we are making the stresses of particles directly down to zero after fracture.

FEA also has a great potential in analyzing the mechanical properties of hierarchal composites but has not been used in the hierarchical composites field. We developed a RVE model of Mg-Al-Al_2O_3 composites in this study to make use of FEA in the hierarchical composites field.

4. Objectives of Research

In this study, a computational model is developed to predict the bulk mechanical behavior of Al_2O_3 particle reinforced 6061 Al alloy-based composites. Especially, our objective of this thesis is that:

- *3D RVE FEA computational model development including the particle damage model to understand the mechanical responses in the PRMMC: Understand the limitation of the RVE FEA model.*

In developing the model, the necessary elastic and plastic physical properties of constituent materials such as Al matrix and ceramic particles are incorporated. In the following chapters (Chapters 2, 3, and 4), the detailed background, previous modeling efforts, and our model development are addressed, respectively. In the result chapter (Chapter 5), the impacts of volume fraction and the morphology such as particle size, particle distribution will be discussed.

References

1. B. Vijaya Ramnath, C. Elanchezhian, RM. Annamalai, S.Aravind. Aluminum metal matrix composites - A review, Rev. Adv. Mater. Sci. 38 (2014) 55-60

2. T. W. Clyne and P. J. Withers. (1993). An introduction to metal matrix composites (New York: Elsevier Science).

3. Andreas Mortensen, Javier Llorca. Metal Matrx Composites. Annu. Rev. Mater. Res. 40 (2010) 243-270

4. Garces G, Rodriguez M, Perez P, Adeva P. Effect of volume fraction and particle size on the microstructure and plastic deformation of Mg–Y2O3 composites. Mater Sci Eng A 419 (2006) 357–64.

5. Nguyen QB, Gupta M. Increasing significantly the failure strain and work of fracture of solidification processed AZ31B using nano-Al_2O_3 particulates. J Alloy Compd 459 (2008) 244–250.

6. Huard G, Angers R, Krishnadev MR, Tremblay R, Dube D. SiCp/Mg composites made by low-energy mechanical processing. Can Metall Q 38 (1999) 193–200.

7. Zheng MY, Zhang WC, Wu K, Yao CK. The deformation and fracture behavior of SiCw/AZ91 magnesium matrix composite during in situ TEM straining. J Mater Sci 38 (2003) 2647–2654.

8. Hassan SF, Gupta M. Development of ductile magnesium composite materials using titanium as reinforcement. J Alloy Compd 345 (2002) 246–251.

9. Perez P, Garces G, Adeva P. Mechanical properties of a Mg-10 (vol.%) Ti composite. Compos Sci Technol 64 (2004) 145–151.

10. Wang HY, Jiang QC, Li XL, Wang JG. In situ synthesis of TiC/Mg composites in molten magnesium. Scripta Mater 48 (2003) 1349–1354.

11. Goh CS, Wei J, Lee LC, Gupta M. Ductility improvement and fatigue studies in Mg-CNT nanocomposites. Compos Sci Technol 68 (2008) 1432–1439.

12. Meisam K. Habibi, Shailendra P. Joshi, Manoj Gupta. Hierarchical magnesium nano-composites for enhanced mechanical response. Acta Materialia 58 (2010) 6104-6114

13. Widas, P. (1997). Introduction to Finite Element Analysis.Virginia Tech Material Science and Engineering. Retrieved

Chapter 2. Background

1. Al-based PRMMCs

A metal matrix composite is a multi-phase material, which contains particles in its composition. Properties such as mechanical, electrical and thermal conduction may differ due to the composition of the materials used during synthesis of the composites. The specific structure and the resultant properties of composites are generally influenced by the type and size of the reinforcements, nature of bonding and chosen processing techniques. The amount, size, and distribution of reinforcing particles in the metal-matrix have important and critical influence on enhancing or limiting the overall properties of the composite material [1]. An example of a general composite is the concrete used in our houses. Reinforced concrete is a composite composed of cement, sand, and metal rod. The composition changes the overall properties of the materials used. It becomes so hard and strong that it can withstand tons of load equally. The mechanical, electrical, thermal, optical and electrochemical properties of the nano-composite will be significantly different from those of the component materials.

Al is the most popular metal-matrix material due to its low density, good thermal conductivity, electrical conductivity, and corrosion resistance [1]. Because of the relative light weight and high specific strength, particulate-reinforced Al composites are attractive structural materials for various fields including automotive and aerospace applications. With these, Al MMCs have a wide range of advanced applications due to the combination of high strength and ductility [2]. For instance, Mazen et al [3]; Mula et al[4] made comparisons of pure Al with 2.0 vol% nano-Al_2O_3 additions and found an increase in yield strength of about 66%, hardness of about 50% and tensile strength increase of about 80%. Dominique et al [5] reported in their

experiment of ultrasonic assisted casting, a disbursement of 2.0 wt% nano-Al_2O_3 (10 nm) in Al matrix. In comparison to pure Al cast by the same method, composite hardness was increased by 92% and the yield strength by 56%, respectively. Hafeez and Senthil [6] concluded that because of the low density, low melting point, high specific strength, and thermal conductivity of Al, a wide variety of reinforcement particulates such as Al_2O_3, SiC, B_4C, Si_3N_4 TiC, TiO_2, TiB_2, and graphite have been used as reinforcements. Among these particulates, it was reported that Al_2O_3, SiC, B_4C, TiB_2 additions can also improve the wear behavior of Al matrix composites.

Although the strength of the materials can be improved by reinforcing particles, the reinforcements can also produce an adverse effect on the fracture toughness and ductility of the materials, which limits the wide applications of the composites [7]. The decreased trends resulted from several reasons [7]; the existence of intrinsic defects within the ceramic particles will create cracks during the deformation of the composites. Also, the residue porosity at the interface between the matrix and reinforcements, the formation of brittle phases resulted from the chemical reaction during the fabrication process, and the poor wettability and significant difference in the thermal expansion coefficient (CTE) between the matrix and the reinforcements might induce the crack nucleation and propagation during plastic deformation.

2. Processing methods

2.1. Powder metallurgy

The basic process of powder metallurgy consists of three major stages [8]. First, the primary material is physically powdered into small individual particles. Then, the different powders of metals and/or ceramics are mixed in the required proportions. Ball milling may be performed to achieve mechanical alloying of powder mixtures to better improve the resultant

mechanical properties. Next, the powder is injected into a mold or dies and compacted on a press to produce a weakly cohesive structure, which closely resembles the dimensions of the object ultimately to be manufactured. Finally, the product is formed by applying high temperature, pressure, long setting times, or any combination thereof. After sintering, secondary operations like extrusion, heat treatment or machining may also be performed.

For example, Mazen and Ahmed [3] mixed pre-weighed pure alumina powder (Al_2O_3) with pure aluminum (Al) powder through the use of a mechanical mixer and four different compositions, Al-0wt%Al_2O_3, Al-2.5wt%Al_2O_3, Al-5wt%Al_2O_3, and Al-10wt%Al_2O_3 were prepared. The Al-Al_2O_3 powder mixture was then hot-pressed at 723K for 4 hours using the hot-pressing setup shown in Fig 2.1. A compaction pressure of 74 MPa on the 24 mm diameter billets was used. The hot-pressed billets were then hot extruded and the extruded rods were used as specimens for different tests. SEM revealed the presence of porosity and particle-rich areas in the matrix as well as debonding of some alumina particles under fracto-graphic examination, due to weak bond strength and large differences between the melting points of Al and Al_2O_3. In liquid phase processing, proper wettability is only achieved at high processing temperatures (>1173 K).

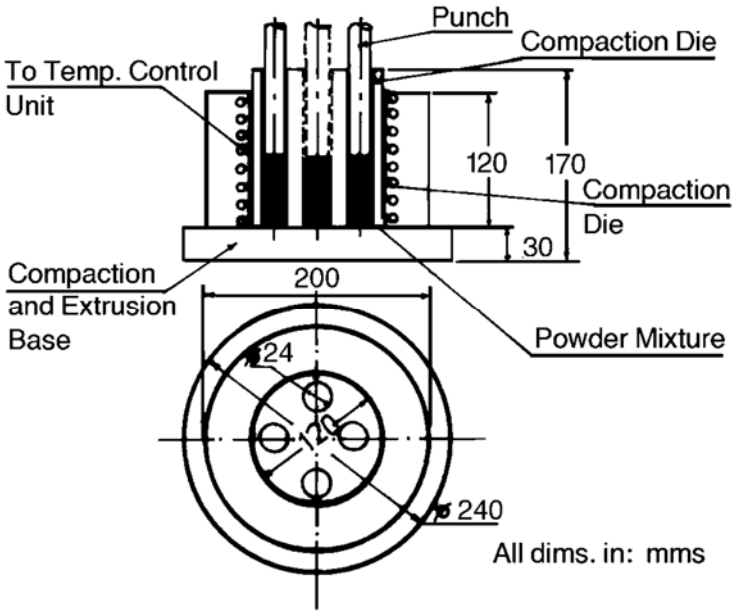

Figure 2.1 Hot pressing and extrusion setup

2.2 Other methods

2.2.1 Mechanical milling

Mechanical milling includes repeated deformation, welding, and fracture. There are many factors that will influence the stages of milling, such as the specific miller type, ball to power weight ratio, characteristics of the balls and their velocity, the milling atmosphere and temperature, and process control [9]. When milling the composite powders, the particle size, types of reinforcement, and most importantly, volume fraction will have influence on the process and concurrent mechanical properties of synthesized composites.

Razavi et al [10] produced Al powder by a nitrogen gas atomization process. The particle size and morphology of the Al powder was determined by a laser particle size analyzer along with SEM, and it was found that the particles are almost spherical with a mean diameter of 48μm. Two grades of α-Al_2O_3 powders with average particle sizes of 35 nm (n-Al_2O_3) and 1μm (Al_2O_3) were studied. Stearic acid powder was used as the process control agent (PCA). The Al powder was

blended with 5 vol% Al_2O_3 and 1.5 wt% PCA in a Turbula T_2C mixer for 20 min. The powder mixtures were then mechanically milled in a planetary ball mill, with a hardened steel vessel under a high purity argon atmosphere for up to 24 h. A rotational speed of 250 rpm and ball to powder weight ratio of 10:1 were employed. In different stages, small amounts of the milled powders were collected for testing. Al powder without Al_2O_3 addition was also processed in the same manner. In their study, the milling stages include plastic deformation, micro-welding, and particle fragmentation. When hard Al_2O_3 particles are added to Al powder, induced fracture occurs earlier, and thus the steady-state condition, i.e., formation of equiaxed particles, is achieved after shorter milling durations. The bulk density of composite powders was found to be higher than that of unreinforced Al. Meanwhile, it was shown that the mechanical milling stages occur earlier in Al–Al_2O_3 micro-composite when compared to the nano-composite.

2.2.2 Casting

Casting is a manufacturing process in which a liquid material is usually poured into a mold, which contains a hollow cavity of the desired shape, and then allowed to solidify. The solidified part is also known as a casting, which is ejected or broken out of the mold to complete the process. Casting materials are usually metals or various cold setting materials that cure after mixing two or more components together; examples are epoxy, concrete, plaster and clay. Casting is most often used for making complex shapes that would be otherwise difficult or uneconomical to make by other methods. [11]

Mazahery [12] used the A356 Al alloy as the matrix material while the mixture of nano-Al_2O_3 particles with an average particle size of 50 nm, and pure Al particles with an average size of 16 μm were used as the reinforcements. The powders were mixed in the ratio of Al/Al_2O_3=1.67,

and ball milled in isopropyl alcohol for 20 min using WC/Co balls. The mixture was then dried in a rotary vacuum evaporator and passed through a 60 mesh screen. The powder mixtures were cold pressed under 200MPa into samples having 60mm×60mm×60mm dimension. The compacted samples were crushed and then passed through 60 mesh screen. For manufacturing the MMCs, 0.75, 1.5, 2.5, 3.5 and 5 vol % Al_2O_3 particles were used. The required amount of Al_2O_3 was calculated according to the ratio of Al/Al_2O_3. The metal-matrix composites have been produced by using a vortex method. Approximately, 450 g of 356 Al alloy was loaded into a crucible made from graphite, and heated up to 800 °C (above the alloy liquidus temperature) for melting. A graphite stirrer fixed on the mandrel of the drilling machine was introduced into the melt and positioned just below the surface of the melt. Approximately, one gram of the powder mixture was inserted into an aluminum foil to form a packet. The packets were added into molten metal in the crucible, when the vortex was formed every 20 seconds. The packet of mixture melted and the particles began to distribute around the alloy matrix. The mixture was stirred for 15 minutes at approximately 600 rpm. Composite slurry was poured into preheated cast iron molds. The composites were shaped in the form of cylinders of 14 mm outer diameter and a length of 140 mm. SEM micrographs indicate that the nano-Al_2O_3 particles are homogeneously dispersed throughout the composite samples. The grain size measurements show that the grain size of aluminum composite is smaller than that of monolithic Al. The porosity levels increased slightly with increasing the particulate content. These results can be attributed to the increased surface area of the nano-Al_2O_3 particles, which can in turn increase the porosity levels. The yield strength, UTS, and ductility of the nano-Al_2O_3 reinforced Al composites improved with an increase in volume fraction of the dispersed nanoparticles. The great enhancement in UTS observed in this experiment, is a function of the small particle size, even distribution of the nano-Al_2O_3 particles,

effective transfer of applied tensile load to the nano-Al_2O_3 particulates, and grain refinement of the aluminum matrix. The hardness of the MMCs increases with the volume fraction of particles in the alloy matrix, due to the increasing ceramic phase in the matrix alloy. The higher hardness of the composites could be attributed to the fact that the nano-Al_2O_3 particles act as obstacles to the motion of dislocations. The maximum hardness was observed in the composite including 2.5 vol% Al_2O_3 and was cast at 800°C.

2.2.3 Pressure infiltration

Pressure infiltration casting is a unique form of liquid infiltration which utilizes pressurized inert gas to force liquid metal into a preform of reinforcement material. The methods and equipment used for pressure infiltration casting allow for inexpensive development of composite materials, prototypes, and net-shape component production [13]. In the pressure infiltration process, there is typically a porous preform of the reinforcement itself, followed by infiltration of its pores with the molten metal [13]. Wetting of the ceramic reinforcement by the molten metal is not easy, therefore, development of the liquid phase properties is not straightforward. Additionally, one must modify the chemistry of the system to overcome the capillary forces that can lead to non-desired wetting. External pressure may also be required to force proper contact and enhance the wettability. Chemical modifications include coating reinforcement, adding special elements to the matrix, or using specific atmospheres, including high temperatures.

For example, Gustafsson et al. [14] milled a powder mixture of Al_2O_3 (mean particle size 0.4 mm) and 4.1 wt% SiC in water for 1.5 h with Si_3N_4 balls. The aqueous suspension had a solid loading of 40vol%, and contained a dispersant. Two doped suspensions were also prepared by adding MgO (0.05 and 0.1 wt% with respect to the Al_2O_3 content) after 1 h of milling. The Al_2O_3:

SiC powder weight ratio was chosen so that the sintered material would have a SiC volume fraction of 5%. After milling, the slurries were screened through a 50 mm mesh, and a pressing aid was added. The slurries were then stirred for 1h, and thereafter screened through a 100mm mesh. Freeze granulation was subsequently carried out by spraying into liquid nitrogen. The ice was removed by freeze drying and the granules were screened so that the fraction larger than 500 mm was removed. Freeze granulation and drying makes it possible to retain the homogeneity of the aqueous suspension in the ceramic green bodies. The granules were hand-pressed into compacts and these were cold isostatically pressed at 300 MPa. The green bodies were placed in a SiC protective powder bed in a graphite crucible and pressureless sintered in a nitrogen atmosphere for 4 h. Two different sintering temperatures, 1750 and 1780°C, were applied The heating rate of the furnace was 1°C/min up to 600 8C, and then 10°C/min up to the holding temperature. The density of the sintered material was determined by the Archimedean method using distilled water. It is possible to pressureless sinter undoped Al_2O_3–5 vol% SiC nanocomposites to near full density (99.3%) at 1780°C. A smaller addition of MgO (0.05 or 0.1 wt% with respect to the Al_2O_3) is an effective densification aid only at lower sintering temperatures (1750°C), while the density of doped and un-doped materials are virtually the same after sintering at a higher temperature (1780°C). The SiC nanoparticles are well distributed and present at predominantly intra-granular positions. The hardness is strongly dependent on the density, and in the range 17.0–18.5 GPa when the material was sintered at 1780°C. The indentation fracture toughness was 2.3–2.4 MPa and did not depend on density, matrix grain size or SiC particle size.

2.2.4 Friction stir process

In the Friction stir process (FSP), plunging of a cylindrical rotating tool with a concentric pin and shoulder into the material surface is done. Also, localized heating must be implemented between the rotating tool and the work piece, in order to raise the local temperature of the material where plastic deformation can be easily induced. The tool is then be traversed along the line of interest when the working temperature is reached. Metal will flow to its back side where it is extruded or forged, consolidated, and cooled under hydrostatic pressure conditions, all induced by the stirring action of the pin tool.

Shafiei-Zarghani [15] used an Al6082 commercial Al–Mg–Si alloy extruded bar as the substrate material. Work pieces were prepared with a thickness, width, and length of 7, 75, and 200 mm, respectively. The hallow groove machined thorough the center surface of the substrate had a width, length, and depth of 1, 160, and 4 mm, respectively. Nano-sized Al_2O_3 powder with an average particle size of ~50nm was filled in the groove. The simplified FSP unit was a modified form of a conventional milling machine. A hardened H-13 tool steel was used that had a shoulder with a diameter of 16mm and a pin with a diameter and length of 5mm and 4mm, respectively. The shoulder tilt angle was fixed at 3°. The tool rotation rate was adjusted to 1250 rpm, and the rotating tool was traversed at a speed of 135 mm/min along the long axis of the work piece. Substrates were subjected to various numbers of FSP passes from one to four. In this investigation, an increase in the number of FSP passes caused a more uniform dispersion of fine cluster of Al_2O_3 particles. A good dispersion of nano-sized Al_2O_3 particles was achieved in the surface composite layer produced by three and four FSP passes. An increasing number of FSP passes resulted in an increase in the hardness value of SCLs due to more uniform distribution of alumina particles and also decreasing the matrix grain size. A maximum average micro hardness value of 312 HV was achieved for the SCL produced by four FSP passes. Hardness and wear resistance of the SCL

produced by four passes was found to be superior to those of the as-received Al substrate. The superior wear behavior of the fabricated SCL was attributed to increased hardness, the presence of hard ceramic particles, and matrix grain refinement. The increased wear resistance of the SCL over the unreinforced Al substrate, improved with increases in the applied load. In other words, the difference in wear rate is more pronounced at higher applied loads. At a relatively lower applied load, SCL produced by four FSP passes exhibited mild wear regime. However, it is changed to slightly severe wear at higher applied loads.

2.3 Comparison of various processing techniques

Process	Advantages	Limitations
Powder Metallurgy	1. Homogeneity of mixture is better controlled, component is produced in near net shape dimension, good ductility, low ball to powder charge ratio provides a better blend homogeneity 2. The gas atomized aluminium particles exhibit a spherical shape with broad size distribution while small satellite particles attached to the large ones 3. The most economical method for manufacturing aluminium MMCs, one can avoid the segregation and agglomeration of the reinforcement particles.	1. In processing of Aluminum, the oxide and hydroxide films coating the powder 2. Metal powders do not act as perfect liquids under pressure and a difference in pressure is established both parallel and perpendicular to the direction of pressing.
Casting	Better matrix–particle bonding, easier control of matrix structure, simplicity, low cost of processing, and nearer net shape	Extremely difficult for the mechanical stirring method to distribute and disperse nanoscale particles uniformly in metal melts due to their large surface to-volume ratio and their low wettability in metal melts

Pressure Infiltration	This method allows the powder particles to be kept in a liquid dispersing medium right up to the point of particle–particle contact during the consolidation step, It avoids problems associated with the formation of hard agglomerates when drying slurries	Abnormal grain growth was noted for samples containing the larger particle size, since the number of particles reduces with increasing particle size. This lowers the potential for grain boundary pinning during sintering, and hence, for limiting grain growth.
Friction Stir Process	1. To form ultrafine-grained structure in Al and Mg alloys 2. To produce a fine-grained microstructure, which exhibits super plasticity	

Table 2.1. Comparison of Various Processing Techniques [2]

3. Mechanical Properties of PRMMC

3.1 Young's modulus

Unidirectional reinforced continuous metal-matrix composites show a linear increase in the longitudinal Young's modulus as a function of fiber volume fraction [16]. Fig 2.2 shows an example of modulus increase as a function of fiber volume fraction for an alumina fiber-reinforced aluminum−lithium alloy matrix composite. The increase in the longitudinal Young's modulus is in agreement with the rule-of-mixtures value, but the modulus increase in a direction transverse to the fibers is much lower. Particle-reinforcement also results in an increase in the modulus of the composite; the increase, however, is much less than that predicted by the rule-of-mixtures. This is understandable because the rule of mixtures is valid only for continuous fiber reinforcement. Fig 2.3 shows increase in Young's modulus in an Al composite with volume fraction of silicon carbide

particles. Due to particle orientation along the extrusion axis, the modulus along the longitudinal orientation (parallel to the extrusion axis) is higher than perpendicular to extrusion (transverse orientation). Thus, there is a loss of reinforcement efficiency in going from continuous fiber to particle [17]. PRMMCs such as SiC particle-reinforced Al can offer a 50−100% increase in modulus over that of unreinforced Al. Which competes with the modulus equivalent of titanium, however, with a density that is about 33% lower. Also, unlike fiber-reinforced composites, the stiffness enhancement in particulate composites is reasonably isotropic.

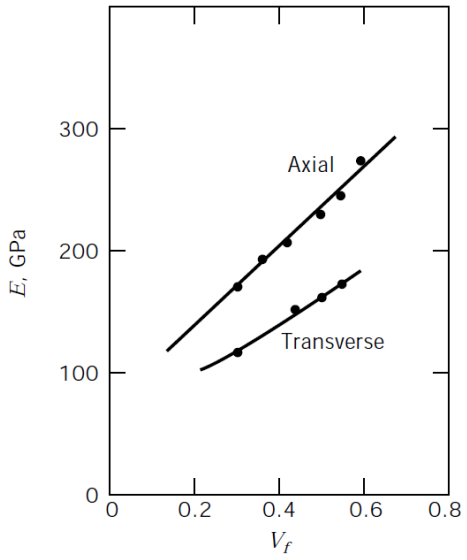

Figure. 2.2 Modulus increase as a function of fiber volume fraction V_f for alumina fiber-reinforced aluminum lithium alloy matrix [16]

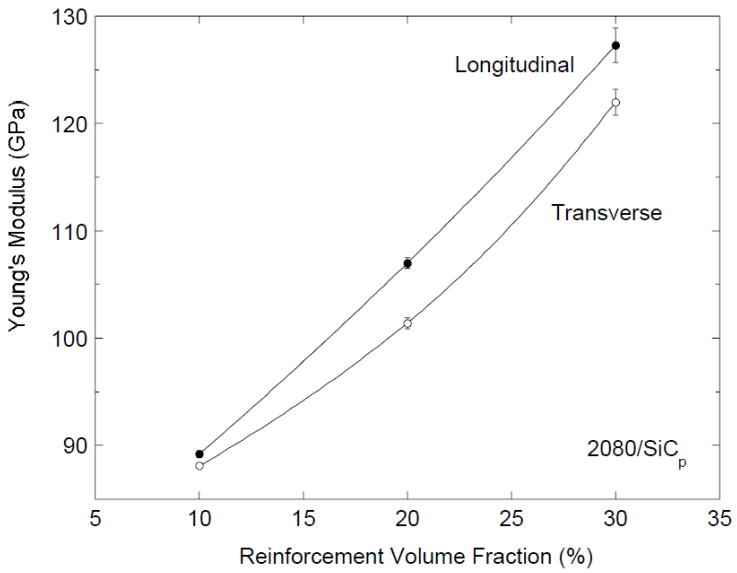

Figure. 2.3 Young's modulus increase in an aluminum composite with SiC particle reinforcement volume fraction [17]

3.2 Strengthening Mechanisms

Prediction of PRMMC strength is more complicated than the prediction of elastic modulus. The high mechanical resistance of PRMMCs is the result of several strengthening mechanism contributions, namely load transfer effect, Hall-Petch strengthening, Orowan strengthening [18-21].

3.2.1 Load Transfer Effect

The load transfer from the soft and compliant matrix to the stiff and hard particles under an applied external load, contributes to the strengthening of the base material. A modified Shear Lag model proposed by Nardone and Prewo [22] is commonly used to predict the contribution in strengthening due to load transfer in particulate-reinforced composites [18-20]:

$$\Delta\sigma_{LT} = v_p\sigma_m\left[\frac{(l+t)A}{4l}\right] \qquad (2.1)$$

where v_p is the volume fraction of the particles in the matrix, σ_m is the yield strength of the unreinforced matrix,l and t are the size of the particulate parallel and perpendicular to the loading direction, respectively. A = l/t is the particulate aspect ratio. For the equiaxed particulates, an increment in yield strength due to load transfer is expressed by:

$$\Delta\sigma_l = 0.5 v_p \sigma_m \qquad (2.2)$$

3.2.2 Hall-Petch Strengthening

The grain size has a strong influence on metal strength since the grain boundaries can hinder the dislocation movement. This is due to the different orientation of adjacent grains and to the high lattice disorder characteristic of these regions, which prevent the dislocations from moving in a continuous slip plane [23]. The Hall-Petch equation relates the strength with the average grain size (d) [23]:

$$\Delta\sigma_{H-P} = \sigma_0 + \frac{k_y}{\sqrt{d}} \qquad (2.3)$$

where k_y is the strengthening coefficient (characteristic constant of each material).

The particles play a fundamental role in final grain size found in metal matrices of composites since they can interact with grain boundaries acting as pinning points, retarding or stopping their growth.The increase of v_p (volume fraction) and the decrease of d_p (particle diameter) lead to a finer structure, as theoretically modeled by the Zener equation [3]:

$$d_m = \frac{4\alpha d_p}{3v_p} \qquad (2.4)$$

where α is a proportional constant.

3.2.3 Orowan Strengthening

The so-called Orowan mechanism consists in the interaction of nano-particles with dislocations. The non-shearable ceramic reinforcement particles pin the crossing dislocations and promote dislocations bowing around the particles (Orowan loops) under external load [23]. The Orowan effect can be expressed by the following expression:

$$\Delta\sigma_{OR} = \frac{0.13bG}{d_p\left(\sqrt[3]{\frac{1}{2}v_p}-1\right)} ln\left(\frac{d_p}{2b}\right) \qquad (2.5)$$

where b is the Burger's vector and G is the matrix shear modulus.

3.2.4 CTE and EM Mismatch

The mismatch in coefficient of thermal expansion (CTE) and in elastic modulus (EM) between the reinforcements and the metal matrix is accommodated during material cooling and straining by the formation of geometrically necessary dislocations (GNDs).

GND density due to CTE and EM mismatch can be estimated by the following expressions [20]:

$$p^{CTE} = \frac{A\Delta\alpha\Delta T v_p}{bd_p(1-v_p)} \qquad (2.6)$$

$$\rho^{EM} = \frac{6v_p}{\pi {d_p}^3}\varepsilon \qquad (2.7)$$

where A is a geometric constant, $\Delta\alpha$ is the difference in CTE and ΔT is the difference between test and processing or heat treatment temperatures. Then, the combined strengthening due to CTE and EM mismatch can be calculated by means of the Taylor equation [24]

$$\Delta\sigma_{CTE+EM} = \sqrt{3}\beta Gb\left(\sqrt{\rho^{CTE}} + \sqrt{\rho^{EM}}\right) \qquad (2.8)$$

where β is a constant.

References

1. B. Vijaya Ramnath, C. Elanchezhian, RM. Annamalai, S.Aravind, T. Sri Ananda Atreya, V. Vignesh and C.Subramanian, Aluminum matrix composites – A review. Rev. Adv. Mater. Sci. 38 (2014) 55-60

2. Dinesh Kumar Koli, Geeta Agnihotri, Rajesh Purohit, A Review on Properties, Behavior and Processing Methods for Al-Nano Al_2O_3 Composites. Procedia Materials Science 6 (2014) 567 – 589

3. Mazen, A.A. and Ahmed, A.Y. Mechanical Behaviour of Al-Al_2O_3 MMC Manufactured by PM Techniques Part I—Scheme I Processing Parameters. Journal of Materials Engineering and Performance 7 (1998) 393-401.

4. Mula, S., Padhi, P., Panigrahi, S.C., Pabi, S.K., Ghosh, S. On structure and mechanical properties of ultrasonically cast Al–2% Al_2O_3 Nanocomposite. Materials Research Bulletin 44 (2009) 1154–1160.

5. Poirier Dominique, Drew Robin, A.L., Trudeau Michel, L., Gauvin Raynald. Fabrication and properties of mechanically milled alumina/aluminium Nanocomposites. Materials Science and Engineering A 527 (2010) 7605–7614.

6. Hafeez Ahamed, V. Senthilkumar, Role of nano-size reinforcement and milling on the synthesis of nano-crystalline aluminum alloy composites by mechanical alloying. Journal of Alloys and Compounds 505 (2010) 772–782

7. Uddin, S.M. Mahmud, T. Wolf, C. Glanz, C. Kolaric, I. Volkmer, C. Höller, H. Wienecke, U. Roth, S. Fecht, H, Effect of size and shape of metal particles to improve hardness and electrical properties of carbon nanotube reinforced copper and copper alloy composites. Comp. Sci. Technol. 70 (2010) 2253–2257.

8. Andrzej Sluzalec, Stochastic characteristics of powder metallurgy processing. Applied Mathematical Modelling 39 (2015) 7303–7308.

9. A. Santos-Beltrán, R. Goytia-Reyes, H. Morales-Rodriguez, V. Gallegos-Orozco, M. Santos-Beltrán, F. Baldenebro-Lopez, R.Martínez-Sánchez, Characterization of Al-Al_4C_3 nanocomposites produced by mechanical milling. Materials Characterization 106 (2015) 368–374

10. Razavi Hesabi, Z., Simch, A., and Seyed Reihani, S.M. Structural evolution during mechanical milling of nanometric and micrometric Al_2O_3 reinforced Al matrix composites, Materials Science and Engineering A 428 (2006) 159–168.

11. Degarmo, E. Paul, Black, J T. Kohser, Ronald A. (2003), Materials and Processes in Manufacturing (9th ed.), Wiley, p. 277, ISBN 0-471-65653-4

12. Mazahery, A., Abdizadeh, H., Baharvandi, H.R. Development of high-performance A356/ nano- Al_2O_3 composites, Materials Science and Engineering A 518 (2009) 61–64.

13. A.J. Cook, P.S. Werner, 2003. Pressure infiltration casting of metal matrix composites. Materials Science and Engineering: A Volume 144, Issues 1–2

14. Gustafsson S, Falk L.K.L, Liden E., Carlstrom E. Pressureless sintered Al2O3–SiC nanocomposites, Ceramics International 34 (2008) 1609–1615.

15. Shafiei-Zarghani A, Kashani-Bozorg S.F, Zarei- Hanzaki A. Wear assessment of Al/Al_2O_3 nano-composite surface layer produced using friction stir processing, Wear 270 (2011) 403–412.

16. A. R. Champion, W. H. Krueger, H. S. Hartman, and A. K. Dhingra, Proceedings of the 2nd International Conference on Composite Materials (ICCM/2), TMS-AIME, New York, 1978, p. 883.

17. V. V. Ganesh and N. Chawla, Metall. Mater. Trans. 35A, 53–62 (2004).

18. Zhang, Z. Chen, D.L, Contribution of Orowan strengthening effect in particulate-reinforced metal matrix nanocomposites. Mat. Sci. Eng. A 483 (2008) 148–152.

19. Zhang Z, Chen D.L, Consideration of Orowan strengthening effect in particulate-reinforced metal matrix nanocomposites: A model for predicting their yield strength. Scripta Mater. 54 (2006) 1321–1326

20. Sanaty-Zadeh A, Comparison between current models for the strength of particulate-reinforced metal matrix nanocomposites with emphasis on consideration of Hall–Petch effect. Mat. Sci. Eng. A 531 (2012) 112–118

21. Luo P, McDonald D.T, Xu, W, Palanisamy, S Dargusch, M.S, Xia. K, A modified Hall–Petch relationship in ultrafine-grained titanium recycled from chips by equal channel angular pressing. Scripta Mater. 66 (2012) 785–788.

22. Nardone V.C, Prewo K.M, On the strength of discontinuous silicon carbide reinforced aluminum composites. Scripta Metal. 20 (1986) 43–48.

23. Hull, D.; Bacon, D.J. Introduction to Dislocations, 4th ed. Butterworth Einemann: Oxford, UK, 2001.

24. Smallman, R.E, Ngan, A.H.W, Physical Metallurgy and Advanced Materials, 7th ed. Butterworth Einemann: Oxford, UK, 2007.

Chapter 3. Previous Research

This chapter contains some examples of the previous experiments and FEA modeling for PRMMC systems and hierarchical composites. For convenience, we have categorized the previous literatures into two groups: experimental PRMMC systems, FEA PRMMC systems and experimental hierarchical composites.

1. Examples of previous experimental PRMMC systems

Al-based metal matrix composites reinforced with Al_2O_3 are being experimentally investigated worldwide in recent years. Here in our review, some important previous studies are introduced.

1.1 Khalid Al-Dheylan et al., 2006 [1]

The objective of their research was to determine the damage and failure mode of PRMMC caused as a result of tensile loadings. The researchers used powder metallurgy to prepare the composites. A blend of 6061 Al alloy powder and Al_2O_3 powder with an average size of 0.7μm was compacted by uniaxial pressing at 200 MPa. They produced 3 types of unique samples, in which volume fractions ranged from 10% to 30%. The microstructural features were examined using scanning electron microscopy (SEM). Microstructures of the resultant 6061 Al alloy reinforced with 10% and 20% volume fraction of Al_2O_3 are shown in Fig 3.1:

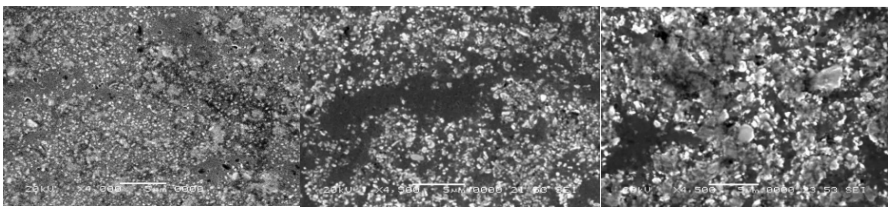

Figure. 3.1 Microstructure of 6061 Al alloy reinforced with 10% (left), 20% (middle), and 30% (right) Al_2O_3 particles [1]

The study is beneficial because it shows the composites' specific values of UTS and Young's modulus. The effect of the reinforcement volume fraction is clearly shown. As shown in Table 1, the experimental results show an increase in elastic modulus with an increase in reinforcement percentage. Young's modulus values ranged from 86.8 GPa for the 10% Al_2O_3 composite to 109.9 GPa for the 30% Al_2O_3 composite. These values correspond to a range of 27.6% to 61.6% increase compared to the elastic modulus of the unreinforced alloy. Furthermore, the increase in the UTS values ranged from 328.22 to 448.77 MPa for the Al 6061-10% Al_2O_3 and Al 6061-30% Al_2O_3 composites, respectively. The strain-to-failure values ranged from 4.72% for the 10% Al_2O_3 composite to 1.42% for the 30% Al_2O_3 composite, compared to a value of 28% for the 6061 alloy. Indicating a dramatic decrease of strain to failure value for the composites.

Volume fraction (%)	**Ultimate Tensile strength (MPa)**	**Young's Modulus (GPa)**	**Persent Strain-to-Failure (mm/mm)×100**
6061 Al alloy	121.53	68.03	29.26
10	328.22	86.81	4.72
20	410.10	104.45	2.29
30	448.77	109.9	1.42

Table 3.1 UTS, Young's modulus, and percent strain-to-failure results with different volume fractions of Al_2O_3 in Al 6061 alloy [1]

1.2 M. Rezayat et al., 2012 [2]

The objective of this study is to investigate the effects of the concentration of Al_2O_3 content on the microstructure, and the mechanical properties of composites. In the study, they used Al_2O_3 powder with a 0.47 μm particle size, with a polyhedral shape to produce the Al-Al_2O_3 composite. Microstructural observations were made using optical microscopy and SEM, in the rolling direction (RD), normal direction (ND), and transverse directions (TD). They produced 3 types of samples with volume fractions of 1%, 2%, and 3%.

As shown in Fig 3.2, the yield strength, ultimate tensile strength, and fracture-to-strain obtained from the engineering stress–strain curves for the composites, as a function of the Al_2O_3 volume fraction.

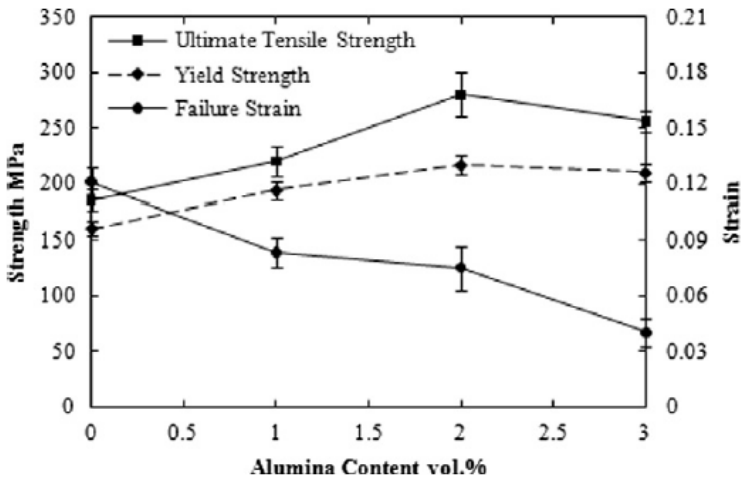

Figure 3.2 Mechanical properties of the Al–Al_2O_3 composite as a function of Al_2O_3 content [2]

In this work, it is shown that the ultimate tensile strength of the composite, as a function of the Al_2O_3 content, has a maximum value in the sample of 2% volume fraction of Al_2O_3, whereas elongation decreased by increasing the Al_2O_3 contents.

1.3 Bharath V et al., 2014 [3]

The researchers synthesized Al 6061-Al_2O_3 particulate MMC using the stir casting method. Al_2O_3 particles with a nominal size of 125 μm and varying amounts of 6, 9, and 12wt% were used. This study is beneficial because it used specific values to show the mechanical behavior of the composites. We can clearly see the effect of the volume fraction on the hardness, yield stress, UTS, as well as the variation in percent of elongation.

Fig 3.3 shows the results of micro-hardness tests conducted on Al 6061 alloys with different wt% Al_2O_3 particles.

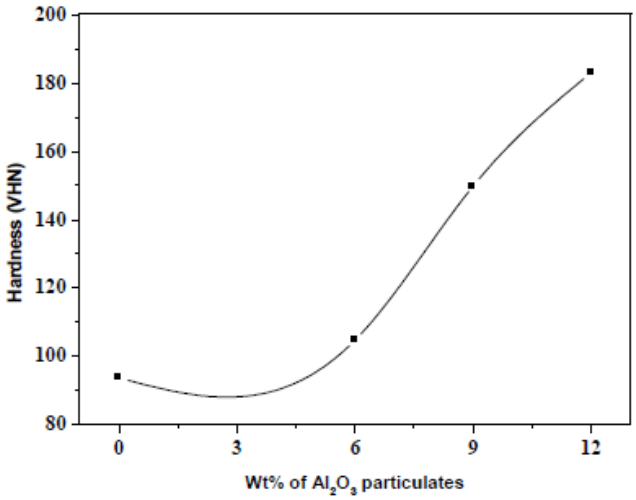

Figure 3.3 Graph showing the variations in hardness of Al 6061 before and after addition of different volume fraction of Al_2O_3 particulates [3]

To investigate the mechanical behavior of the composites, tensile testing was conducted using a computerized uni-axial tensile testing machine. Three specimens were used for each test and the average value was reported. The tensile properties including tensile strength, yield strength, and percent elongation were extracted from the stress-strain curves and are represented in Table 3.2.

Weight percentage of Al_2O_3 particles (%)	**Yield Stress (MPa)**	**Ultimate Tensile strength (MPa)**	**Extent of Improvement in UTS Value (%)**
0	138.06	149.76	-
6	145.51	167.93	12.12
9	155.94	173.61	15.92
12	178.91	193.47	29.18

Table 3.2 the tensile test results of cast Al6061, with addition of 6, 9, and 12% of Al_2O_3 particulates to Al6061 [3]

It is clear that the fracture strength of composites (6, 9, and 12 wt %) is higher than that of cast Al6061, while the ductility of the composite is lesser than the unreinforced alloy. It is also clear from Table 3.2 that the tensile strength increased with increasing the amount of reinforcement, while there is decrease in ductility with an increase in reinforcement percentage.

2. Examples of previous FEA-PRMMC systems

Experiments towards PRMMCs always cost a lot, so a cheaper way to understand the mechanical properties of PRMMCs is necessary in recent years. As a suitable way to solve this problem, FEA has received considerable attention. Here are some examples to prove the reliability of FEA in this field.

2.1 M. Guagliano, 2015 [4]

Research was presented by M. Guagliano about the mechanical behavior of a 6061 aluminum alloy reinforced with Al_2O_3 particles. Experimental tests were carried out to evaluate the mechanical characteristics of this type of material under static and fatigue loading. A microscale finite-element model (FEM) of this material was developed to investigate the mechanical behavior of the composite material following a thermal treatment and implies a tensile load applied along direction.

The finite-element model is based on a unit cell of an Al_2O_3 particle surrounded by the matrix. Particles were equal to 18 mm long and 9 mm wide, resulting in a dimensional ratio of 1:2, which was similar to the one observed experimentally. Fig 3.4 shows the mesh of the composite material, particular of the particle.

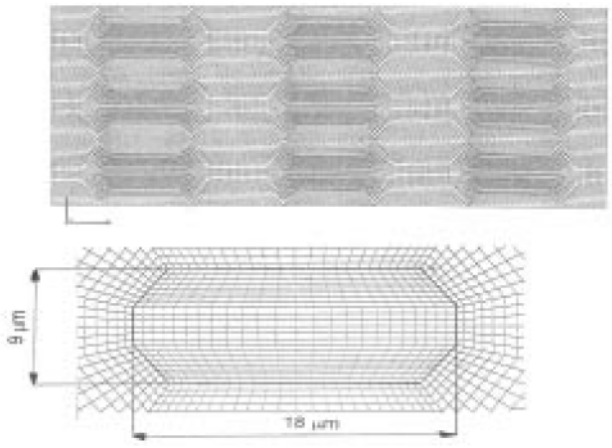

Figure 3.4 Mesh of the composite material, particular of the particle [4]

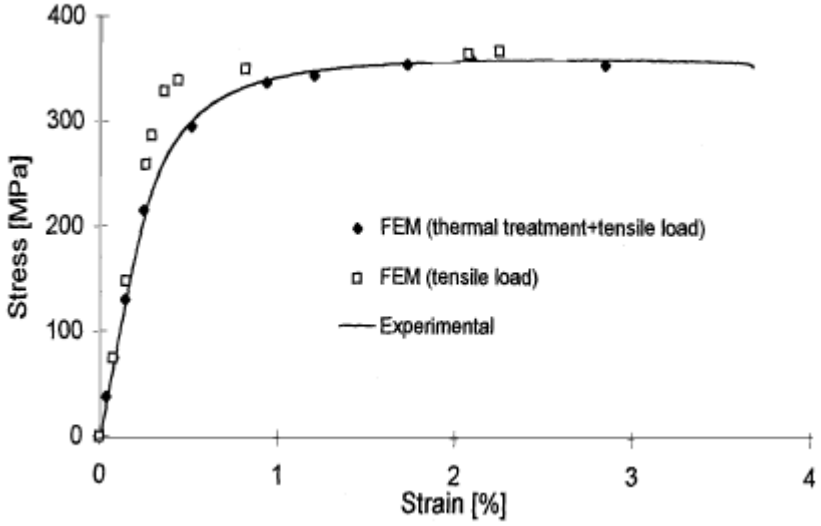

Figure 3.5 Tensile stress-strain curves obtained numerically and experimentally [4]

This study is meaningful because it provided the comparison between the stress-strain curves obtained experimentally and numerically. As shown in Fig 3.5, agreement is good until the highest load is applied, which can be considered as validation of the FEM microstructure model. The global elastic modulus is practically equal to the experimental modulus (Eexp = 92.800 MPa, E_{FEM} = 93.200 MPa), whereas the value numerically obtained without considering the thermal treatment is 10% higher (E_{FEM} = 101.800 MPa, without residual stresses). This can be attributed to local plasticization of the matrix near the sharp corners at the interface with the reinforcement [4]. Due to the presence of residual stresses, this occurs for low applied loads and globally reduces the elastic modulus. Furthermore, the presence of the tensile residual stresses in the matrix causes yields for low loads. This also is in concordance with the experimental evidence.

2.2 Hai Qing 2013 [5]

In this research, the effect of particle volume fraction, composite microstructure and boundary conditions on the deformation behavior of an Al alloy/SiC metal matrix composite was numerically studied. Finite element method (FEM) was used to conduct the numerical simulations. A program is developed for the generation of 2D micromechanical FE-models with randomly distributed SiC particles. In order to simulate the damage process in aluminum alloy matrix and SiC particles, the maximum principal stress criterion based elastic brittle damage model are developed within Abaqus/Standard Subroutine USDFLD, respectively. The FE-models are shown in Fig. 3.6

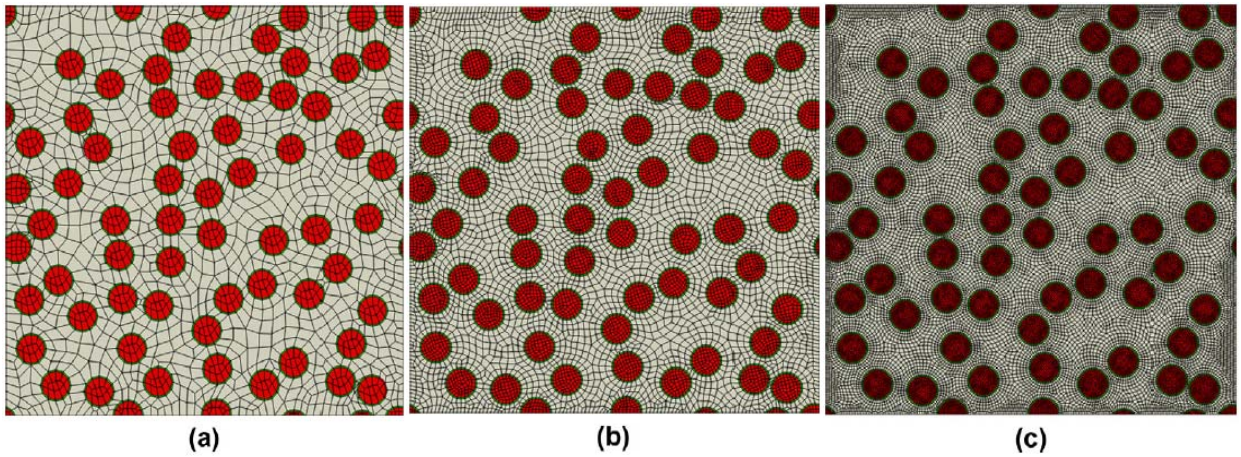

Figure 3.6 Examples of the 2D RVE containing 64 identical particles and 25% reinforcement volume content with mesh seed: (a) 12, (b) 24 and (c) 48. [5]

This study is a very good example of previous particle damage model, although it didn't analyze the stress condition on the ceramic particles. As shown in Fig 3.7, the stress-strain curves of the composites show a large drop when the particles start to fracture. Ultimate tensile stress and strain to failure can be extracted at the very beginning point of particles' fracture.

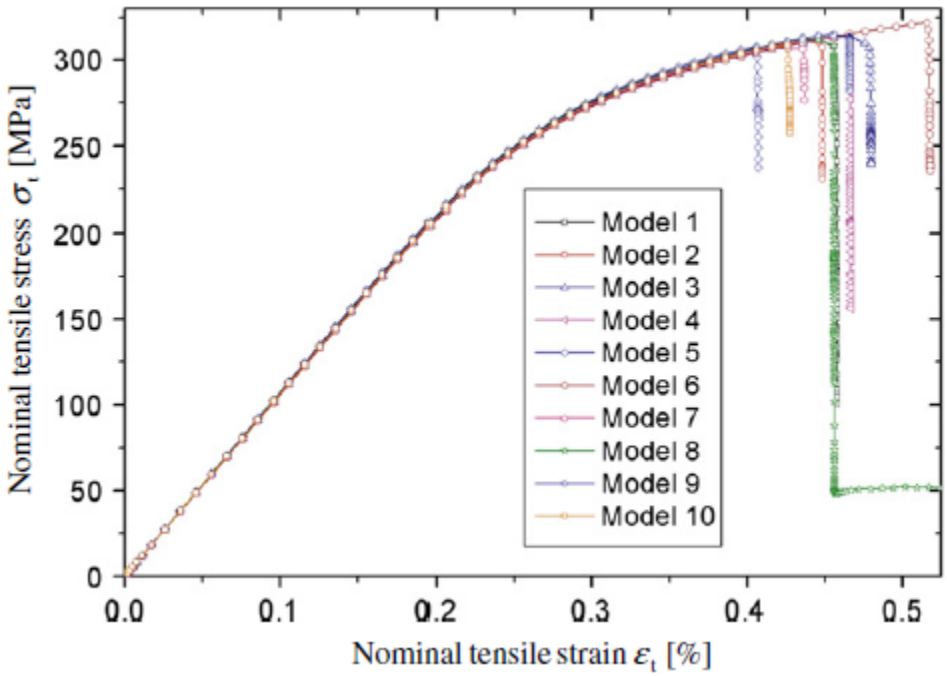

Figure 3.7 Stress–strain relationships of different micromechanical models containing 64 particles [5]

2.3 N. Chawla et al., 2011 [6]

In this research, the effect of particle distribution on the deformation behavior of an Al (6061) /SiC metal matrix composite was numerically investigated. Finite element method (FEM) was used to conduct the numerical simulations. The software used to perform the finite element analysis was ABAQUS (Standard Implicit module; version 6.6-3, Pawtucket, RI). [6] The SiC ceramic phase is taken as elastic. The SiC particles were modeled as purely elastic, while the Al matrix was modeled as elastic–plastic. The SiC particles were represented as two-dimensional circular particles of uniform diameter. Three particle distributions – ordered, random, and clustered were evaluated. The degree of particle clustering was quantified using the coefficient of variance

of the mean near-neighbor distance method. [6] The whole FE-model as well as the meshed matrix phase are shown in Fig. 3.8

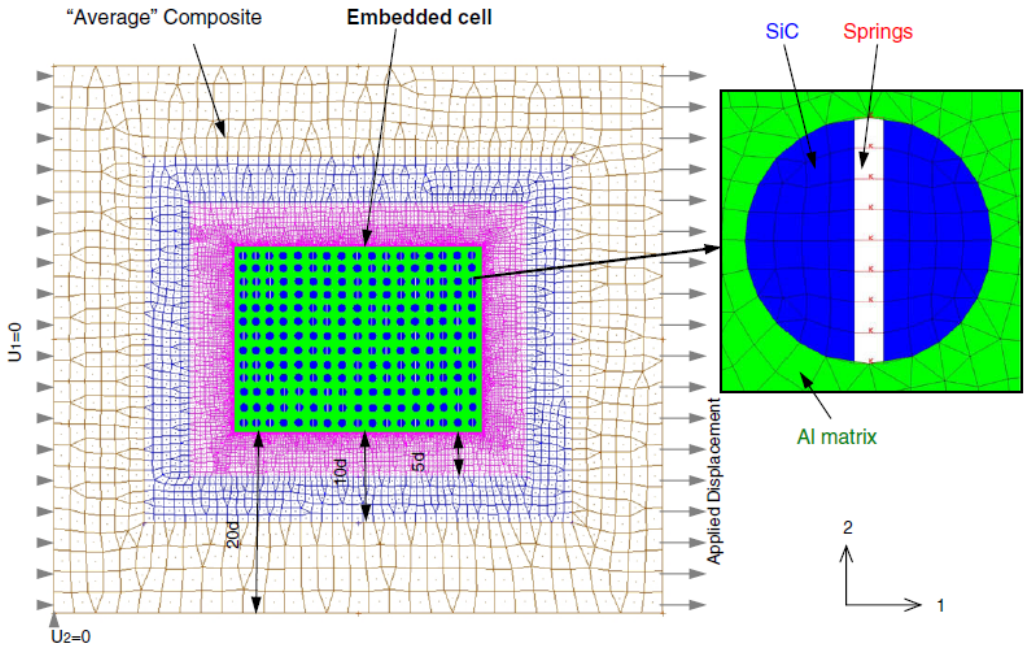

Figure 3.8 Description of the numerical model [6]

This study is meaningful because it applied particle damage model to the simulation and the simulation has taken the stress condition of ceramic particles into consideration. As shown in Fig 3.9 (a), the fracture of particles can been clearly observed as the stress-strain curve start to decrease drastically. The stress-strain curves of SiC particles are shown in Fig 3.9 (b). The particle damage model in this research has the limitation that the stress on the SiC particles didn't drop to zero after the fracture of particles.

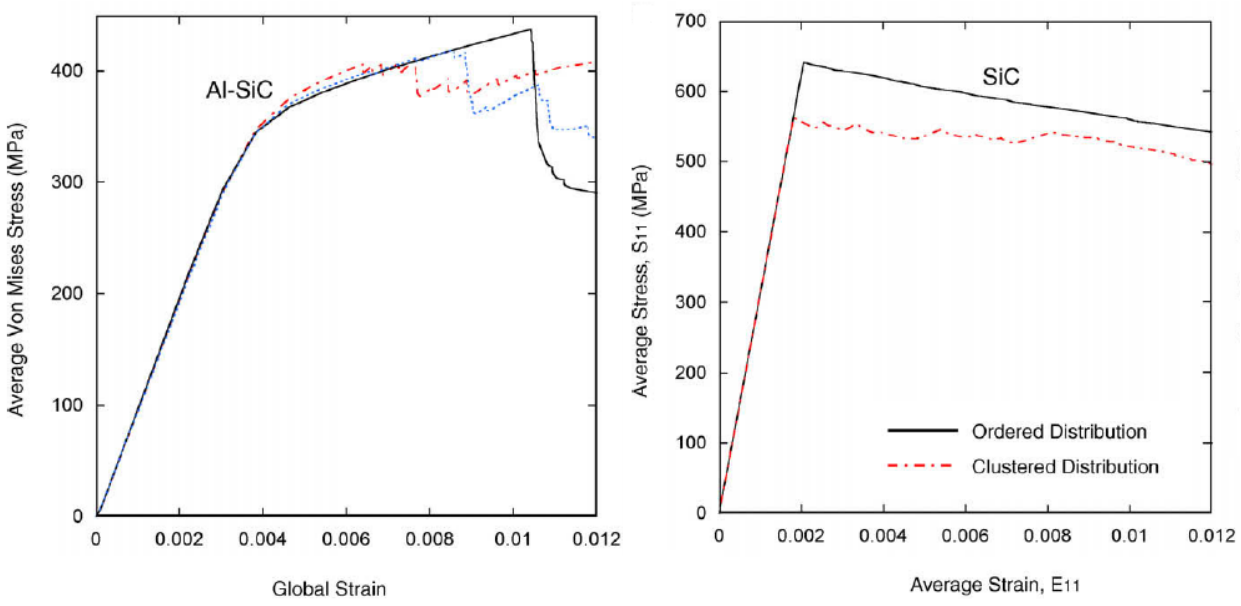

(a) (b)

Figure 3.9 Average Von Mises stresses versus Global strain for (a) Al–SiC composites and (b) SiC particles [6]

3. Examples of previous experiments for hierarchical composites

In recent years, several attempts have been made to use different types of reinforcement to enhance the mechanical response of magnesium (Mg) by different processing routes [7-10], but to date, only Manoj Gupta's group studied the effect of a hybrid reinforcement on the mechanical response of magnesium. In this sub-section, we introduce the only exact studies in this hierarchical composites field.

3.1 Meisam K. Habibi et al., [11]

Meisam K. Habibi et al have opened the area of study of using a hybrid reinforcement to enhance the mechanical response of magnesium (Mg). The objective of their study was to synthesize and investigate the mechanical performance of a hierarchical magnesium (Mg)

composite with a novel micro-architecture including a reinforcing constituent that is a composite in itself. Specifically, they developed a composite (alternatively referred to as a level II composite) with pure Mg as the matrix, reinforced by another level I composite comprising a sub-micron pure aluminum (Al) matrix in which are embedded alumina (Al_2O_3) particles. The sub-micron Al and Al_2O_3 were combined through a ball milling process, getting the level I composite, which was then combined with pure Mg to form a level II composite [11].

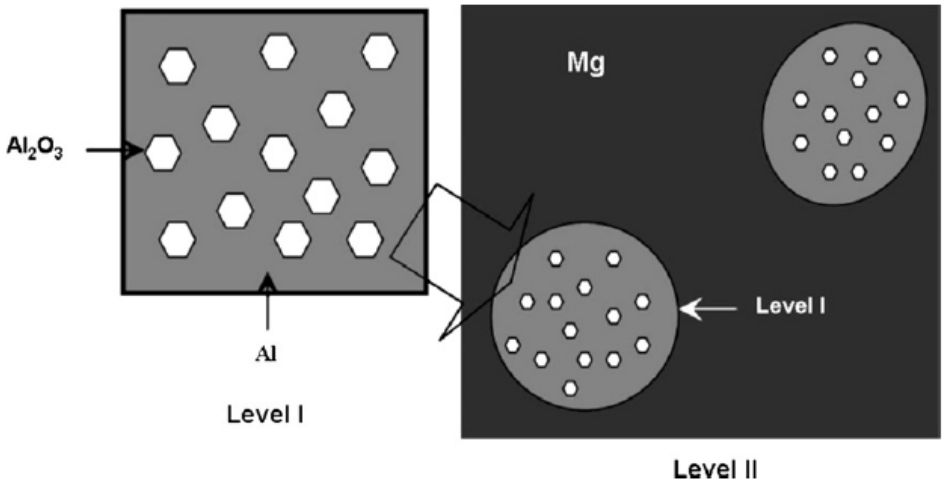

Figure 3.10 Schematic of the hierarchical Mg nano-composite synthesized in Habibi's work [11]

Fig. 3.10 illustrates the underlying concept of hierarchical Mg composite synthesized in their work. This study is meaningful because it is considered as the first attempt to study the effect of a hybrid reinforcement to enhance the mechanical response of magnesium (Mg). The uniaxial tensile true stress–true strain curves of the hierarchical composite samples for different Al volume fraction along with the response of pure Mg are shown in Fig 3.11.

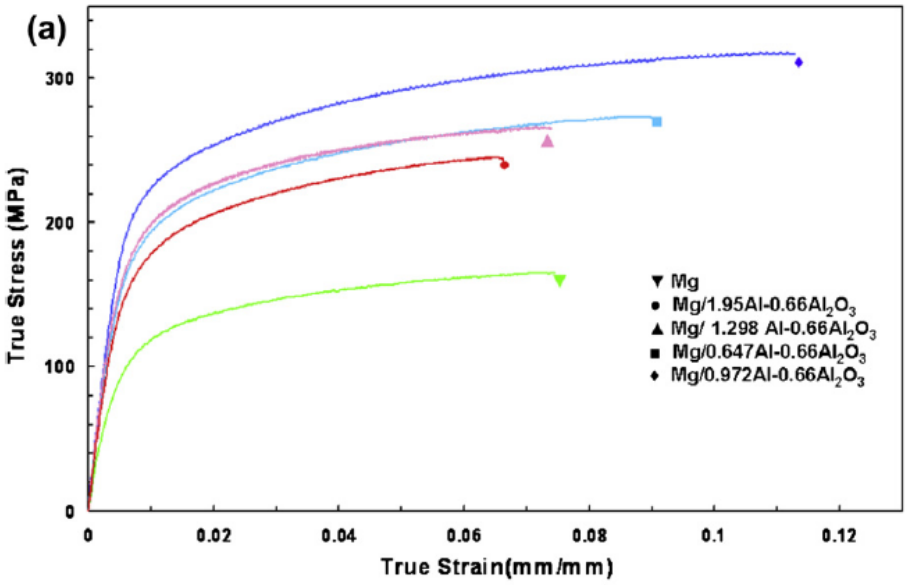

Figure 3.11 True stress–true strain curves for pure Mg and hierarchical composite specimens [11]

References

1. Khalid Al-Dheylan, Syed Hafeez, Tensile failure micromechanisms of 6061 Aluminum reinforced with submicron Al_2O_3 metal-matrix composites. The Arabian Journal for Science and Engineering, Volume 31, Number 2C.

2. M. Rezayat, A. Akbarzadeh, A. Owhadi, Production of high strength Al–Al_2O_3 composite by accumulative roll bonding. Composites: Part A 43 (2012) 261–267.

3. Bharath V, Madev Nagaralb, V Auradib, S. A. Koric, Preparation of 6061Al-Al_2O_3 MMC's by Stir Casting and Evaluation of Mechanical and Wear Properties. Procedia Materials Science 6 (2014) 1658 – 1667.

4. M. Guagliano, A Numerical Model to Investigate the Role of Residual Stresses on the Mechanical Behavior of Al/Al_2O_3 Particulate Composites. JMEPEG (1998) 7:183-189

5. Hai Qing. Automatic generation of 2D micromechanical finite element model of silicon–carbide/aluminum metal matrix composites: Effects of the boundary conditions. Materials and Design 44 (2013) 446–453.

6. A. Ayyar, G.A. Crawford, J.J. Williams, N. Chawla. Numerical simulation of the effect of particle spatial distribution and strength on tensile behavior of particle reinforced composites. Computational Materials Science 44 (2008) 496-506.

7. Goh C.S., Wei J., Lee L.C. and Gupta M. (2006) "Simultaneous enhancement in strength and ductility by reinforcing magnesium with carbon nanotubes". Materials Science and Engineering A, 423 (2006) 153-156.

8. Han B.Q. and Dunand D.C. (2000) "Microstructure and mechanical properties of magnesium containing high volume fractions of yttria dispersoids". Materials Science and Engineering A, 277 (2000) 297-304.

9. Hassan S.F. and Gupta M. (2007) “Development of nano-Y2O3 containing magnesium nanocomposites using solidification processing”. Journal of Alloys and Compounds.429 (2007) 176-183.

10. Paramsothy M., Hassan S.F., Srikanth N. and Gupta M. (2009) “Enhancing tensile/compressive response of magnesium alloy AZ31 by integrating with Al_2O_3 nanoparticles”. Materials Science and Engineering A, 527 (2009) 162-168.

11. Meisam K. Habibi, Shailendra P. Joshi, Manoj Gupta, Hierarchical magnesium nano-composites for enhanced mechanical response. Acta Materialia 58 (2010) 6104–6114

Chapter 4. Model Development

A typical FEA for PRMMC contains several important pre-processing steps. We first need to generate the proper geometries including all components. Components are regarded as separate parts in these pre-processing steps. Then, FEA meshes are required for all the components. These FEA meshes can be routinely obtained directly from the computer-generated solid models. We must also incorporate relevant material properties for each component and combine all the components into a total composite model. Proper boundary or loading conditions should also be applied. Finally, a suitable solution method must be chosen. In this chapter, these steps for FEA of PRMMC are addressed.

1. Structure Generation

In analyzing PRMMC, a representative volume element (RVE) is created. In the theory of composite materials, the RVE (also called the unit cell) is the smallest volume over which a measurement can be made that will yield a value representative of the whole [1]. This is generally the principle adopted, and it leads to the fact that the RVE must include a large number of the composite microheterogeneities (grains, inclusions, voids, fibers, etc.). It must, however, remain small enough to be considered as a volume element of continuum mechanics [1]. RVE in this thesis is a square that can be divided into two parts: metal-matrix and the reinforcement particles. For the entire FEA process of the PRMMC, the first step is to generate suitable geometries for individual constituent components. Geometries for the metal-matrix and the ceramic particles are required. Toward this, we employed the commercial autoCAD software, Rhinoceros 5.0 by Robert McNeel & Associates. Using this software, squares and spheres were created at the same time to represent the metal-matrix and particulates, respectively.

1.1 Model geometries generated for the investigation of particle size effect

All of the squared computation boxes were created in 10×10×10 mm^3 format. Three types of spheres were created with same volume fraction (10%) but different radii that are range from 0.96 to 2.88mm. Fig 4.1(a) shows the square matrix single particle inside matrix. Models with 8 particles and 27 particles are shown in Fig 4.1 (b) and (c).

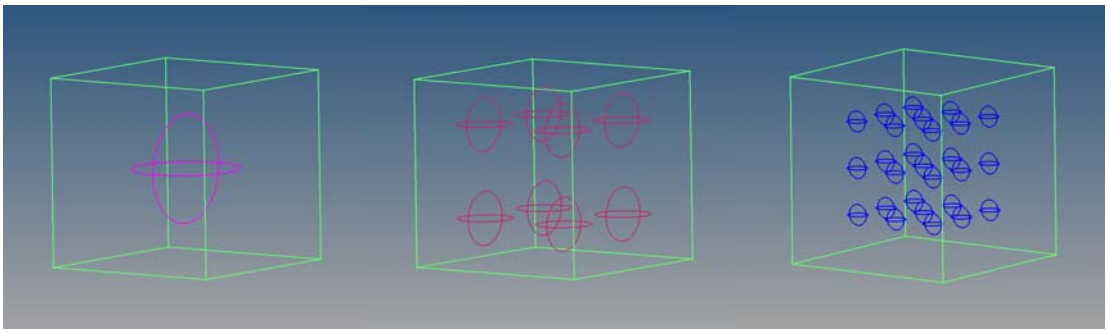

(a) (b) (c)

Figure 4.1 Simulated microstructures of the PRMMCs with different particle sizes

1.2 Model geometries generated to study the particle distribution effect

With the fixed particle volume fraction of 10% and fixed particle number of 27, models with random and clustered particle distributions were created. The two simulated particle distributions are shown in Fig 4.2. Each distribution has 27 particles all with a constant radius of 0.96mm. The degree of particle clustering in the simulated in the simulated microstructures was quantified by the coefficient of variance of the mean near-neighbor distance (COV_d) technique [2]. The COV_d is defined as:

$$COV_d = \frac{\sigma_d}{d} \qquad (4.1)$$

where σ_d^2 is the variance in the mean near-neighbor distances for all particles. The higher the COV_d, the more "clustered" the distribution of the particles. The coordinates of all the 27 particles are generated by Excel Rand function.

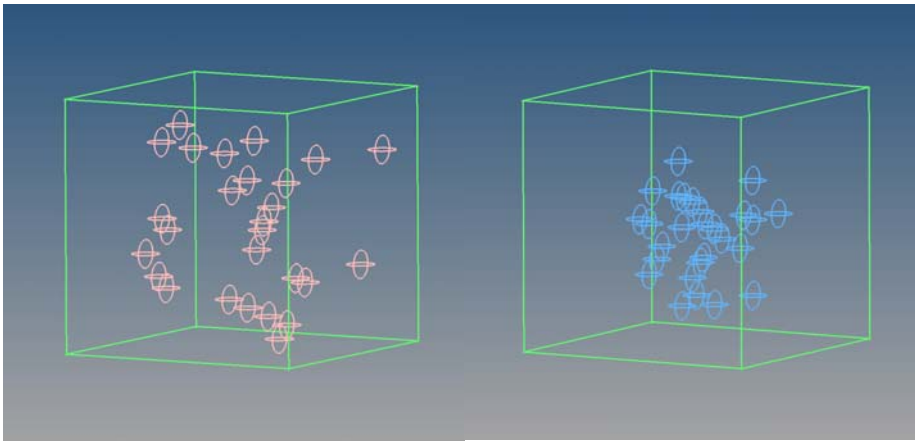

(a) (b)

Figure 4.2 Simulated microstructures with two different particle distributions: (a) random distribution: $COV_d = 0.32$ (b): Clustered distribution: $COV_d = 0.69$.

1.3 Model geometries generated to investigate the volume fraction effect

With the random distributed and fixed particle number of 27, models with different volume fractions were created by changing the radius of the particles. All the models have the same COV_d as 0.32. Fig 4.3 shows the three simulated microstructures with different volume fractions from 10% to 30%.

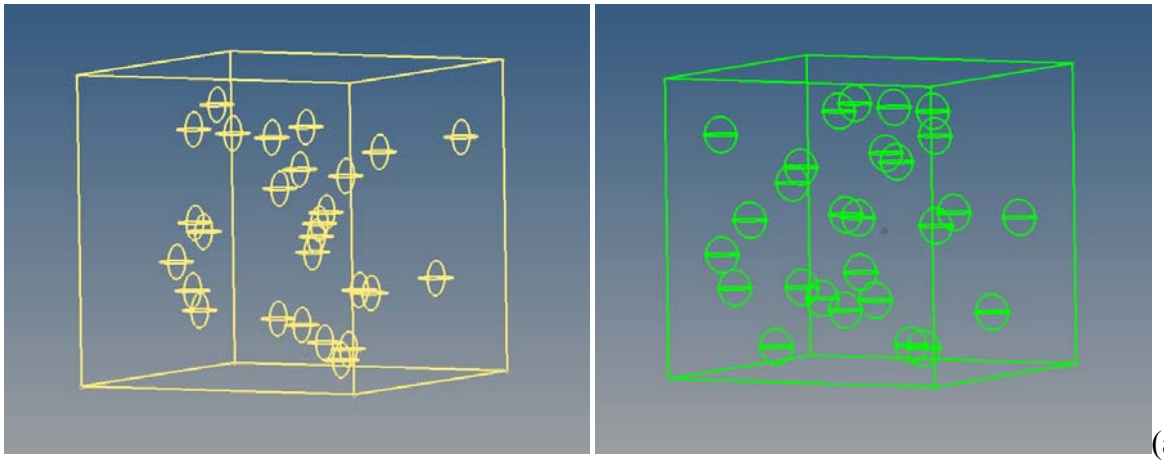

(a)

(b)

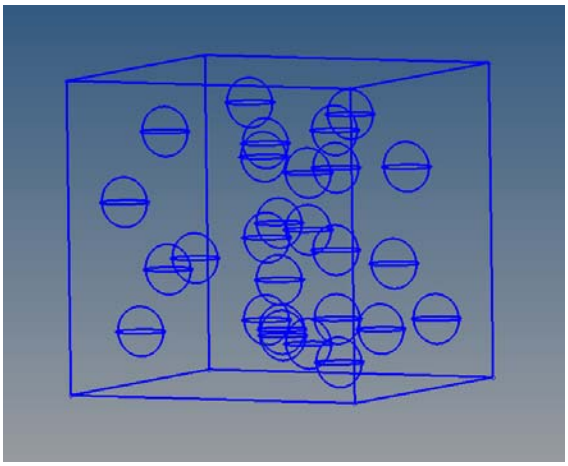

(c)

Figure 4.3 Simulated microstructures with different particle volume fractions: (a) 10%, (b) 20% (c) 30%

1.4 Model geometries generated for hierarchical composites

For the geometries of hierarchical composites, because the reinforcement particle itself is a composite, we created two kinds of particles: the very inner ceramic particles and the outer Aluminum particles. Fig 4.4 shows an example of the geometry of the hierarchical composites.

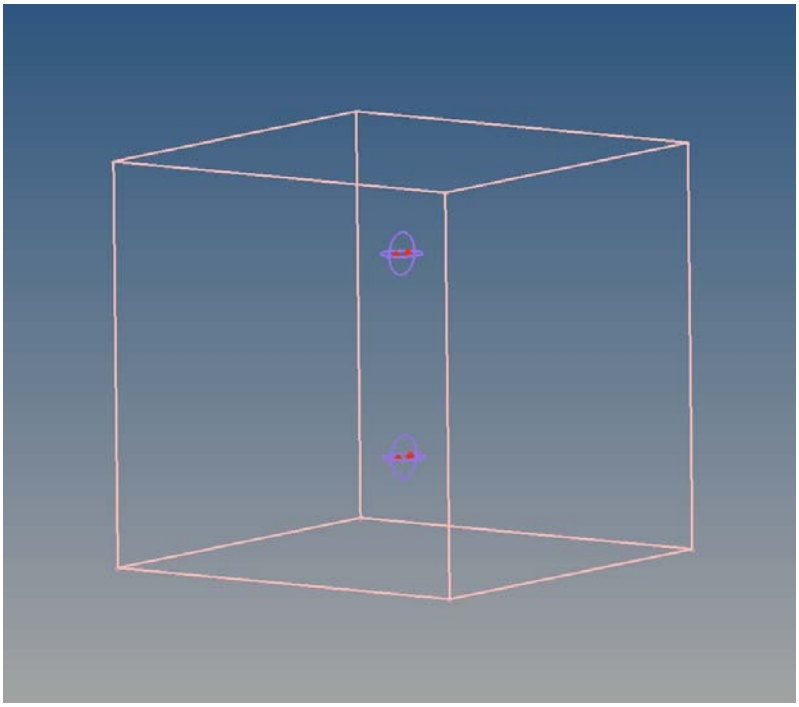

Figure 4.4 Geometry of hierarchical composites

2. Mesh Generation

After geometry generation, these solid models need to be discretized into suitable FEA meshes. The most convenient way is to use “tetramesh”, an option in the commercial Hypermesh software 11.0 by Altair Engineering, to directly mesh the matrix and the particle into different tetrahedron meshes. Here, a suitable and optimized mesh size needed to be determined. Fig 4.5 illustrates the mesh sample of a sphere with radius 2.88 mm and Fig 4.6 shows a cross section of a matrix containing one particle.

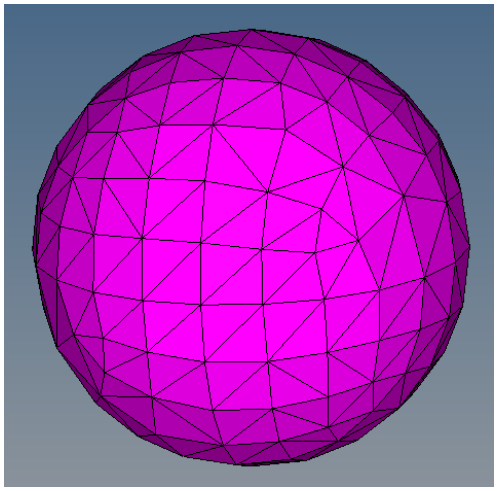

Figure 4.5 Example of a particle FEA mesh with radius of 2.88 mm

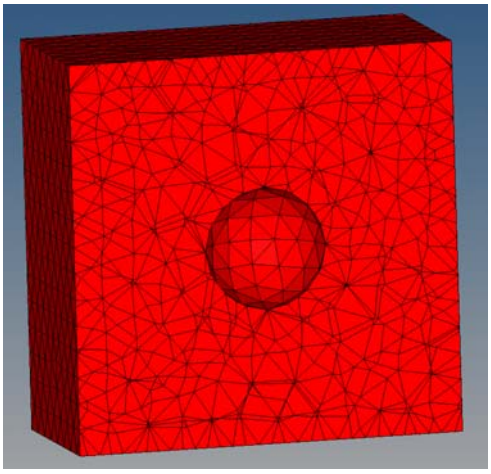

Figure 4.6 Example of a cross-section of matrix FEA mesh containing one particle in the center

RVE models for hierarchical structures were generated. Different from the structure of PRMMC, hierarchical structure requires the reinforcement itself is a composite. In our study, the reinforcement particle of the whole hierarchical composite also has two parts: the matrix shell and the inner particle. Fig 4.7 shows the cross section of the matrix shell. Thus, the whole hierarchical composite can be divided into three parts: the outer matrix, the inner matrix shell and the particle. Fig 4.8 shows the cross-section of it. Same as PRMMC, all the squared computation boxes that

are used as the matrix of the hierarchical composites were created in 10×10×10 mm^3 format. Only one type of particle was generated with radius of 1.16 mm and volume fraction of 0.66%. Two types of inner matrix shells were created with volume fraction of 0.647% and 0.972%.

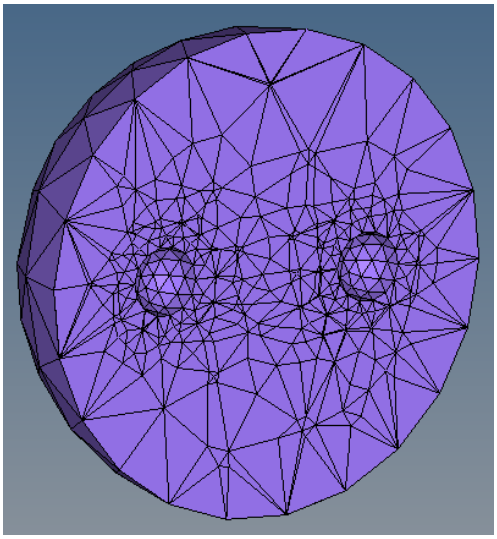

Figure 4.7 Example of a cross-section of matrix shell of hierarchical composites

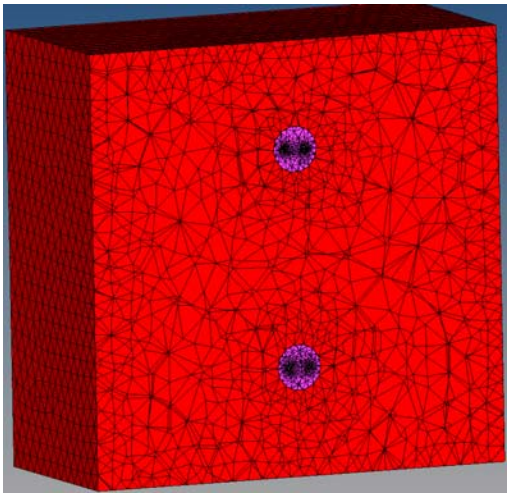

Figure 4.8 Example of a cross-section of whole hierarchical composite structure

3. Material Properties

Before performing any simulations, the adequate material properties of all the components must be fully defined.

3.1 Material properties of Al6061 alloy and Al_2O_3

As discussed in the previous chapter, Al (or Al alloys) is used as the matrix and ceramic is used as the particles. To compare with the experimental results, Al 6061 alloy is chosen as the material of the matrix and Al_2O_3 is chosen as the ceramic particles. The behavior of Al 6061 alloy is elastic–plastic in nature and its response to uniaxial loading could be highly non-linear [3]. The young's modulus is 68.03 GPa with 0.33 as the poisson's ratio [4]. These plasticity models can be defined using the data obtained from an experimental test with the grain size of 16.6 μm. [3] Most of the previous studies including this thesis treat Al 6061 alloy as a homogeneous, isotropic, and incompressible material. Fig. 4.9 shows the stress-strain curve that was employed in this thesis for the Al 6061 alloy [3].

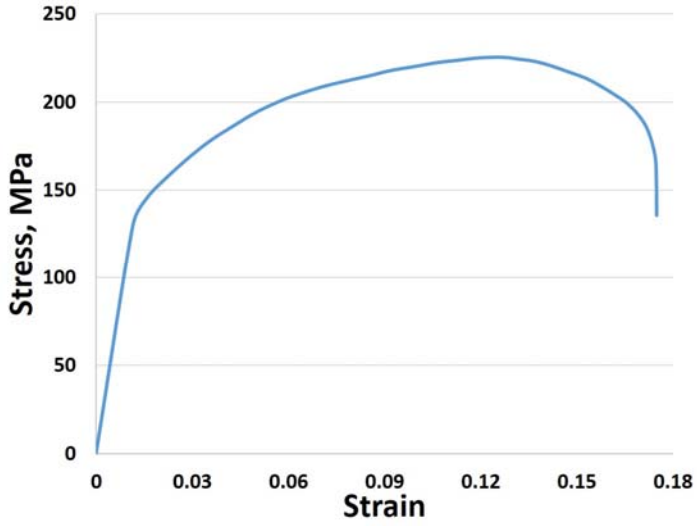

Figure 4.9 Stress-strain curve of Al 6061 alloy [2]

On the other hand, the Al_2O_3 particles were assumed to behave in a linear elastic manner until the ultimate strength was reached, followed by the stress drop to zero. The strength of the Al_2O_3 particles has been reported to be between 1 and 2 GPa [5]. In our studies, all SiC particles were assumed to have uniform fracture strengths of 1100 MPa. We used 390GPa as the young's modulus and 0.2 as the poisson's ratio. The grain size is 10μm. [5]

3.2 Material properties of Al6061 alloy with different grain size

In order to simulate the effect of matrix grain size on the tensile properties of PRMMC, we used Ludwik's Equation [6] to calculate different plastic properties of Al6061 alloy with different grain sizes. The equation can be expressed as:

$$\sigma = \sigma_y + k\varepsilon_p^n [6] \qquad (4.2)$$

where k is the strength coefficient, and n is the strain hardening exponent. Adnan N. Abood et al. [7] found Al6061 alloy has the property that k= 480MPa and n= 0.052. σ_y is the yield stress of Al6061-T6 alloy and can be expressed as:

$$\sigma_y = \sigma_0 + \frac{k'}{\sqrt{d}} \qquad (4.3)$$

where σ_0 (=276MPa for Al6061[8])is the original strength of the material. k' (=83.79 MPaμm^{-1} for Al6061 [8]) is a constant depending on the material. Fig 4.10 presents the calculated plastic stress-strain curves with different grain size from 10μm to 50μm:

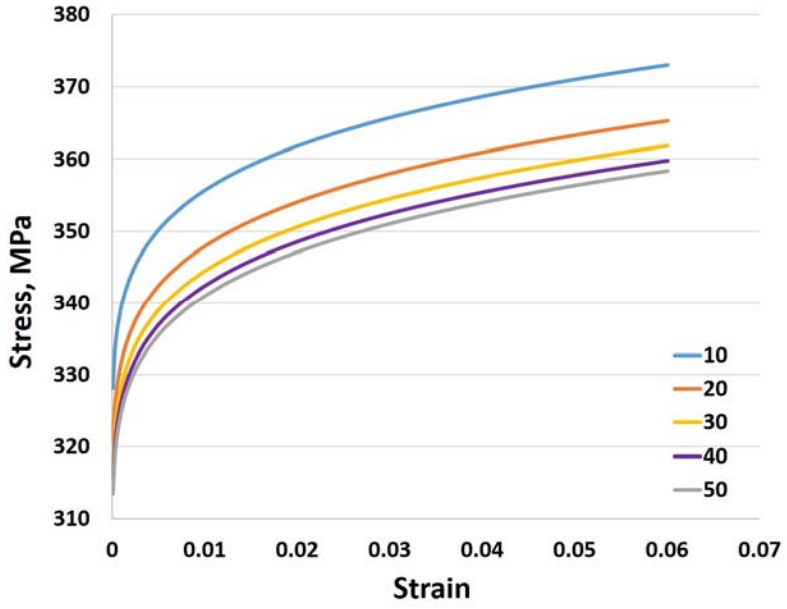

Figure 4.10 Calculated plastic stress-strain curves of Al6061 alloy with different grain size

Because grain size has no influence on the elastic modulus of Al6061 alloy, we used 68.02 GPa as the Young's modulus and 0.33 as the Poisson's ratio [4].

3.3 Material properties of pure Al and pure Mg

For the modeling of hierarchical composites, we used pure Mg as the outer matrix, pure Al as the inner matrix shell and Al_2O_3 as the particle. Ludwik's Equation was used to calculate the plastic properties of pure Mg:

$$\sigma = \sigma_0 + \frac{k'}{\sqrt{d}} + k\varepsilon_p^n \qquad (4.4)$$

where σ_0 is the yield stress of pure Mg, which is 35 MPa. k' is the Hall-Petch coefficient (280MPa $\mu m^{\frac{1}{2}}$ [9]). In order to compare with the real experimental results, d is chosen to be 8 μm. k and n are 210 and 0.39 respectively [10]. Fig 4.11 gives the calculated plastic stress-strain curve of pure

Mg and Fig 4.12 shows the stress-strain curve of pure Al, which is extracted from Dobes et al. [11].

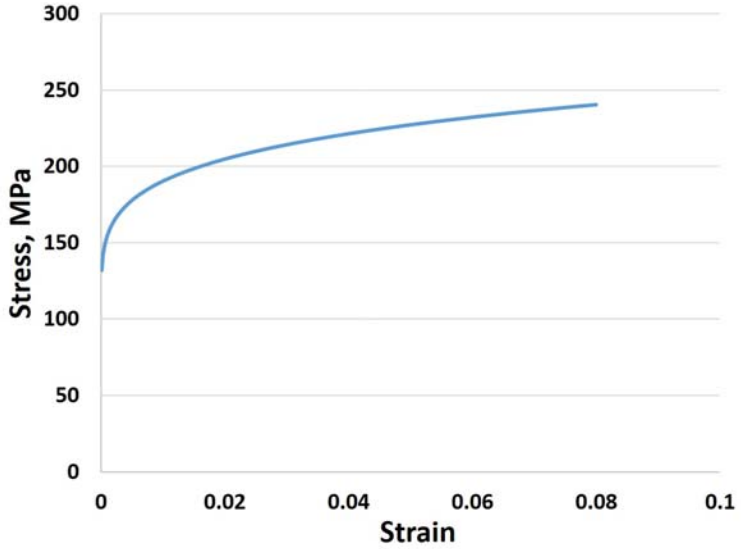

Figure 4.11 Calculated plastic stress-strain curve of pure Mg

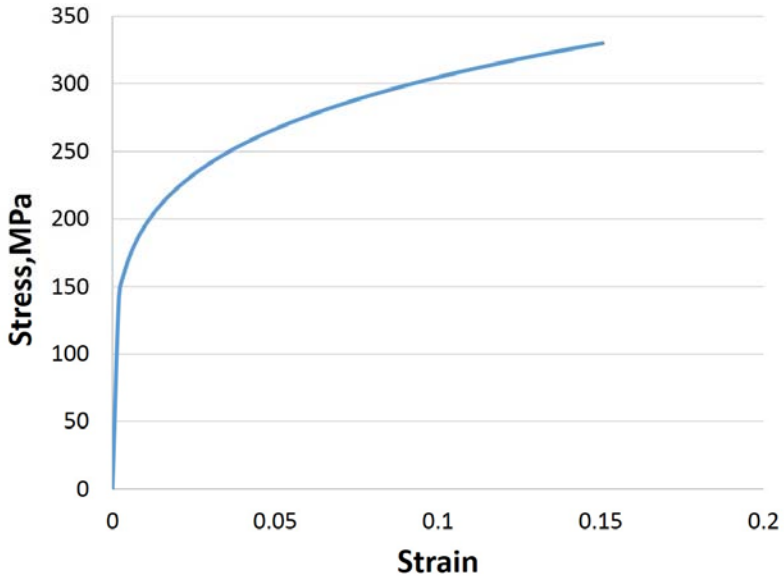

Figure 4.12 Stress-strain curve of pure Al

4. Boundary Conditions and Interface Conditions

In analyzing the mechanical behavior of the PRMMC models, several types of boundary conditions can be prescribed on RVE. In our study, we applied the displacement control as the loading method. Fig. 4.13 shows the displacement boundary conditions that were applied on the RVE model. Identical values of displacements were assigned on the two planes that perpendicular to Y direction, so the stresses were applied on the RVE models along Y direction.

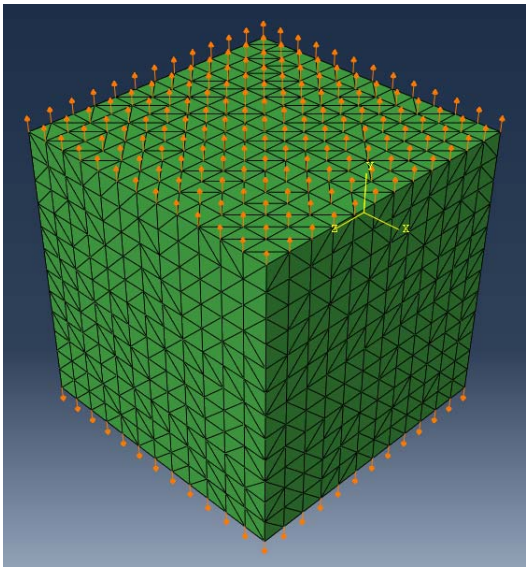

Figure 4.13 Boundary conditions applied on RVE model of PRMMC

One of the features in the current thesis is to alter the tie conditions between the interfaces of matrix and particles. Generally in previous studies, a complete tie boundary condition is applied on the interface, which means the outer surface of the particles are 100% tied with the inner hole surfaces of the matrix. However, in case of our study, in an effort to simulate the incoherency of the matrix-particle interfaces, we have applied 3 different types of tie boundary conditions on the RVE models, i.e., 50%, 75%, and 100% tied interface surfaces. The results of them are then

compared with each other. Fig 4.14 shows the examples of 50%, 75%, and 100% tied boundary conditions.

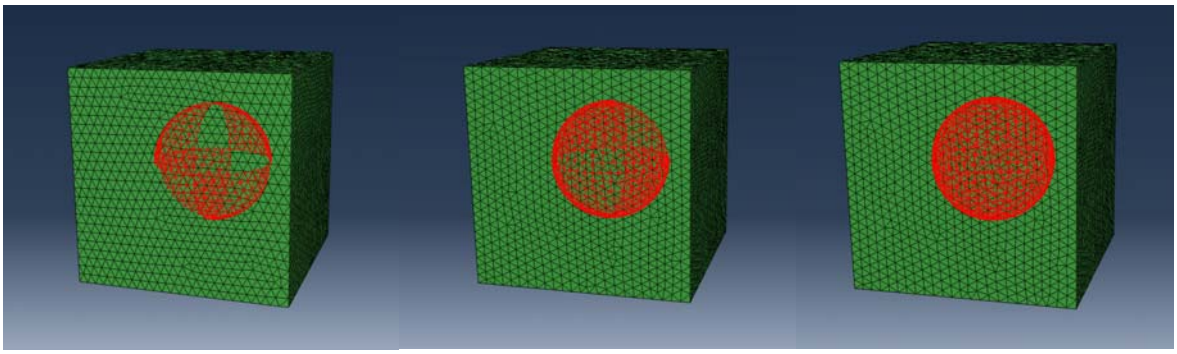

(a) (b) (c)

Figure 4.14 Examples of (a) 50%, (b) 75%, and (c) 100% tied boundary conditions

In addition, flat surface boundary conditions were also applied for realistic computations to represent a meso-scopic volume. As shown in Fig 4.15, by using an Abaqus option named "constraints", we controlled all the nodes that located on every single surfaces move by a same amount so that all the surfaces on the RVE model keep to be perfect flat surfaces all the time.

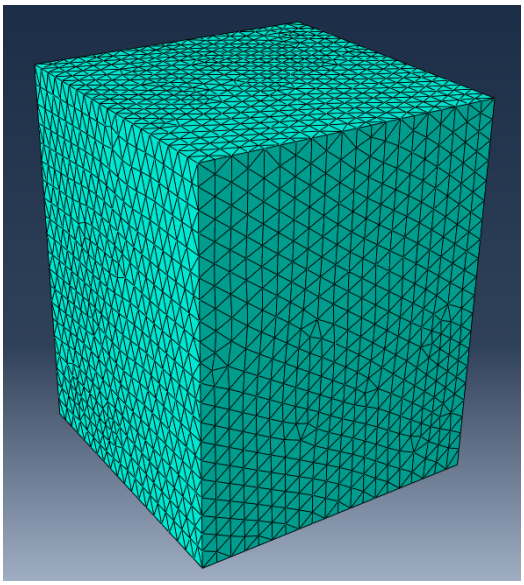

Figure 4.15 Example of RVE model that has flat surfaces after the simulation

5. Fracture of Ceramic Particulates

Proper estimation for the fracture of the ceramic particles is one of the most challenging roadblocks to obtain reliable results. A particle damage model was developed to simulate the fracture of ceramic particulates, we divided the computation into three steps. Step one determines the general stress-strain curve of the model, then we find the fracture points of the particles according to the particle ultimate strength of 1100 MPa. [12] The step two will start at the beginning of particle fractures. Unlike step one, we untie the particles with the matrix in step two so that the stresses on the particles decrease significantly. After observing the failure strain of the composite in step two, the overall stress-strain curve of the composite is obtained from step three.

Let's use composite with 27 regular distributed particles as a specific example. We assigned the strain of the composite as 0.18 in step one to get a general stress-strain curve without particles damage. Fig 4.16 shows the comparison between experimental and FEA results after step one.

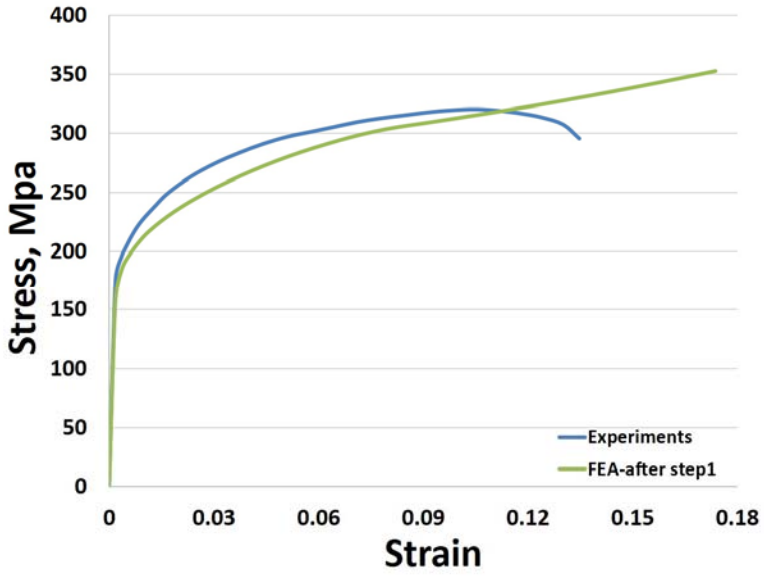

Figure 4.16 Comparison of experimental and FEA results after step one

As we can see in Fig 4.16, FEA result shows a similar stress-strain curve with the experimental result, but the stress didn't decrease as the experimental stress-strain curve. After the simulation of step one, the analysis of the stress condition on the particles were conducted to find the fracture point, in which the stress on every single particle reaches 1100 MPa. The stress condition of the whole composite was assigned as the beginning stress condition of step two. In order to figure out the failure strain of the composite, we set the strain of model in step two as 0.16, which is big enough to see a straight line in the stress-strain curve obtained in step two due to the fracture of matrix. Because the straight line is caused by the failure of the matrix, the strain of the beginning point of the straight line is the failure strain of the whole composite. The stress-strain curve obtained from step two is shown in Fig 4.17.

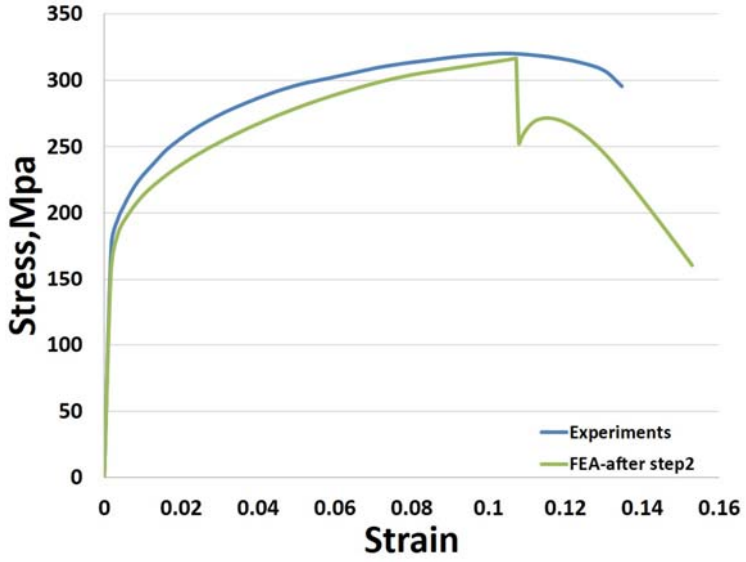

Figure 4.17 Comparison of experimental and FEA results after step two

The final step was to determine the actual failure stress so that the whole stress-strain curve can been obtained from our particle damage model. We did same simulation as step two and the only difference is the strain we assigned. We used the failure strain observed from step two as the strain of this simulation. Finally, the stress-strain curve of the whole composite was extracted from step three, which is compared with experimental stress-strain curve and is shown in Fig 4.18.

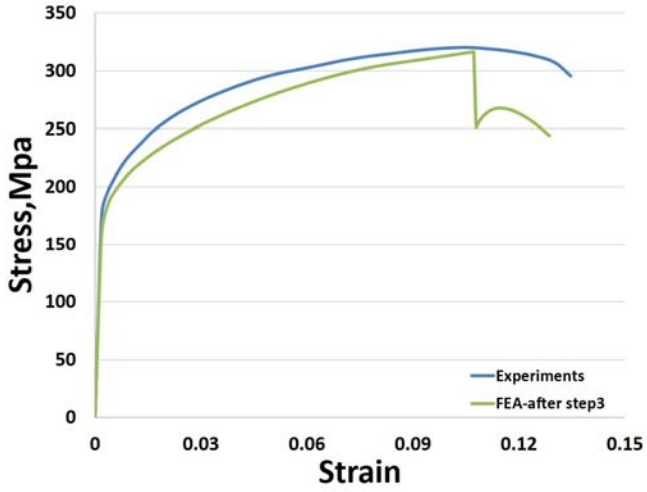

Figure 4.18 Comparison of experimental and FEA results after step three

Fig 4.19 shows the tensile stress distributions on the cross-section surfaces of composites after step1, step2 and step3.

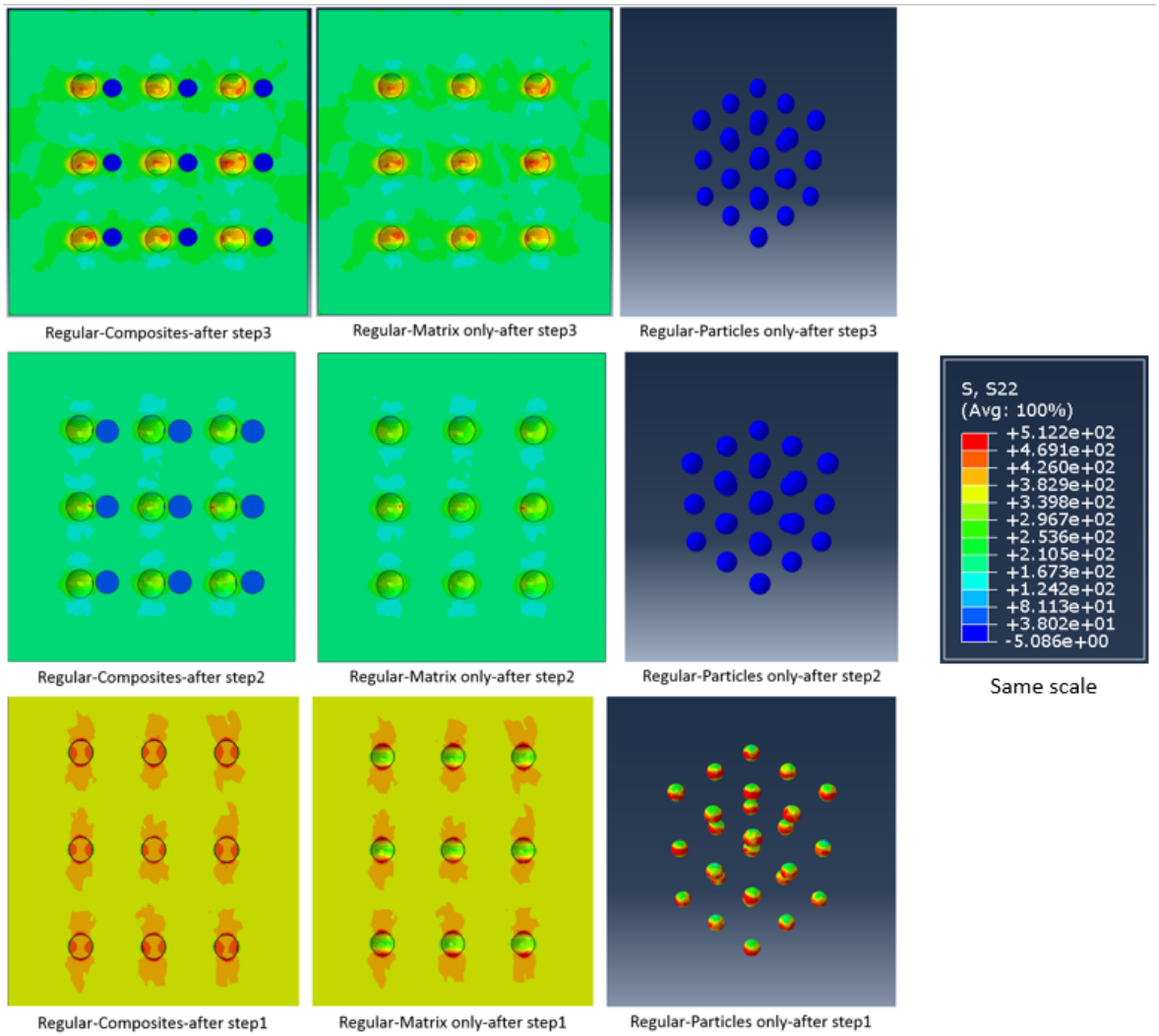

Figure 4.19 Contour plots of tensile stress distributions on the cross-section surfaces of composites after step1, step2 and step3

References

1. S. Balasivanandha Prabu, L. Karunamoorthy. Microstructure-based finite element analysis of failure prediction in particle-reinforced metal–matrix composite. Journal of materials processing technology 207 (2008) 53-62

2. A. Ayyar, G.A. Crawford, J.J. Williams, N. Chawla. Numerical simulation of the effect of particle spatial distribution and strength on tensile behavior of particle reinforced composites. Computational Materials Science 44 (2008) 496–506.

3. Yoshimasa Takahashi, Takahiro Shikama. Effect of additional magnesium on mechanical and high-cycle fatigue properties of 6061-T6 alloy. Materials Science & Engineering A 641 (2015) 263-273

4. Khalid Al-Dheylan, Syed Hafeez, Tensile failure micromechanisms of 6061 Aluminum reinforced with submicron Al_2O_3 metal-matrix composites. The Arabian Journal for Science and Engineering, Volume 31, Number 2C.

5. C.A. Lewis, P.J. Withers. Weibull modelling of particle cracking in metal matrix composites. Acta Metallurgica & Materialia. Volume 43, Issue 10, October 1995, Pages 3685-3699.

6. Jacob Lubliner. Platicity Theory. 2005

7. Adnan N. Abood, Ali H. Saleh & Zainab W. Abdullah, Effect of Heat Treatment on Strain Life of Aluminum Alloy AA 6061, Journal of Materials Science Research; Vol. 2, No. 2; 2013

8. Woei-Shyan Lee, Zih-Chao Tang, Relationship between mechanical properties and microstructural response of 6061-T6 aluminum alloy impacted at elevated temperatures, Materials and Design 58 (2014) 116–124

9. Meisam K. Habibi, Shailendra P. Joshi, Manoj Gupta. Hierarchical magnesium nano-composites for enhanced mechanical response. Acta Materialia 58 (2010) 6104–6114

10. G.D. Fan, M.Y. Zheng, X.S.Hu, K. Wu, W.M. Gan, H.G. Brokmeier. Internal friction and microplastic deformation behavior of pure magnesium processed by equal channel angular pressing. Materials Science & Engineering A 561 (2013) 100–108.

11. FerdinandDobes, PetrDymacek. Estimation of the mechanical properties of aluminium and an aluminium composite after equal channel angular pressing by means of the small punch test. Materials Science & Engineering A 626 (2015) 313–321

12. J. Lorca, A. Martin, J. Ruiz, M. Elices. Particulate fracture during deformation of a spray formed Metal-Matrix composite. Metall. Trans. A 24 (1993) 1575-1588

Chapter 5. Results and Discussions

In this chapter, the computational results with various factors will be analyzed and discussed. The parameters that we have explored in this thesis include reinforcement volume fraction, matrix grain size, degrees of bonding, particle size and reinforcement distributions. The tension stresses are put on Y directions of different RVE models and the focus of the analysis is primarily on young's modulus, yield stress, ultimate tensile stress and failure stress of different composite structures. In addition, the properties of hierarchical composites are also investigated. Computational results are also compared with previous experimental and theoretical results.

1. Theoretical results of Particle Reinforcement Metal Matrix Composites (PRMMC) models.

The enhanced strength and hardness observed in the particle reinforced metal matrix composites compared with pure Al or Al alloy is attributed to the presence of the particles, which activated multiple strengthening mechanisms acting in tandem [1]. These include, but may not be limited to: (a) Orowan strengthening [2]; (b) grain size strengthening [3]; (c) effective load transfer from the matrix to the reinforcement [4]; (d) generation of geometrically necessary dislocations (GNDs) to accommodate the coefficient of thermal expansion (CTE) and elastic modulus mismatch between the matrix and the particles [5].

Due to the limitation of computational modeling, only load transfer effect is applicable to our PRMMC models. As we discussed in chapter 2, the load transfer from the soft and compliant 6061 Al alloy matrix to the stiff and hard Al_2O_3 particles under an applied external load, contributes to the strengthening of the matrix material. Because equiaxed particles are used in our

models, equation(1) should be used to calculate the contribution in yield stress due to load transfer in particlate-reinforced composites:

$$\Delta\sigma_{LT} = \frac{1}{2} v_p \sigma_m \qquad (5.1)$$

where v_p (~0.1-0.3) is the volume fraction of the particles. σ_m (=131.8797MPa [6]) is the yield stress of the unreinforced 6061Al alloy matrix.

Thus, the prediction results of load transfer effect on the yield stress of our models can be summarized in Fig 5.1:

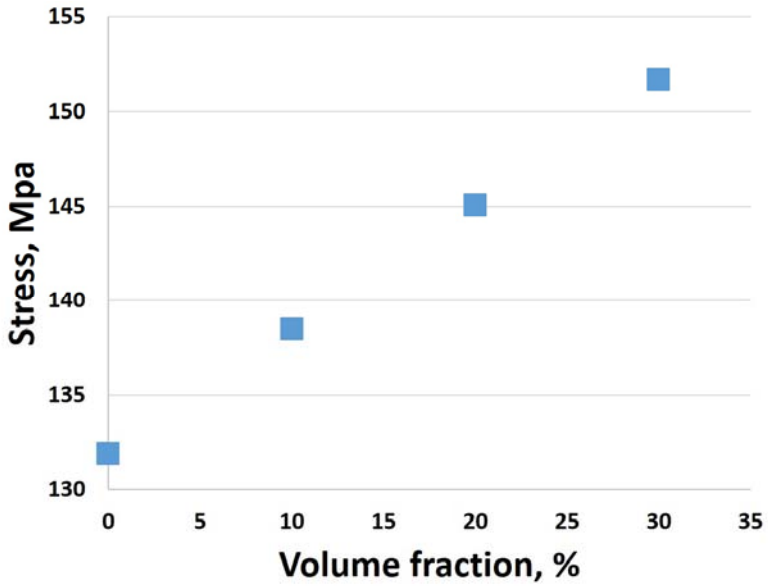

Figure 5.1 Calculation results of load transfer effect on the yield stress of PRMMC

2. Issues and limitations of our approach

Before conducting the parameterization study, the prerequisite step is to understand the issues and limitations of our FEA approach. In order to do that, we compare the results from our RVE models with the real experiments conducted by A.J. Knowles et al [7] and H.R. Ezatpour [8].

First set of simulations were applied to compare with A.J. Knowles's experiments that analyzed the mechanical properties of SiC particles reinforced metal matrix composites. The paper clearly showed the stress-strain curves of 6061 Al alloy and 10%wt SiC particles reinforced composite. We inputted the stress-strain curve of 6061 Al with proper young's modulus and poisson's ratio as the material properties of the matrix in our model. Also, material properties of SiC particles were same with the paper. Three models with both 10% volume fraction but different particle distributions (regular, random and clustered) were created to compare with the real experiments' model. Fig 5.2 shows the stress-strain curves obtained from the three FEA simulations and the real experiment. Fig 5.3 illustrates the tensile stress profiles on the cross-section surfaces of composites with three different particle distributions. We used same stress scale to show the stress distributions on the particles, matrix and composites.

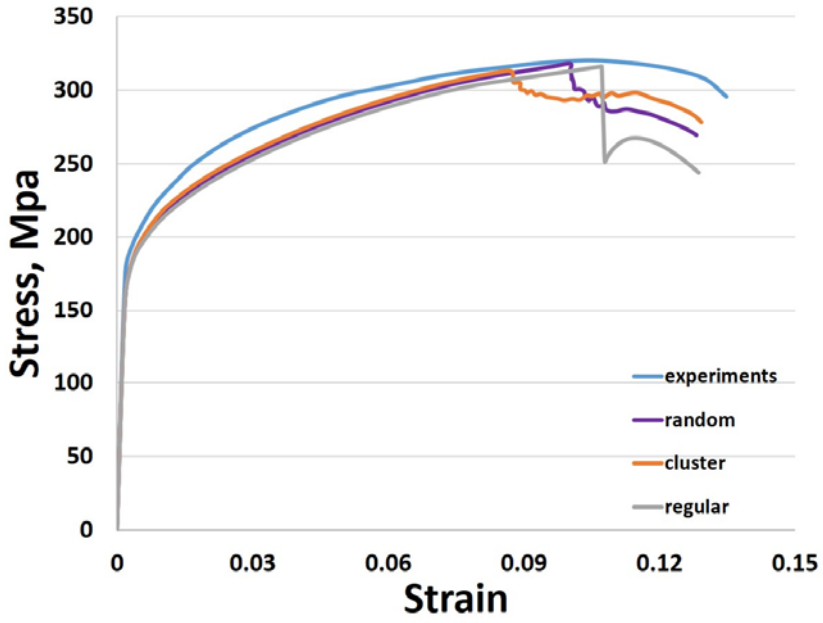

Figure 5.2 Comparison between three FEA results and experimental results conducted by A.J. Knowles et al [7]

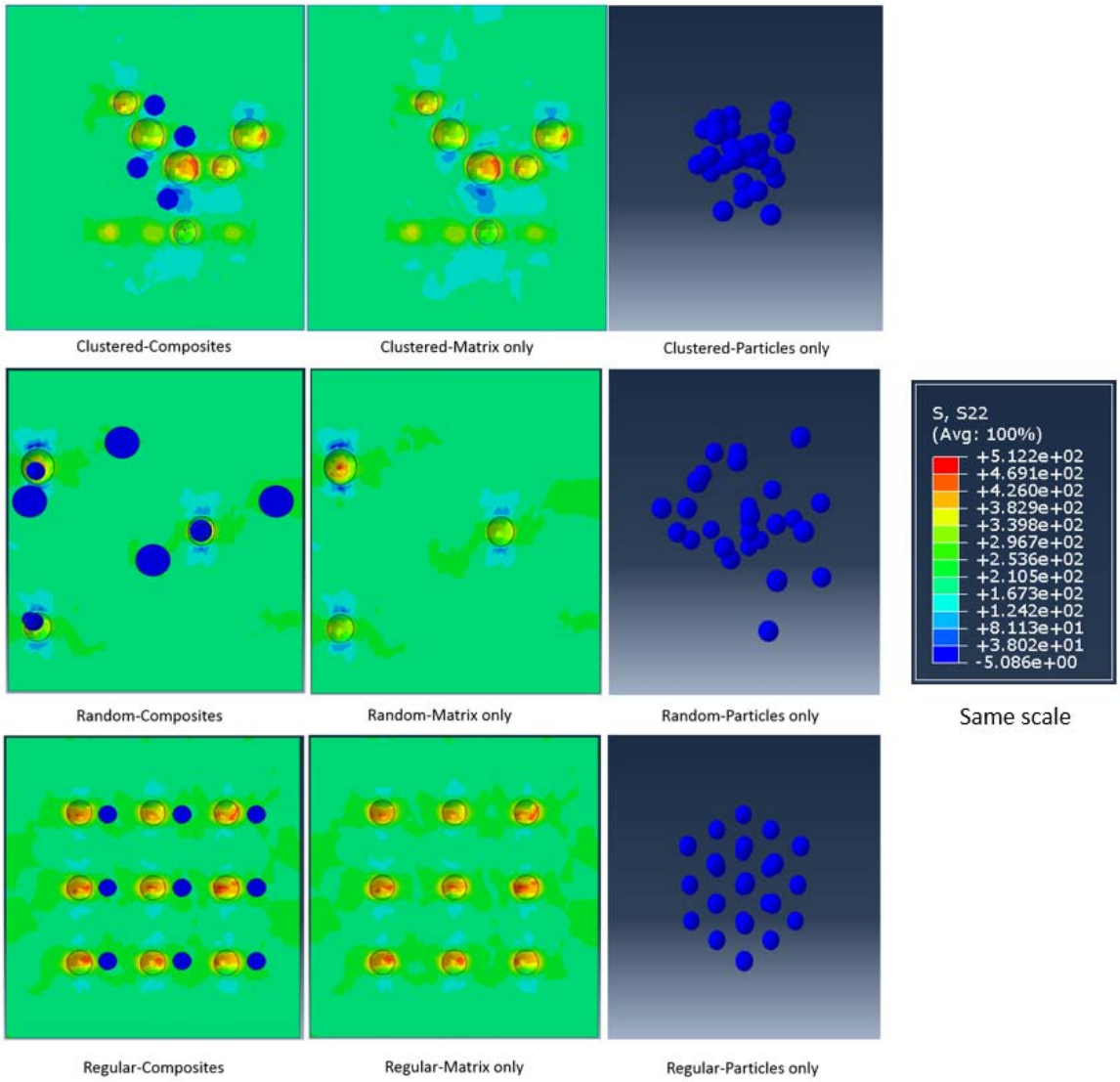

Figure 5.3 Contour plots of tensile stress distributions on the cross-section surfaces of composites with different particle distributions of Al6061-SiC model at the end of the simulations

From Fig 5.2, it is seen that all the three models have very similar young's modulus and yield stress. Before particles fracture, composites with cluster particle distribution has the highest stress among the three composites. But the point of first particle fracture was also observed in the clustered distribution model. The model with random particle distribution has the highest ultimate

tensile stress, which is closest to the experimental result. However, the three FEA results have considerable differences of strain to failure and failure stress with the experimental result, which is due to the limitation of our particle damage model to predict the strain to failure and failure stress of the composites.

H.R Ezatpour, M. Parizi and S. A. Sajjadi studied the mechanical properties of Al_2O_3 particles reinforced pure Al matrix composites in the extruded state. We inputted the stress-strain curve of pure Al in extruded state as the material properties of the matrix in our model. Three models with both 5% volume fraction but different particle distributions (regular, random and clustered) were created to compare with the real experiments' model. Fig 5.4 shows the stress-strain curves obtained from the three FEA simulations and the real experiment. Fig 5.5 illustrates the tensile stress profiles on the cross-section surfaces of composites with three different particle distributions.

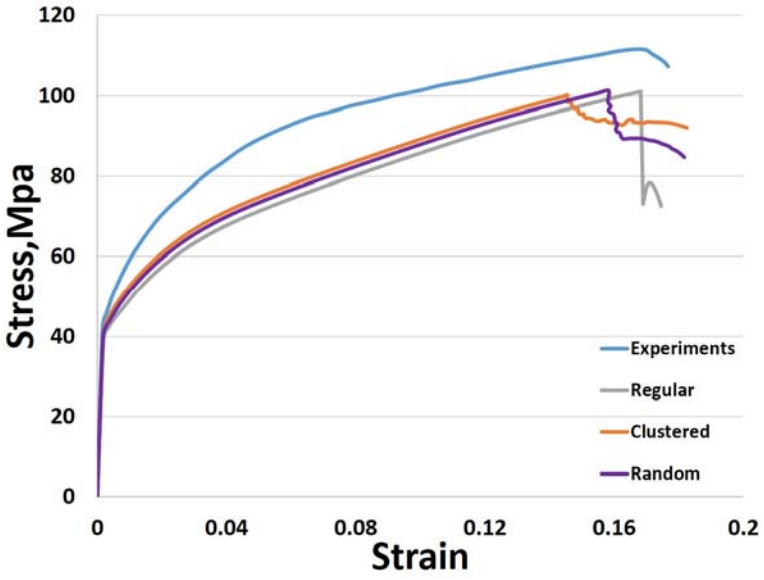

Figure 5.4 Comparison between three FEA results and experimental results conducted by H.R. Ezatpour [8]

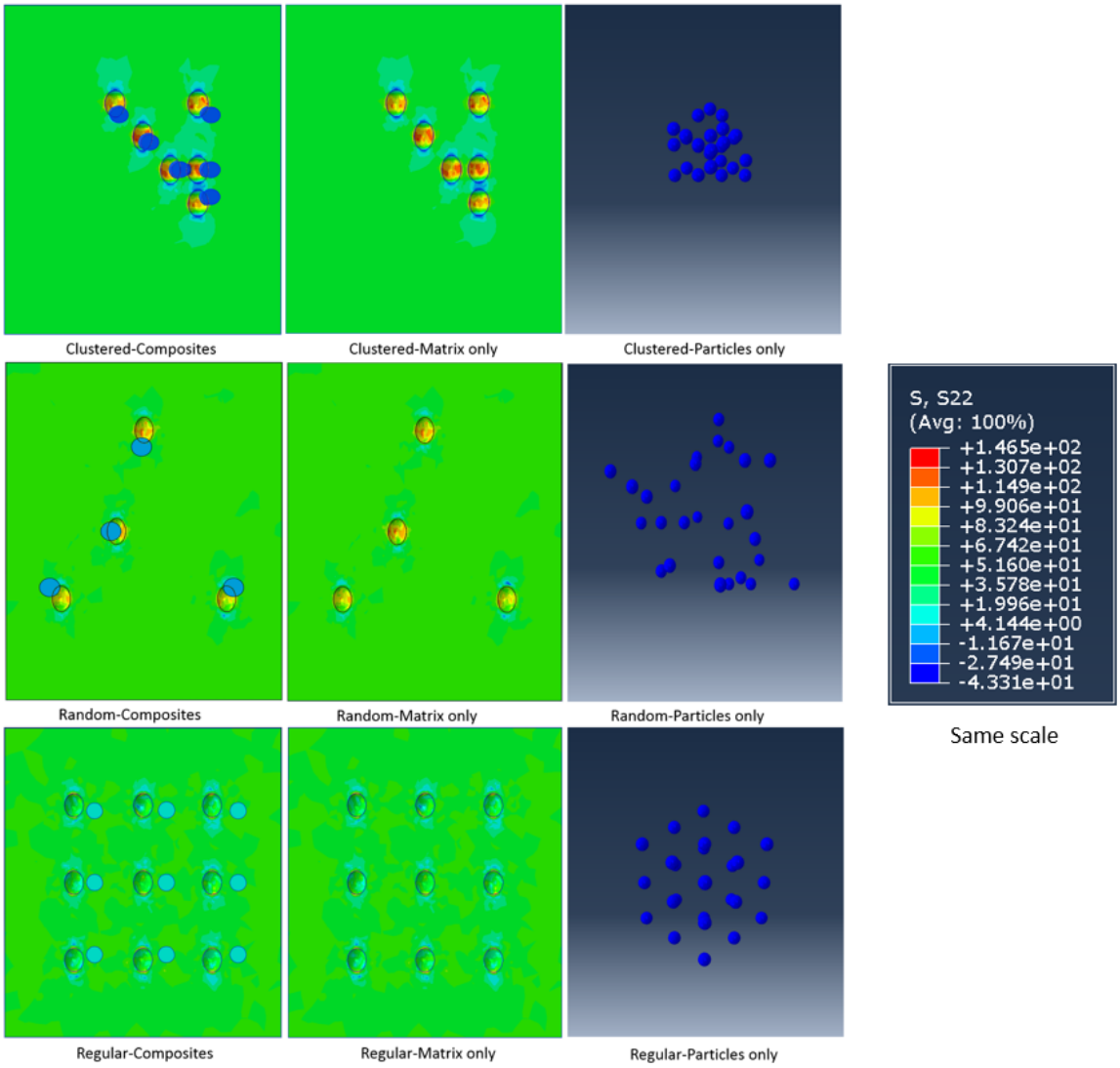

Figure 5.5 Contour plots of tensile stress distributions on the cross-section surfaces of composites with different particle distributions of pure Al-Al_2O_3 model at the end of the simulations

Due to the limitations of initial materials resources, we are unable to include the extrusion effect into the materials properties that we used in the simulations, so there is in general a clear difference between FEA and the experimental results.

3. Computational results of RVE models of PRMMC

Because particles are most likely to randomly distribute in the matrix in the real experiments, we are using models with 27 random distributed particles in this sub-section to analyze the influence of particle volume fractions, particle size, particle distribution and matrix grain size on the mechanical behavior of Al_2O_3 reinforced 6061 Al matrix composites. In addition, results of models with three types of boundary conditions are compared with each other to investigate the effect of degrees of bonding on the mechanical properties of Al_2O_3 reinforced 6061 Al matrix composites.

3.1 Impacts of particle volume fractions

Firstly, in order to investigate the effect of particle volume fraction, models with particle volume fractions of 10%, 20% and 30% were created. All the models have 27 random distributed particles inside the matrix. Fig. 5.6 shows different stress-strain curves of whole composites with different volume fractions. Fig 5.7 gives the values that extracted from Fig. 5.6 to show the variation of young's modulus, yield stress and ultimate tensile stress with different volume fractions. Stresses were applied on the Y directions of all the models. Fig 5.8 and Fig 5.9 show the stress distributions on the cross-section surfaces of composites with different volume fractions when the stress of the composites reaches ultimate tensile stress and yield stress, respectively.

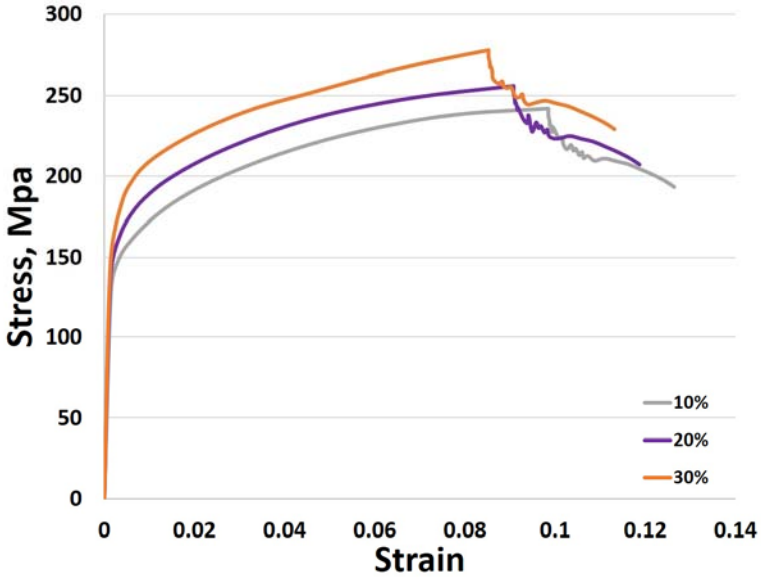

Figure 5.6 Plots showing the stress-strain relationships of RVE models with 10%, 20% and 30% volume fractions

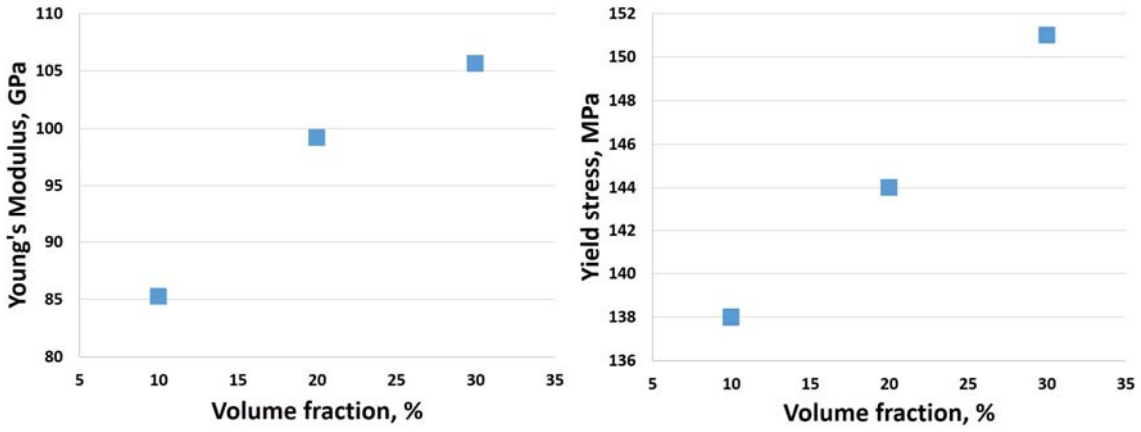

(a) (b)

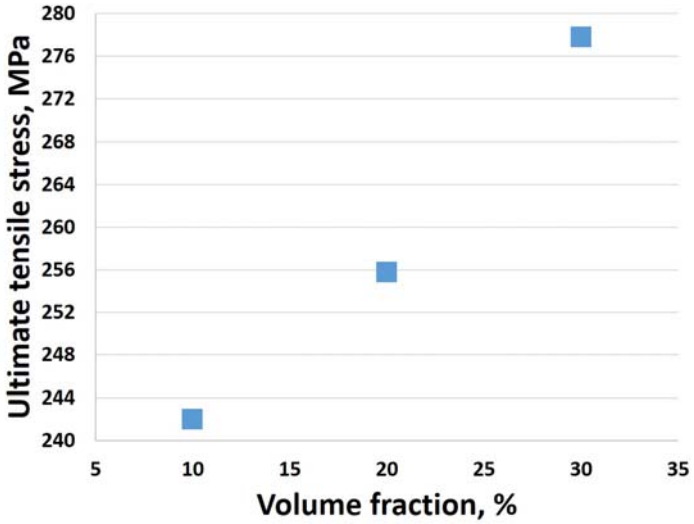

(c)

Figure. 5.7 Variation of (a) Young's modulus, (b) Yield stress, (c) Ultimate tensile stress with different particle volume fractions

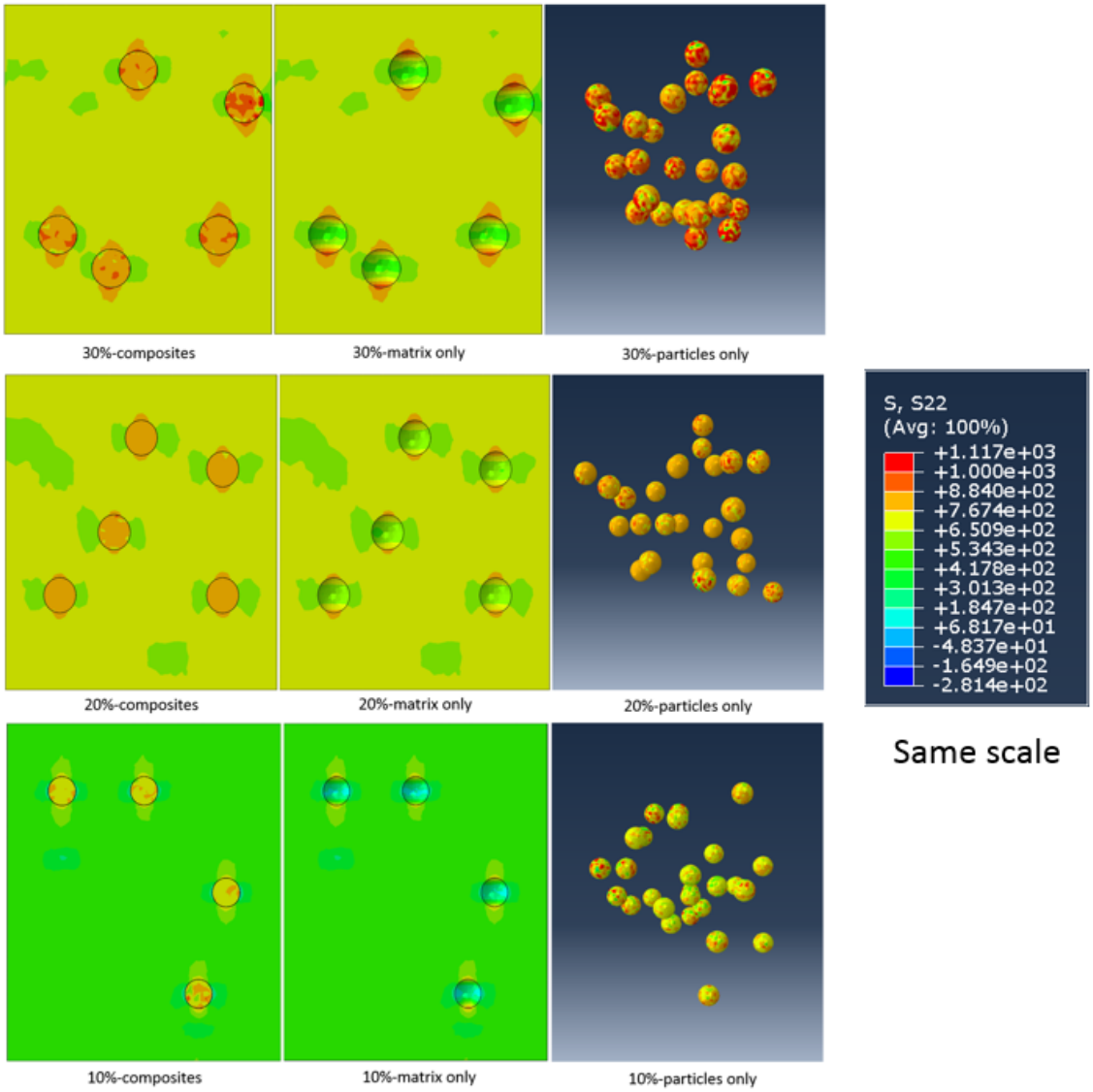

Figure 5.8 Y direction stress distributions on the cross-section surfaces of composites with different volume fractions when the stress of the composites reaches ultimate tensile stress.

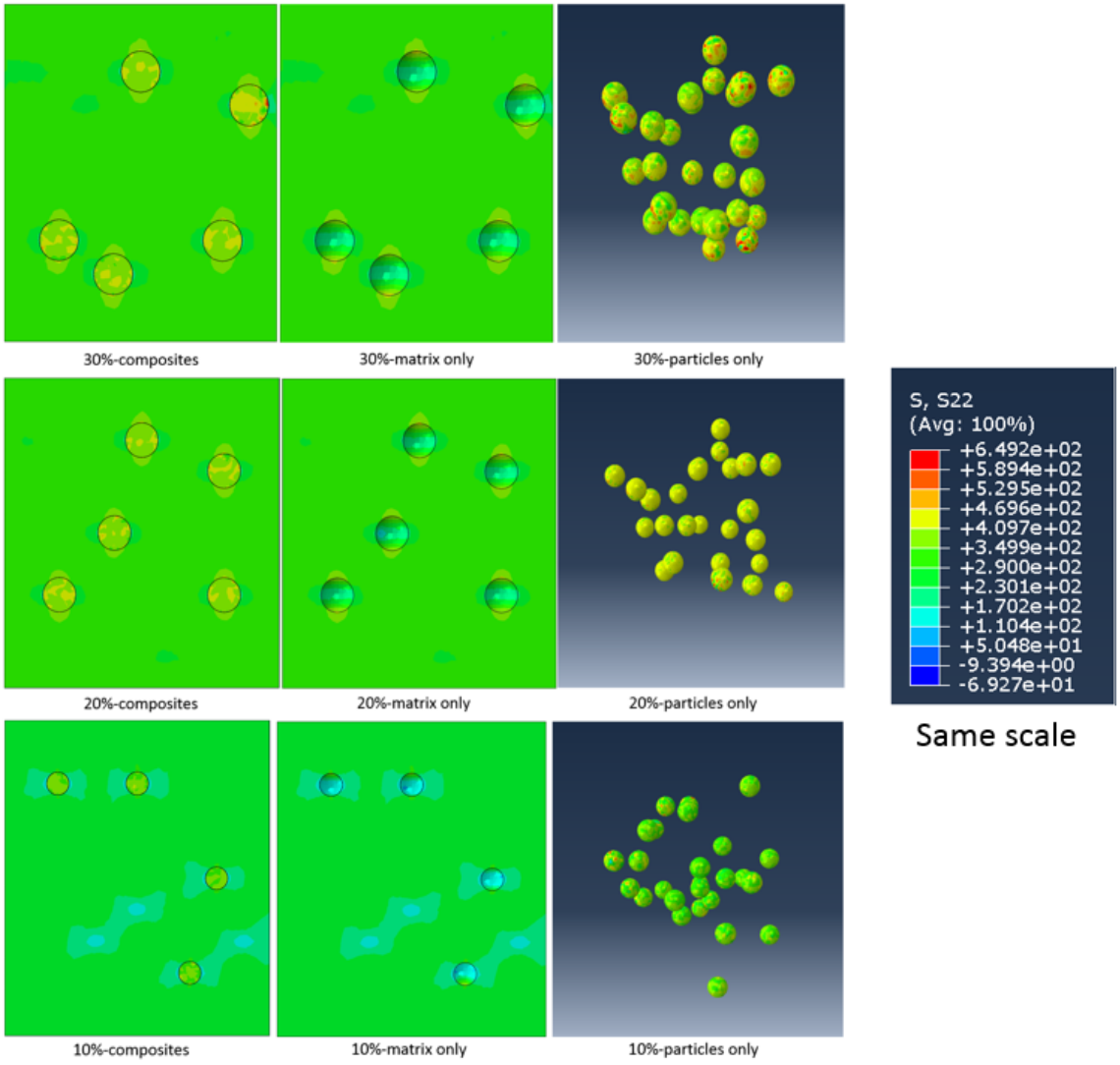

Figure 5.9 Y direction stress distributions on the cross-section surfaces of composites with different volume fractions when the stress of the composites reaches yield stress.

From Fig 5.7, it is possible to conclude that: the values of yield stress (0.2% proof strength) increased with increasing volume fraction of particulate, but the rate of increase in the stress decreased with the increasing volume fraction. There is also an increase in UTS values when volume fraction is increasing. Different from yield stress, the rate of increase in the UTS increased

with the increasing volume fraction. Increase in strength is possibly due to the load transfer between the metallic matrix and the reinforcement.

In addition, the results of young's modulus showed similar trends with the yield stress. Higher value of young's modulus is clear indication of the fact that the presences of particulates in the matrix have improved the overall young's modulus of the composites. This is true because aluminum is a soft material and the reinforced Al_2O_3 particles being hard, contributes positively to the young's modulus of the composites, so the increase of young's modulus of composites could be attributed to the relatively high young's modulus of Al_2O_3 itself.

However, the composite materials with higher volume fractions exhibited lower elongation than that of lower volume fractions. It is obvious that plastic deformation of the mixed soft Al matrix and the ceramic reinforcement is more difficult than the base Al itself. As a result, the ductility of the higher volume fraction composites drops down when compared to that of lower volume fraction and unreinforced material.

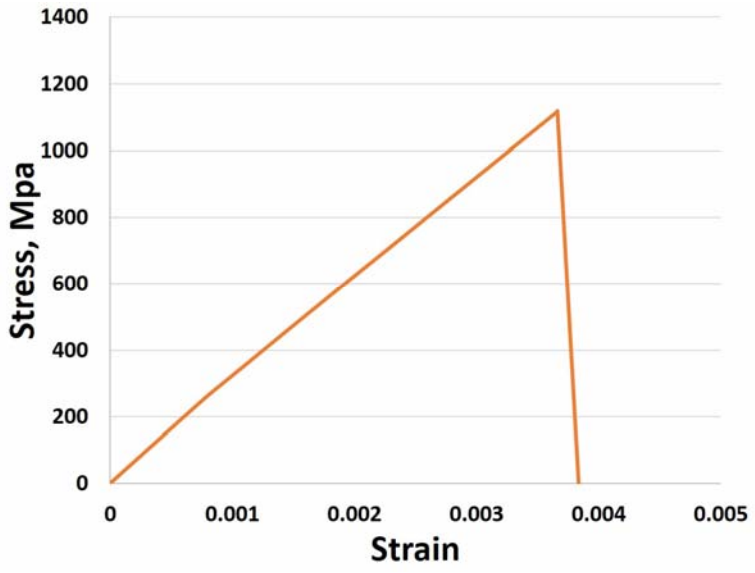

Figure. 5.10 Stress-strain relationship of ceramic particles during the whole simulation

Fig. 5.10 shows the stress strain curve of the ceramic particles. The fracture of ceramic particles take place on the very end of step one, where the stress of Al_2O_3 reaches the ultimate point. Thus, the stress of the ceramic particles increased linearly before the fracture and directly decreased to zero after the fracture. Once the particles fracture, they will influence the average stress and strain values of the composites, making the values decrease drastically, so the three stress-strain curves in Fig 5.6 all have an obvious decrease part after the particles' fracture.

3.2 Impacts of particle size

In order to figure out the effect of the particle size, three different composite structures with same particle volume fraction but different radius of particle reinforcements were created. The model with smallest particle radius, which is 0.96mm, has 27 regular particles inside the matrix. In order to have same volume fraction with the first one, model with particle radius of 1.44mm owns eight particles inside the matrix. The third one has the same volume fraction with the others but a biggest particle radius, which is 2.88mm and with only one particle inside the matrix. All the models have 10% volume fraction. Fig 5.11 gives the tension stress-strain curves obtained from the three RVE models above.

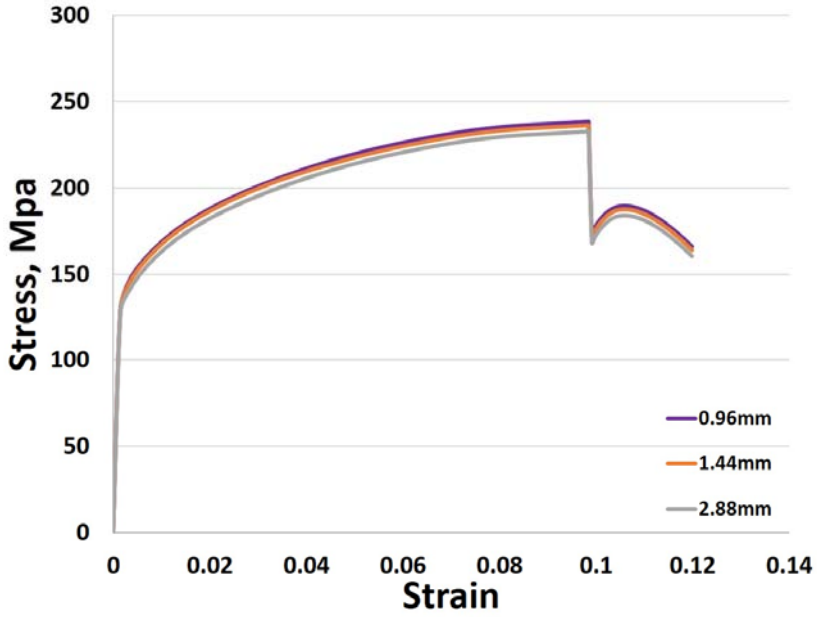

Figure 5.11 Plots showing the stress-strain relationships of RVE models with different particle sizes

Fig 5.12 gives the variation of young's modulus, yield stress and ultimate tensile stress with different particle sizes. Fig 5.13 and Fig 5.14 show the stress distributions on the cross-section surfaces of composites with different particle sizes when the stress of the composites reaches ultimate tensile stress and yield stress, respectively.

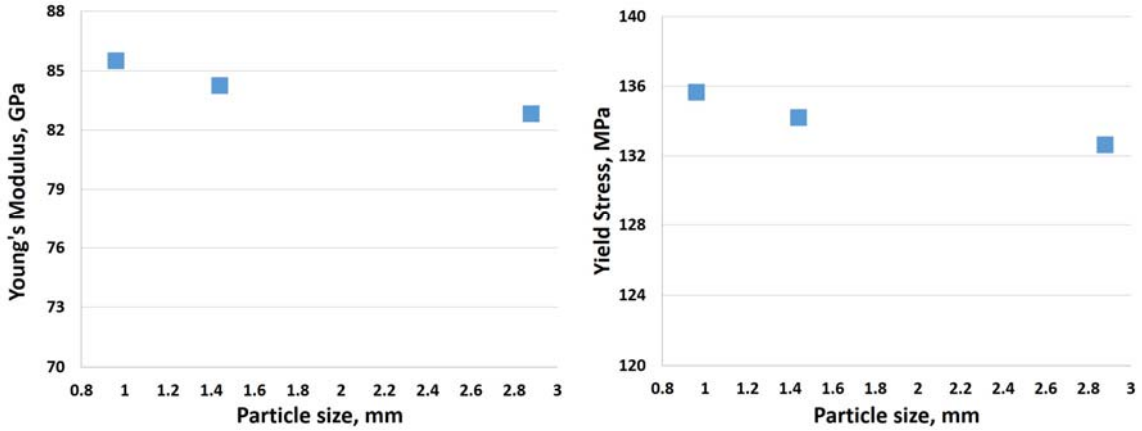

(a) (b)

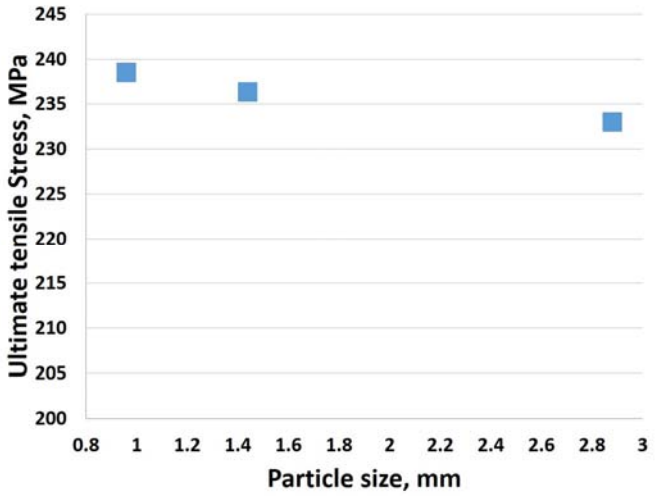

(c)

Figures 5.12 Variation of specific (a) Young's modulus, (b) Yield stress, (c) Ultimate tensile stress with different particle sizes

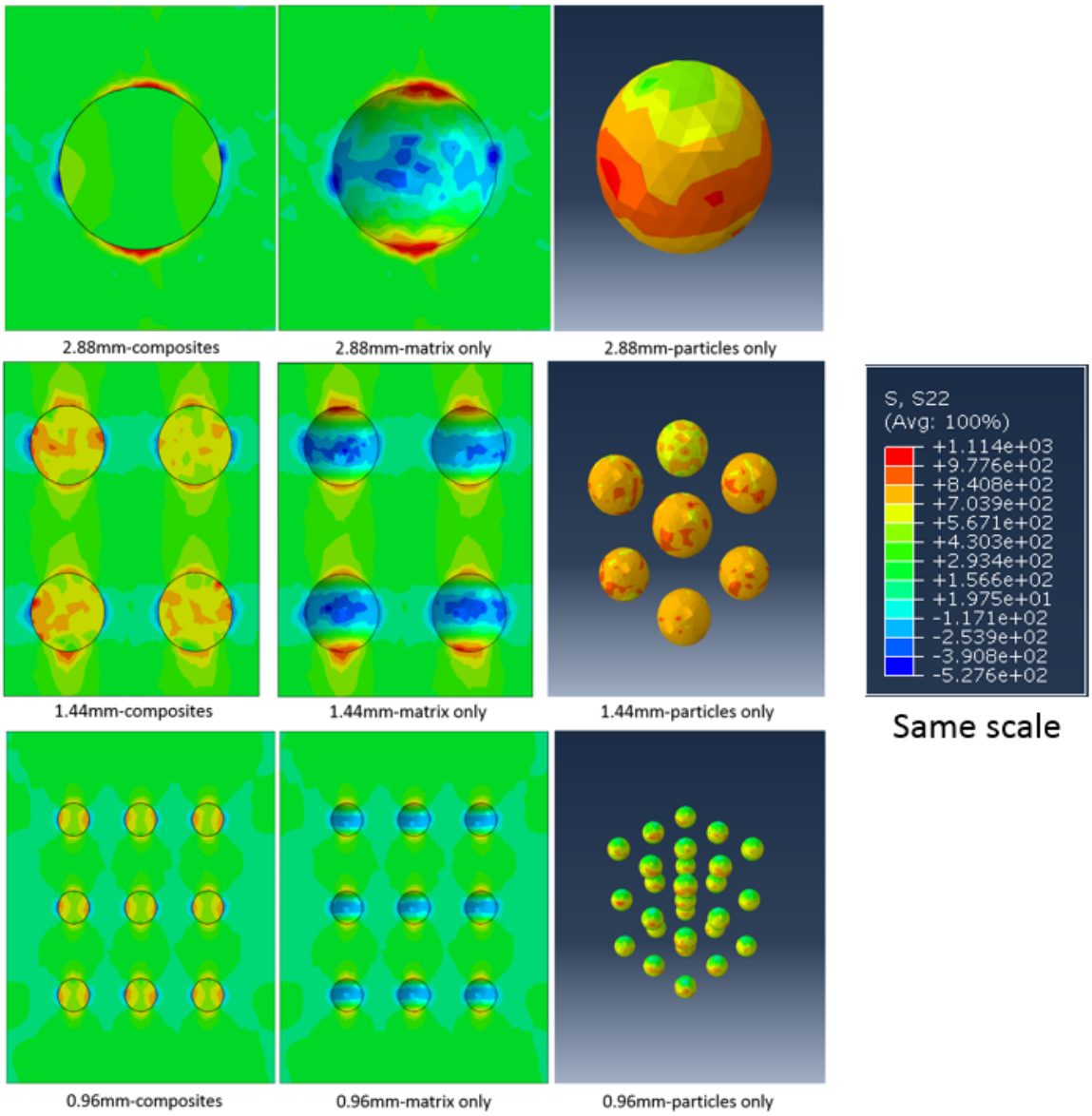

Figure 5.13 Y direction stress distributions on the cross-section surfaces of composites with different particle sizes when the stress of the composites reaches ultimate tensile stress.

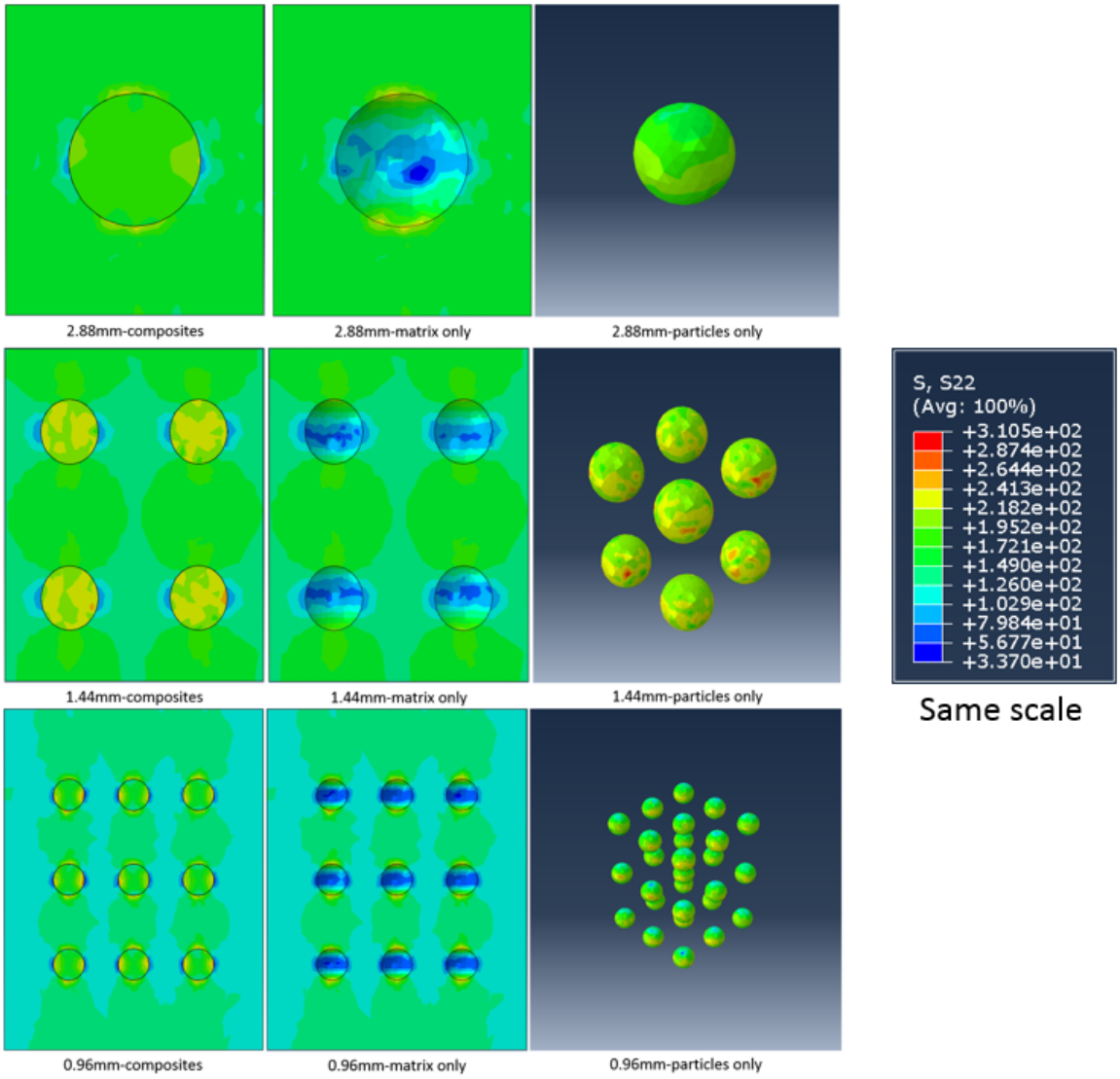

Figure 5.14 Y direction stress distributions on the cross-section surfaces of composites with different particle sizes when the stress of the composites reaches yield stress.

Figure 5.11 and Figure 5.12 show that particle size has very limited effect on the young's modulus and yield stress of composites. Although the values of young's modulus and yield stress show a decrease trend with increasing particle size, all the three models have very close values of young's modulus and yield stress. Compared with young's modulus and yield stress, stronger increase in UTS can be obtained with decreasing particle size, owing to a greater number of

particles for the same volume fraction. At the same time, ductility is preserved. In general, RVE models with smaller particle size has relatively higher strength.

3.3 Impacts of particle distribution

As for the investigation of particle distribution, seven RVE models were generated with exactly same volume fraction and particle size. All the models have 27 particles inside the matrix and all the volume fractions are 10%. As shown in Fig 5.15, the distribution of (b) random and (c) clustered types were created to compare with the (a) regular one.

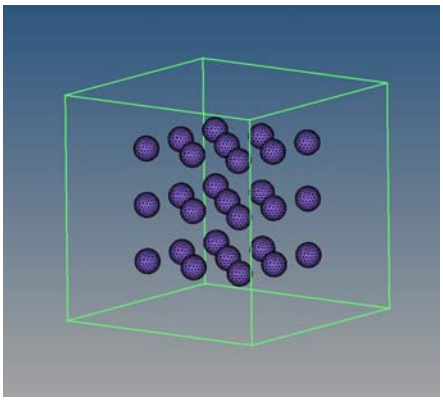

(a)

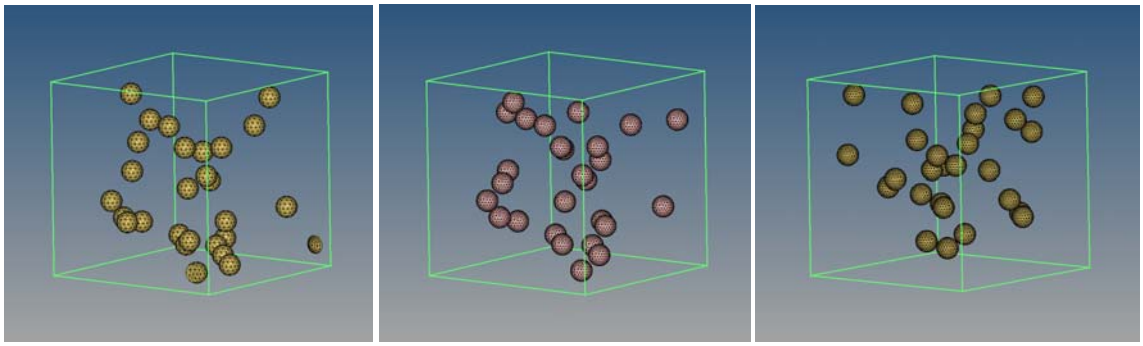

(b)

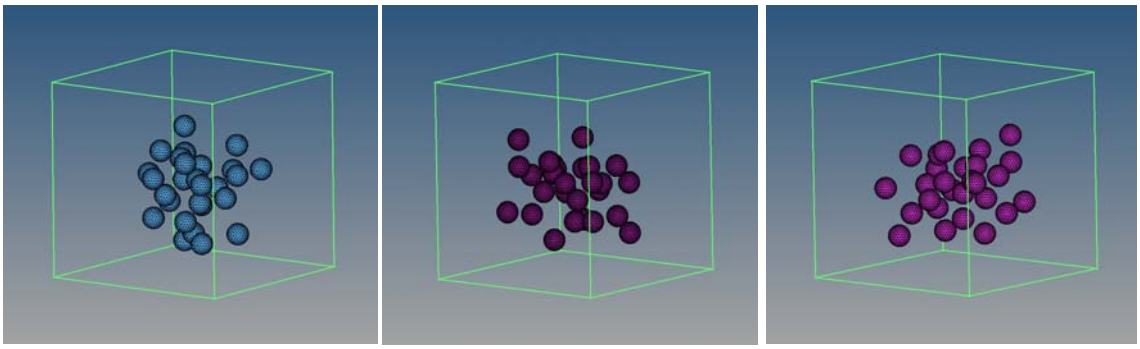

(c)

Figure 5.15 View of (a) regular, (b) random and (c) clustered particle distributions in the RVEs models

For random and clustered distributions, three stress–strain curves were computed for each distribution. As shown in Fig 5.16, both random and clustered show three very close stress-strain curves. In order to accurately represent the stress-strain relationships of random and clustered distribution, we calculated the average values of the three stress-strain curves of each distribution to compare with the stress-strain curve of regular distribution. The comparison results are plotted in Fig 5.17.

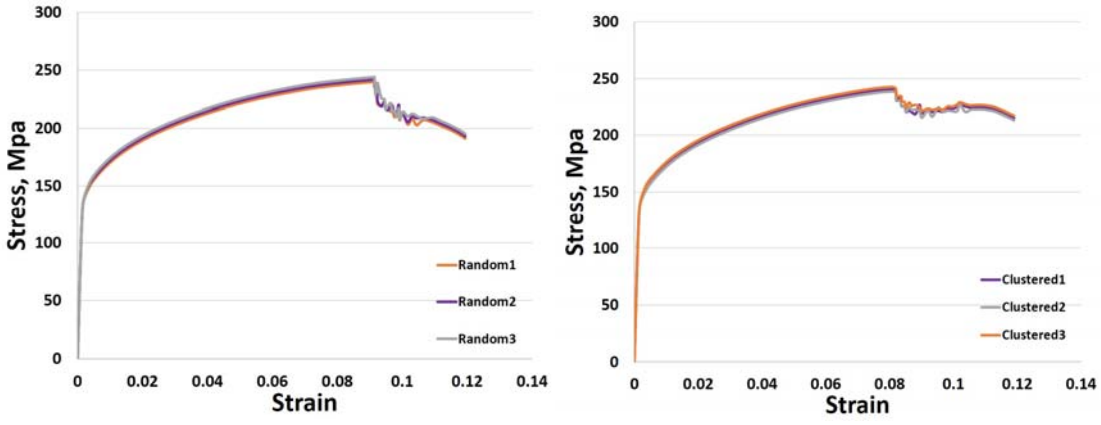

(a) (b)

Figure 5.16 Plots of stress-strain curves of random and cluster distributed PRMMCs

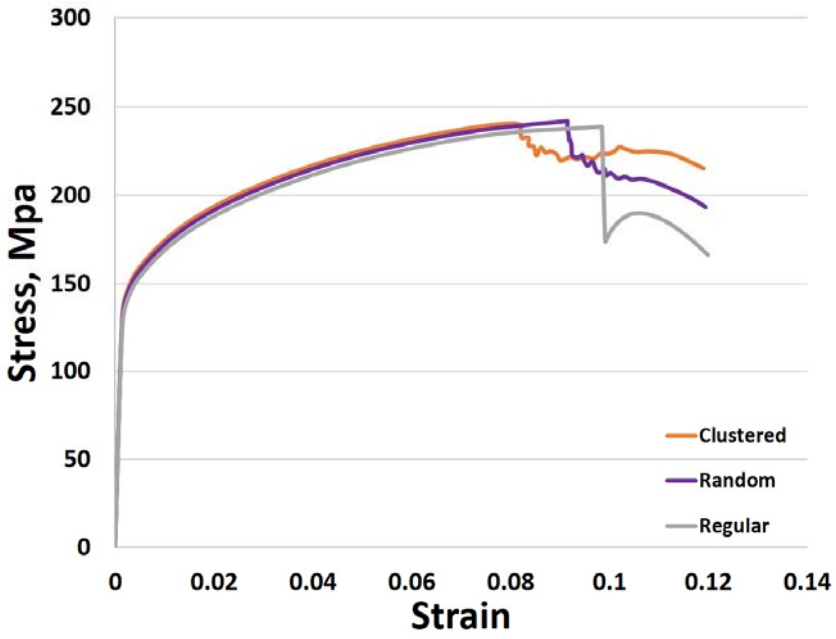

Figure 5.17 Comparison of stress-strain curves of models with three types of particle distributions

Similar as the conditions in particle size sub-section, particle distributions have weak influence on the young's modulus and yield stress of the composites and relatively stronger effect on the UTS. Before particles' fracture, the model with the clustered particle distribution (COV_d = 0.69) had the highest tensile stress followed by those of the random particle distribution (COV_d = 0.32) and the regular particle distribution (COV_d = 0.09). However, the point of first particle fracture was also observed in the clustered distribution model at a strain of 8%. Although higher cluster degree of particle distribution makes the composites have higher young's modulus and yield stress, models with random particle distribution have the highest ultimate tensile stress. Fig

5.18 and Fig 5.19 show the stress distributions on the cross-section surfaces of composites with different particle distributions when the stress of the composites reaches yield stress and ultimate tensile stress, respectively.

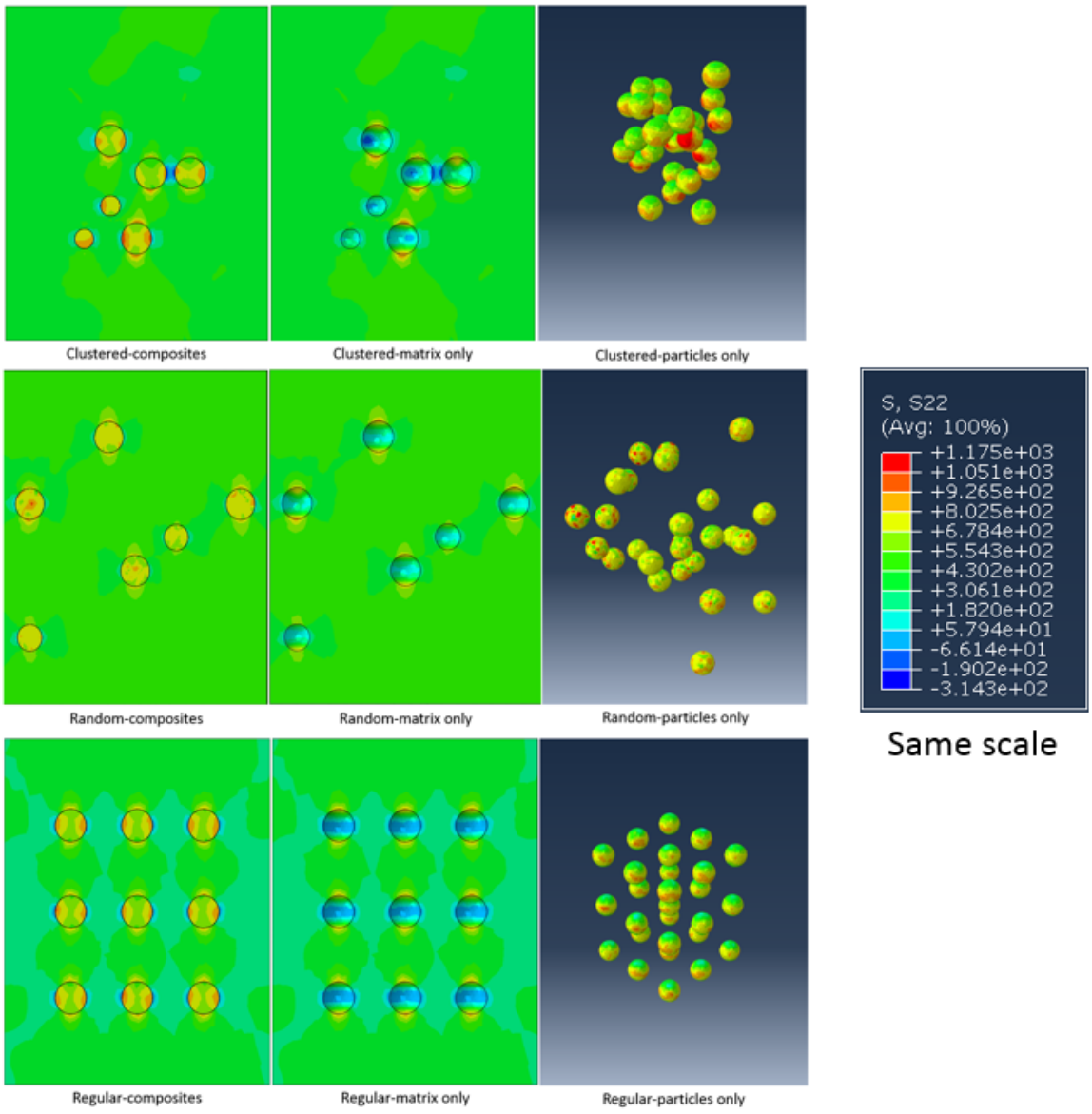

Figure 5.18 Y direction stress distributions on the cross-section surfaces of composites with different particle distributions when the stress of the composites reaches ultimate tensile stress.

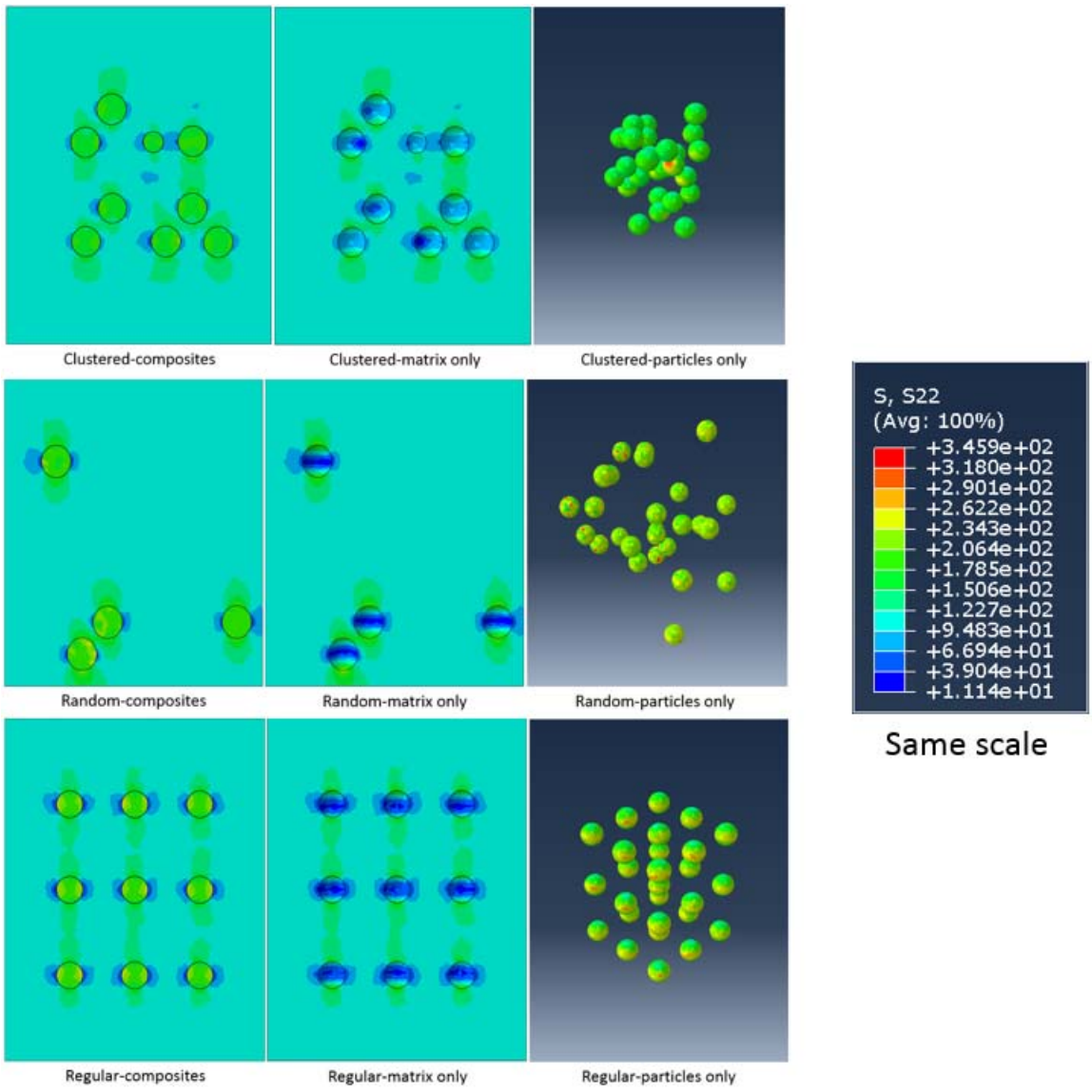

Figure 5.19 Y direction stress distributions on the cross-section surfaces of composites with different particle distributions when the stress of the composites reaches yield stress.

3.4 Impacts of matrix grain size

Influence of the matrix grain size was also investigated for the next set of the study. 6061 Al alloys with different grain sizes have different plastic stress, the stress-strain curves are shown

in Fig 4.7. Based on the data of Fig 4.7, five models with different matrix grain sizes (~10-50 μm) were created. All the models have only one particle inside the matrix and have the same volume fraction of 10%. Fig. 5.20 shows different stress-strain curves of whole composites and the specific yield stresses and ultimate tensile stress values are shown as a function of matrix grain size in Fig 5.21. Fig 5.22 and Fig 5.23 show the stress distributions on the cross-section surfaces of composites with different matrix grain sizes when the stress of the composites reaches yield stress and ultimate tensile stress, respectively.

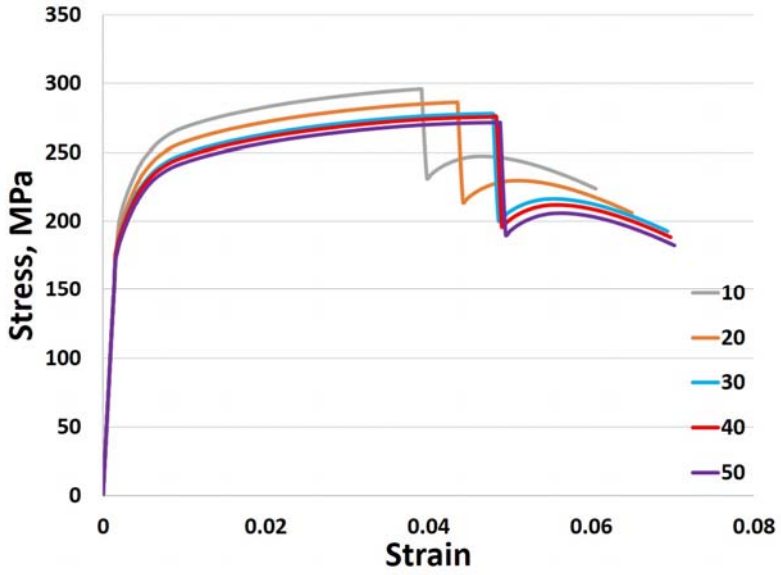

Figure 5.20 Plots showing the stress-strain relationships of RVE models with different matrix grain sizes

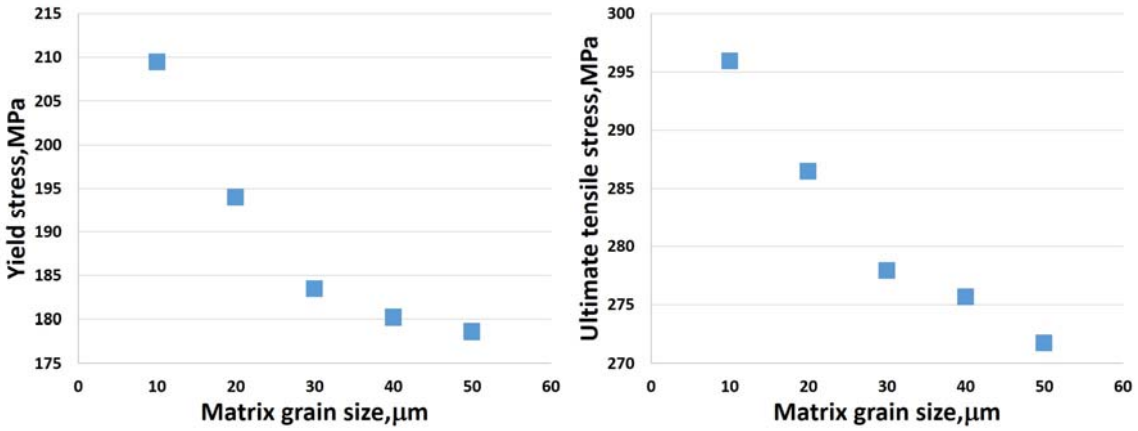

Figure 5.21 Variation of yield stress with different matrix grain size

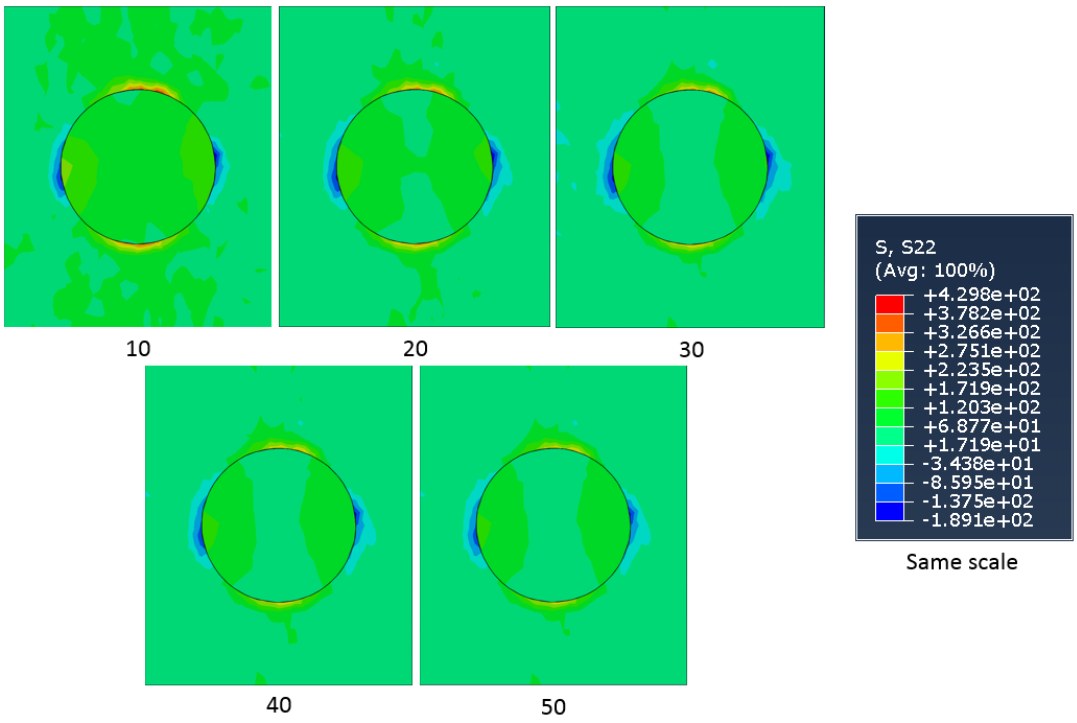

Figure 5.22 Y direction stress distributions on the cross-section surfaces of composites with different matrix grain size when the stress of the composites reaches yield stress.

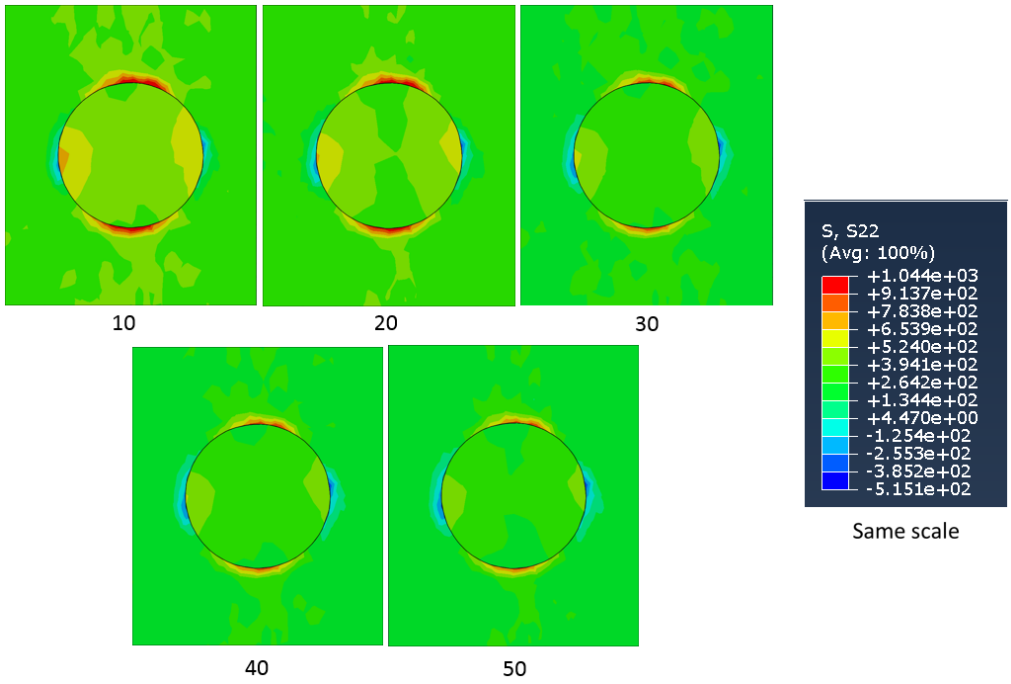

Figure 5.23 Y direction stress distributions on the cross-section surfaces of composites with different matrix grain size when the stress of the composites reaches ultimate tensile stress.

The results give us that the increase of matrix grain size decrease the yield stress and ultimate tensile stress. The effect decrease with increasing matrix grain size. The decrease effect is likely the result of the fact that yield stress of pure 6061Al alloy also decrease a lot if the grain size of increases. To be specific, RVE model with 10μm grain size has the biggest yield stress of 209.455MPa and ultimate tensile stress of 295.924MPa. An increase of grain size from 10μm to 30μm caused 25.985MPa decrease of yield stress and 18.02MPa of ultimate tensile stress. However, if the grain size continues to increase from 30μm to 50μm, there is only 4.88MPa decrease in yield stress and 6.15MPa in ultimate tensile stress.

Thus, reducing matrix grain size can significantly increase the yield tress when the size is under 30μm.

3.5 Influence of degrees of bonding

In the previous studies regarding RVE models of PRMMC, the surfaces of particles and matrix are always 100% tied together to each other during the whole simulation processes. But in real experiments, some gaps are also likely to exist in the matrix-particle interfaces due to the deformation of the particles and some cracks that occurs on the matrix holes' surfaces. Thus, it is worth to study the effect of degree of bonding on the tension behavior of RVE models.

Two more RVE models with 75% and 50% degrees of bonding were generated to compare with the 100% tied model. They have exactly same with volume fraction (10%), particle size (2.88mm) and particle numbers (one particle inside) except the tie boundary conditions. Same tension stresses are applied on all of the three models. Fig 5.24 gives the results of comparison between models with different degrees of bonding.

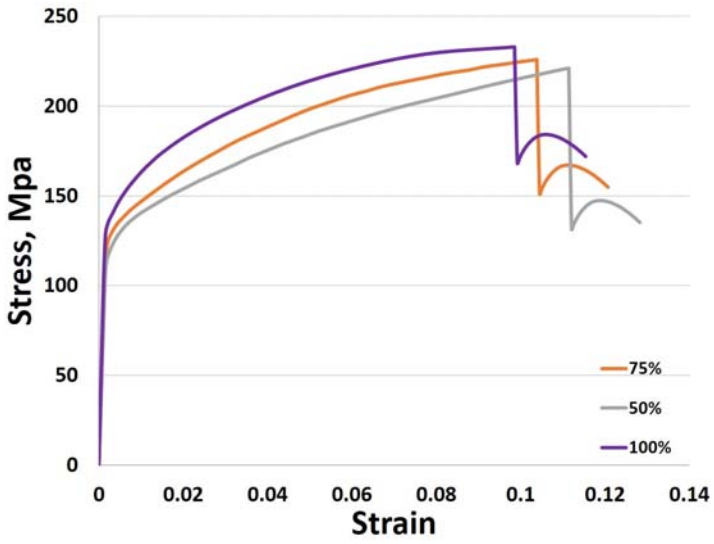

Figure 5.24 Predictions of the stress-strain curves of 50% to 100% degrees of bonding

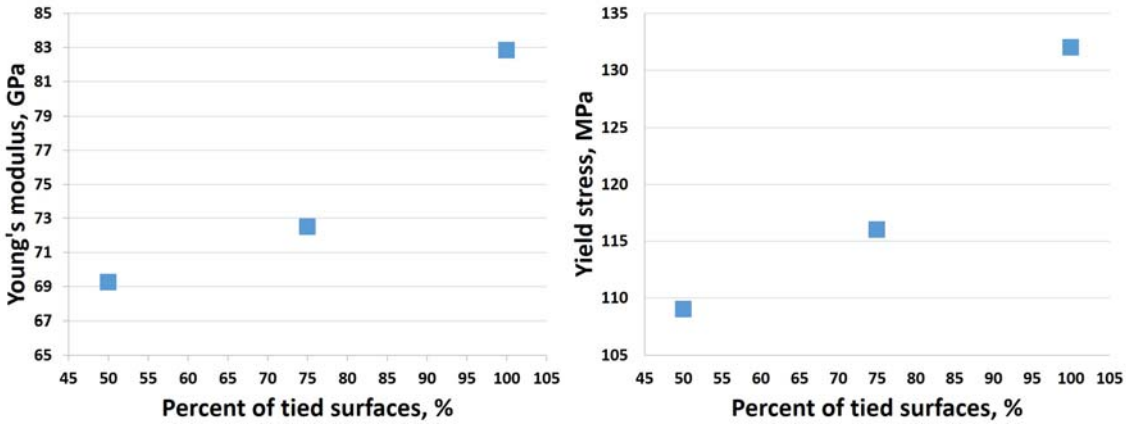

(a)

(b)

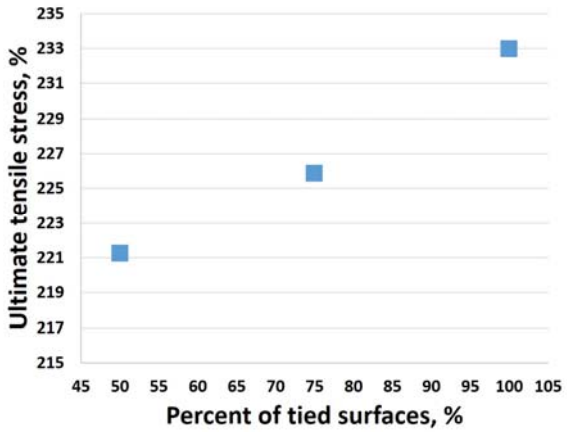

(c)

Figure 5.25 Scatter diagrams of (a) Young's modulus, (b) Yield stress (c) Ultimate tensile stress for 50% to 100% degrees of bonding

Fig 5.24 shows that the tie boundary condition has a significant effect on the yield stress, young's modulus and ultimate tensile stress. Fig 5.25 shows a clearer view of the influence of degrees of bonding on the values of (a) Young's modulus, (b) Yield stress and (c) Ultimate tensile stress. Fig 5.26 and Fig 5.27 show the stress distributions on the cross-section surfaces of composites with different degrees of bonding when the stress of the composites reaches yield stress and ultimate tensile stress, respectively.

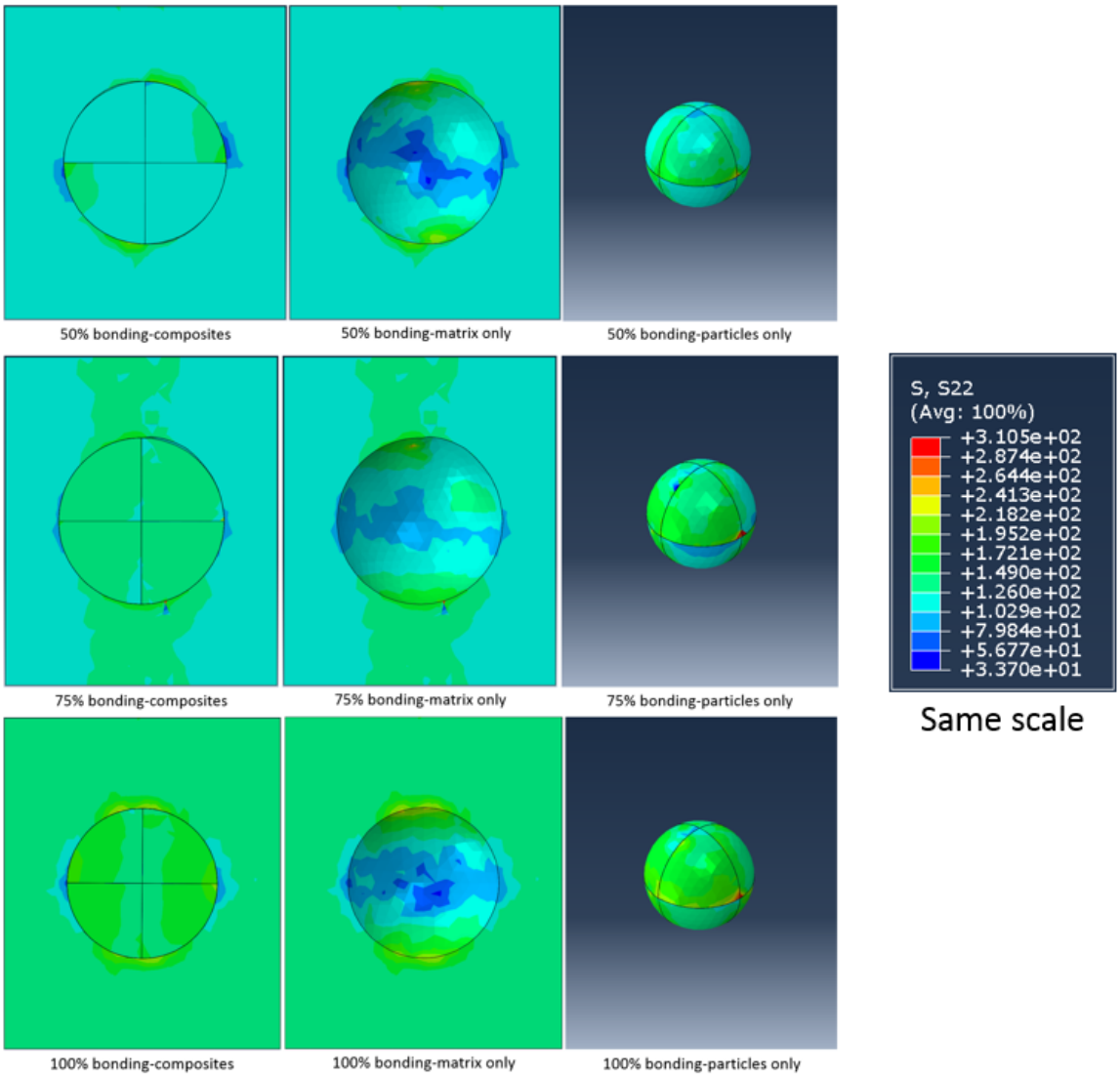

Figure 5.26 Y direction stress distributions on the cross-section surfaces of composites with different degrees of bonding when the stress of the composites reaches yield stress.

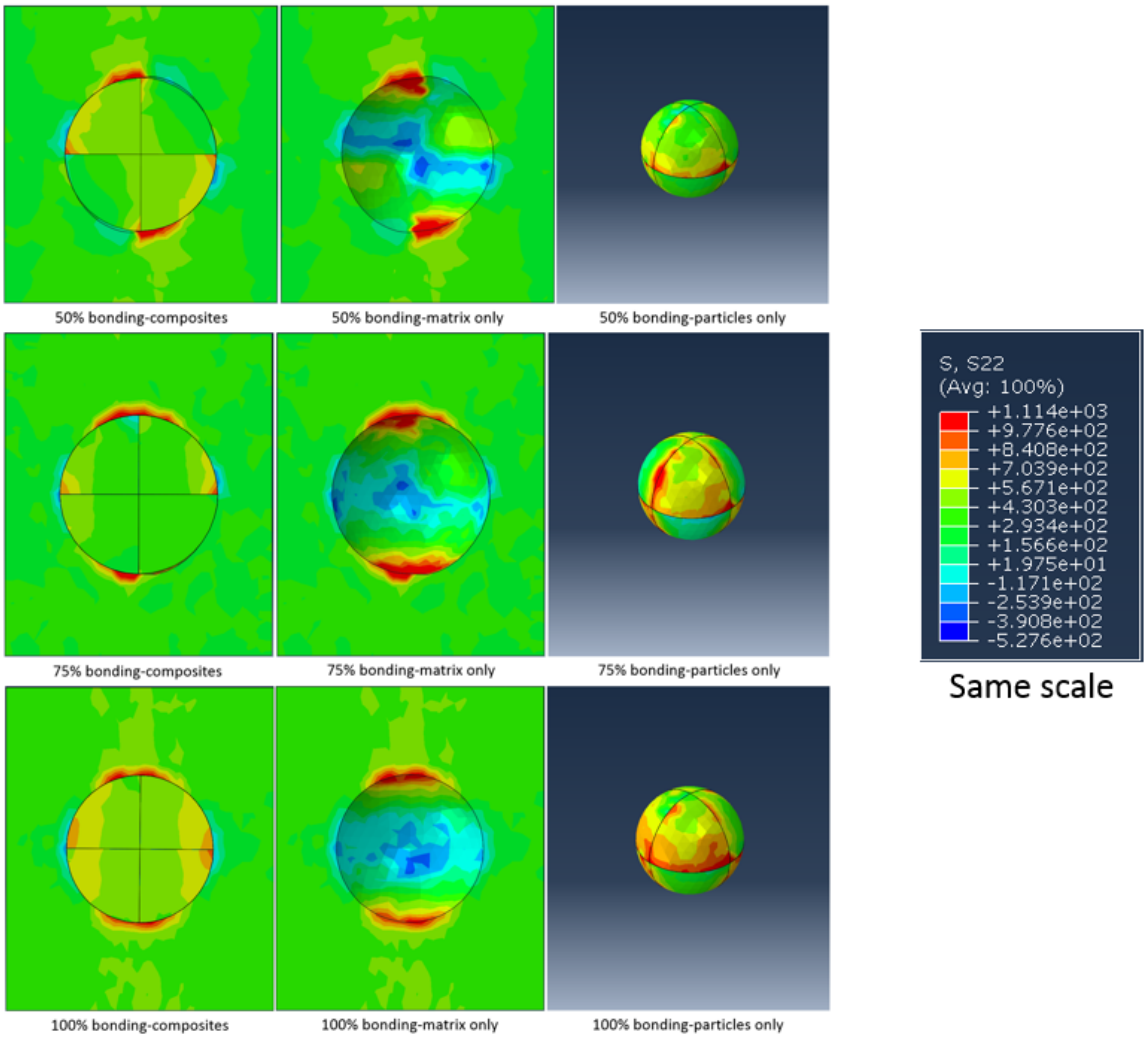

Figure 5.27 Y direction stress distributions on the cross-section surfaces of composites with different degrees of bonding when the stress of the composites reaches ultimate tensile stress.

As discussed in the previous sub-sections, young's modulus, yield stress and ultimate tensile stress of the composites are strongly influenced by the particulate volume fraction. The three models have a same particle inside the matrix but different percent surfaces tied with the matrix, which will result in different strengthening effects on the composites. Models with higher percent of the tied surfaces will have higher young's modulus, yield stress. Because models with

higher percent of the tied surfaces will result in higher stress on the particle, particle in the 100% tied model will fracture first, followed by 75% and 50%.

As for the stresses on the particles, models with three different degrees of bonding (100%, 75% and 50%) have similar results, which are shown in Fig 5.28. The only difference is the strain. Bigger strain is needed for particle with less percent of surface tied with the matrix.

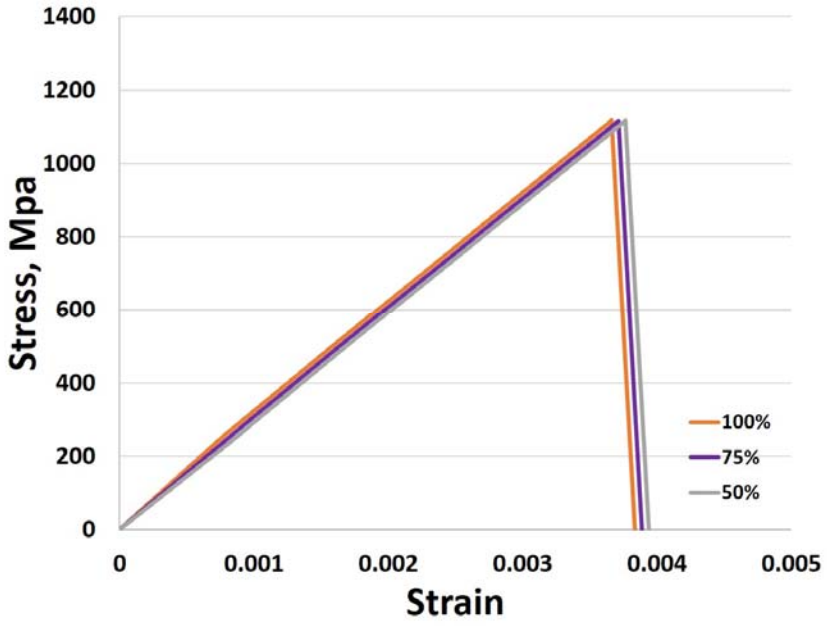

Figure 5.28 Plots of stress-strain curves for particles in different tie condition models

4. Comparison between FEA and experimental results of PRMMC

Up to this point, we have separately discussed theoretical and FEA results of PRMMC. In this sub-section, we do a comparison between theoretical, FEA and experimental results. Theoretical and computational results are compared with the experimental results of 6061 Al alloy reinforced by Al_2O_3 particles.

4.1 Comparison between FEA and Al-Dheyla et al. [9]

The main objective of their study is to determine the damage and failure processes of PRMMC, which consists of a uniform distribution of strengthening ceramic particles embedded within a metal matrix. The composites were prepared by powder metallurgy. A blend of 6061 aluminum alloy powder and Al_2O_3 powder were compacted by uniaxial pressing. Metallographic samples from 10%, 20%, and 30% volume fractions reinforced composites were used and uniaxial tensile tests were performed on the samples.

Al-Dheyla's data of Young's Modulus is shown in Fig 5.29 along with our FEA predictions.

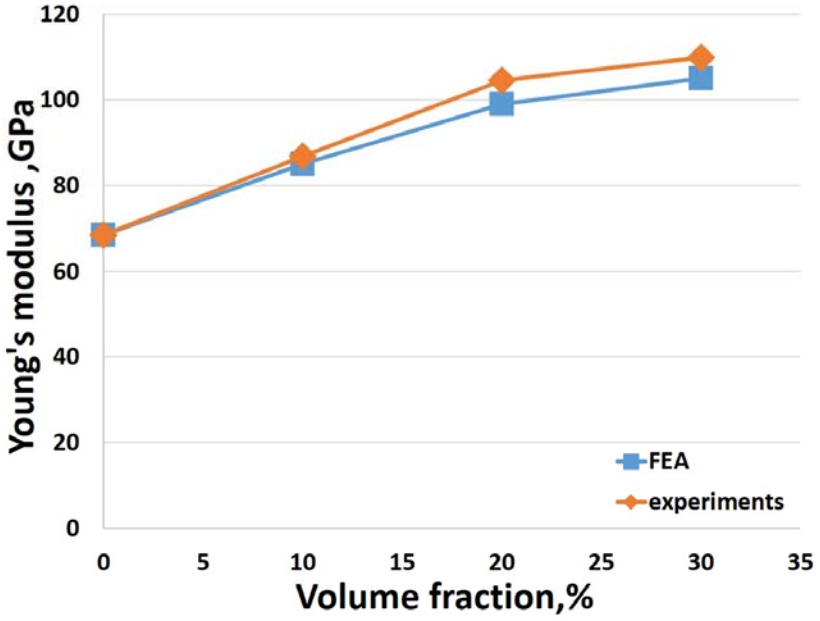

Figure 5.29 Comparison of Young's modulus between FEA and Al-Dheyla [9]

Experimental results showed an increase in young's modulus with increasing reinforcement volume fraction, where the values ranged from 86.8GPa for the 10% volume fraction Al_2O_3 composite to 109.9GPa for the 30% volume fraction. Al_2O_3 composite. FEA results

showed a lower increase of young's modulus from 85.22GPa to 98.63GPa. Under the condition that our computational modeling used same initial material property (Young's modulus) with the experiments, FEA and experiments have closest young's modulus values (only 1.6MPa difference) when volume fraction of Al_2O_3 particles is 10%. However, with the volume fraction increases, the difference between FEA and experimental results are also increasing. There are 13.2MPa and 12.3MPa differences between FEA and experiment results with volume fractions of 20% and 30%, respective. These diversities are due to the differences between our FEA simulation approaches with the experimental procedures that the paper used. In the microstructure observation of the experimental samples, particle clustering and particle depleted regions were observed on the polished surfaces [9]. As we can see in Fig 5.30: compared with the 10% Al_2O_3 composite, particles in samples with 20% and 30% volume fractions group together, in which a few large Al_2O_3 particles intermingled with smaller, uniform, and regularly shaped particles. Because of particles clustering, porosity is elevated in these particles clustered regions [9]. Thus, higher dislocation densities are expected to present in samples with 20% and 30% volume fractions. However, this clustering condition is not applicable in our computational modeling. We keep the particle distributions same with the increasing volume fractions and we do not take porosity and dislocations into consideration. That is why our FEA results have a reasonable agreement when the volume fraction is 10% but show bigger diversities when the volume fraction reaches 20% and 30%.

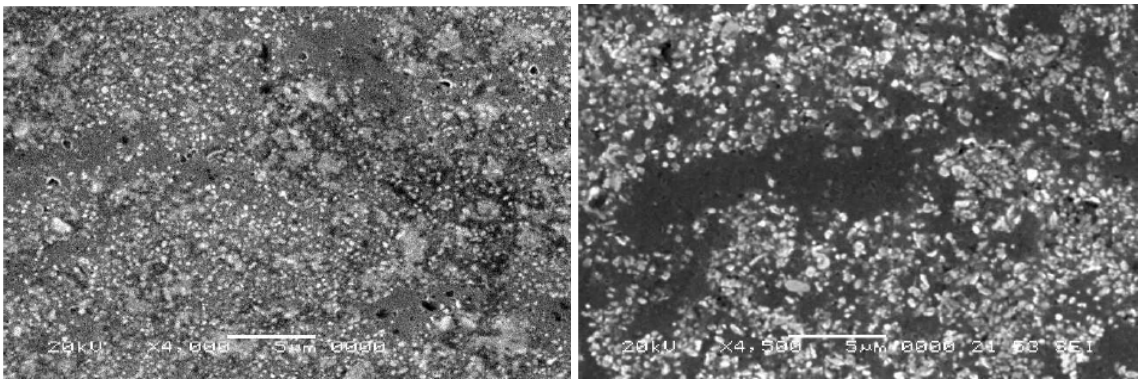

(a) (b)

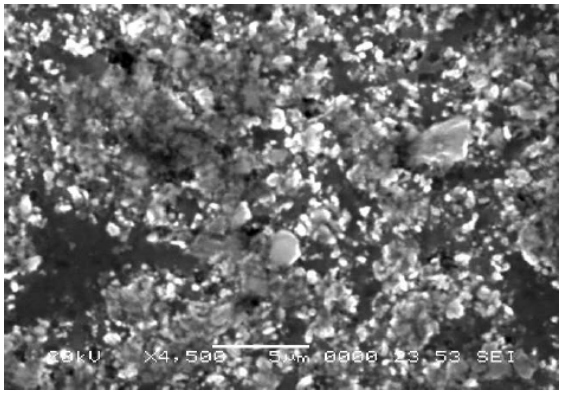

(c)

Figure 5.30 Microstructure of 6061 aluminum alloy reinforced with (a) 10%, (b) 20% and (c) 30% Al_2O_3 Particles [9]

4.2 Comparison between theoretical models, FEA and B. G. Park et al. [10]

A systematic examination of the effect of particulate volume fraction on the mechanical properties of an Al_2O_3-Al MMC has been undertaken in Park group's research. The material used was AA 6061 alloy reinforced with a polycrystalline 20 μm diameter microsphere Al_2O_3 reinforcements. The volume fraction was varied systematically from 5% to 30%. Metal powder

and microspheres were blended, compacted by cold isostatic pressing. All samples were extruded into 19 mm diameter rod. Then, tensile testing was performed.

We compared the data extracted from Park's experimental results with that of our computational models. The comparison results are shown in Fig 5.31.

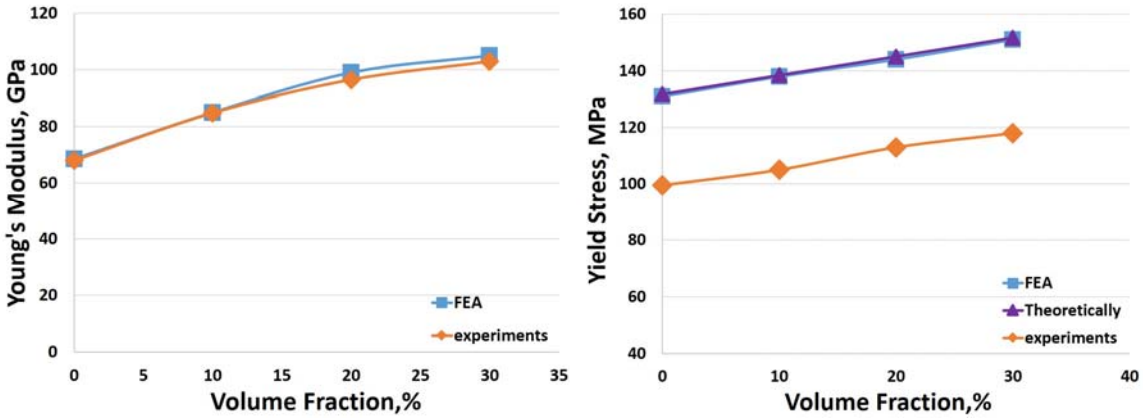

(a) (b)

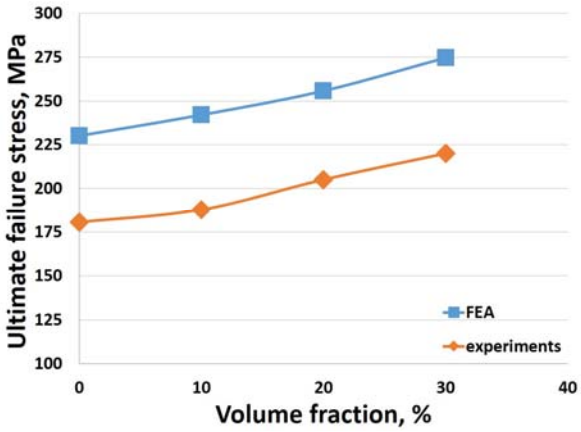

(c)

Figure 5.31 Comparison of (a) Young's modulus, (b) Yield stress and (c) UTS between FEA and B.G.Park et al [10].

In analyzing Fig 5.31 (a), it was found that: the elastic modulus of both FEA and experiments increase with increasing volume fraction of Al_2O_3 particles. Under the condition that

our computational modeling used same initial material property (Young's modulus) with the experiments, FEA and experiments showed almost same young's modulus values when the volume fraction of Al_2O_3 particle is 10%. However, with the increasing of volume fractions, the diversity increases to 3GPa. The FEA results of elastic modulus show reasonable agreement with that of experiments at low volume fractions but exhibit an increasing deviation from the experimental results as the volume fraction increases. The paper revealed that broken particles were present in the composites and that the level of particle fracture increased with volume fraction [10]. However, in our FEA approaches, we treat Al_2O_3 particles as a whole unit. As long as the max principal stress of the particles reach 1100 MPa, we would regard the whole particle is entirely fractured. The paper has also shown that particle fracture reduces the elastic modulus in AA 6061 reinforced with Al_2O_3 particles. Since the level of particle fracture increased with volume fraction [10], an increasing deviation from linear behavior would be expected and this may account for the diversities between our FEA results and B.G.Park's results.

As we can see in Fig 5.31 (b), the simulation results show a qualitatively consistent prediction of yield stress to the theoretical results in all the volume fractions.

As for the comparison between FEA and experimental results, the initial material property of 6061Al alloy that used in our computational modeling is different from that in the paper. As we can see in Fig 5.31 (b) and (c), when the volume fraction is zero, there is a 32.5MPa and 46.7MPa difference between our computational modeling and experimental results in yield stress and ultimate tensile stress, respectively.

The differences are due to different grain sizes of 6061 Al alloy. We used 6061 Al alloy with 1.22μm [7] in our computational model but the paper used the alloy with grain size of 20μm [10]. As we know from previous papers, 6061 Al alloy with smaller grain size usually shows a

higher strength. Based on these initial differences in the material properties, our FEA results show constantly higher values than the experimental values when the volume fraction increase from 0 to 10%. Thus, if we can input the same initial material property with the experiments in our computational modeling, we are possible to expect our computational modeling show a close result with the experiments when the volume fraction is below 10%. However, if we continue to increase the volume fraction from 10% to 30%, the differences between our FEA and experiments slightly reduced. In the experiments, there are a number of factors that contribute to the strengthening effect of the composites, including residual elastic stresses, increased dislocation densities and increased plastic constraint. Their combined effect increases linearly with volume fraction [10]. Because we are unable to simulate these effect in our computational modeling and the dislocation density, residual stresses and the level of plastic constraint would be expected to increase progressively with volume fraction [10], our FEA results show an increasing difference in yield stress and UTS with experimental results as volume fraction increase from 20% to 30%.

Thus, from what discussed in sub-sections of 4.1 and 4.2, we can conclude that results of our RVE models can best represent the mechanical properties (including yield stress, young's modulus and UTS) of real PRMMCs samples when the Al_2O_3 particle volume fraction is below 10%. Although there are slight diversities between our FEA and experimental results if we increase the volume fraction of reinforcement, there is in general a significant agreement in the stress variation trends between them.

5. Results of hierarchical composites

Mechanical properties of Mg-Al-Al_2O_3 hierarchical composites were also investigated for the final set of the study. Two RVE models were created. Y direction tension stresses were applied on these RVE models. FEA results were compared with Mei K. Habibi et al. [11]

5.1 FEA results of hierarchical models.

We tested two different models with volume fraction of Mg/0.647%Al-0.66%Al_2O_3 and volume fraction of Mg/0.972%Al-0.66%Al_2O_3. Fig. 5.32 shows the stress-strain curves of these two models under the exactly same boundary conditions.

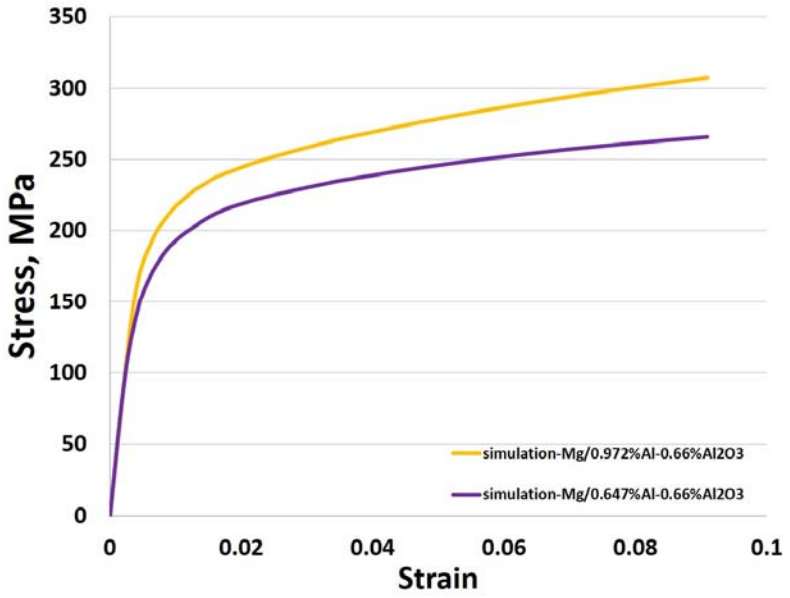

Figure 5.32 Plots of stress-strain curves of two hierarchical models

In investigating the stress-strain curves of the two hierarchical models, it was found that the two models show close young's modulus and yield stress. Same as PRMMCs, the model with higher reinforcement volume fraction shows higher young's modulus and yield stress.

5.2 Comparison between FEA and Mei K. Habibi [11]

Meisam K. Habibi et al. [11] have synthesized and investigated the mechanical performance of a hierarchical magnesium (Mg) nano-composite with a reinforcing constituent that is a composite in itself. Specifically, they developed a composite with monolithic Mg as the matrix, reinforced by another composite comprising a pure aluminum (Al) matrix in which are embedded Al_2O_3 particles. The level II composite was obtained by adding a small volume fraction of the ball-milled level I composite to Mg using the powder metallurgy route followed by microwave-assisted rapid sintering and hot extrusion. The smooth bar tensile properties of the monolithic and hierarchical Mg extruded rods were determined.

Fig 5.33 shows the uniaxial, tensile true stress–true strain curves of both FEA and experimental hierarchical composite samples for different Al volume fraction along with the response of monolithic pure Mg. Fig 5.34 shows stress distributions on the cross-section surfaces of hierarchical composites with different Aluminum volume fractions when the simulations were finished.

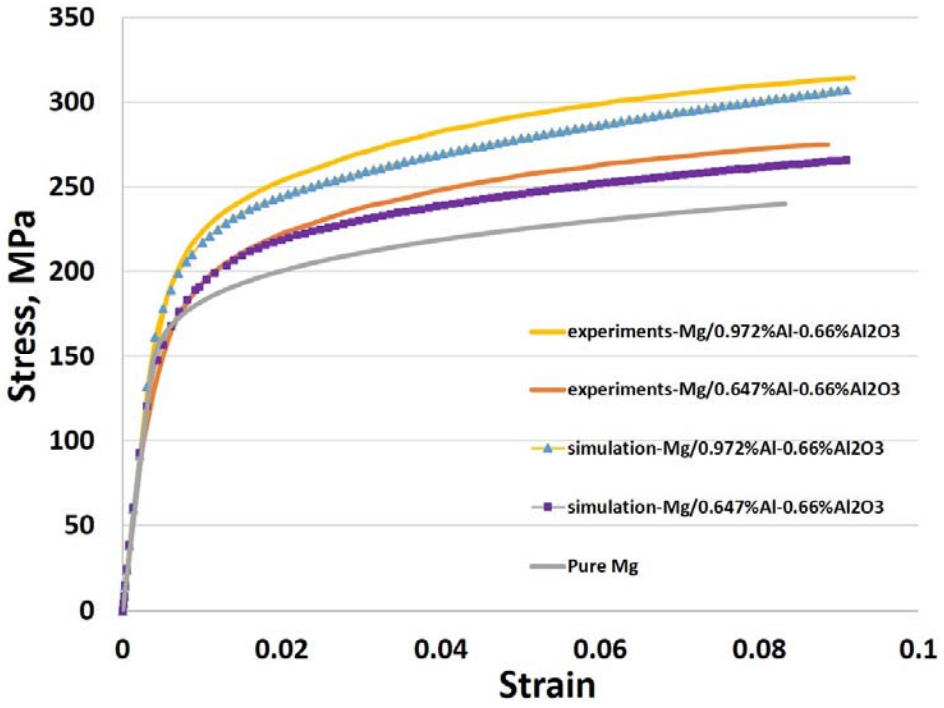

Figure 5.33 Stress–strain curves for FEA predictions, monolithic Mg and hierarchical composite specimens

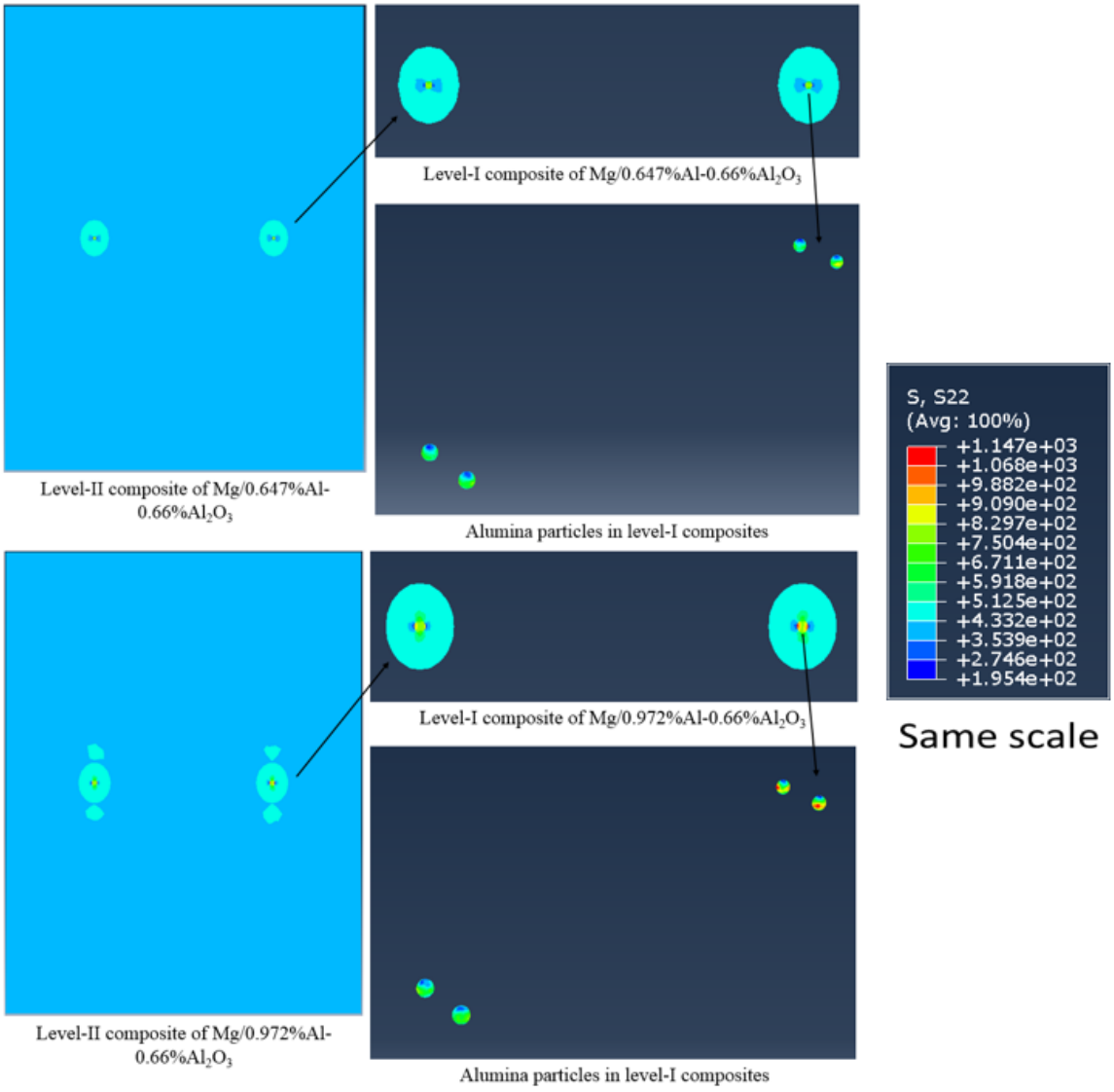

Figure 5.34 Y direction stress distributions on the cross-section surfaces of hierarchical composites with different Aluminum volume fractions.

Fig. 5.33 gives us that there is a significant improvement in the specific strengths of the hierarchical composites compared with the pure Mg with increasing volume fraction of Al in the level I composite. The stress-strain curves obtained by RVE models also exhibited an overall superior response compared with pure Mg. However, there are some diversities between our FEA results and experimental ones. The two stress-strain curves of our simulations are just in the middle

of that of experiments. Under the condition that our FEA simulations used same material properties as the paper, different strengthening mechanisms can be the very reason of these diversities. The enhanced strength and hardness observed in the hierarchical nano-composites compared with monolithic Mg is attributed to the presence of the level I composite, which activated multiple strengthening mechanisms acting in tandem [11]. These include: (a) Orowan strengthening; (b) grain size strengthening; (c) effective load transfer from the matrix to the reinforcement; (d) generation of geometrically necessary dislocations (GNDs) to accommodate the coefficient of thermal expansion (CTE) and elastic modulus mismatch between the Mg matrix and the level I composite ; (e) activation of non-basal slip modes. However, our RVE models are very limited models that can only take load transfer and grain size strengthening into consideration. There is no Orowan strengthening in our models because our simulations are not in nano-size. We do not have temperature changes during the simulation process, so we are unable to simulate the CTE mismatch.

References

1. Joshi SP, Ramesh KT. An enriched continuum model for the design of a hierarchical composite Scripta Materialia 57 (2007) 877–880.

2. Hull, D.; Bacon, D.J. Introduction to Dislocations, 4th ed. Butterworth Einemann: Oxford, UK, 2001.

3. Nardone V.C, Prewo K.M, On the strength of discontinuous silicon carbide reinforced aluminum composites. Scripta Metal. 20 (1986) 43–48.

4. Sanaty-Zadeh, A. Comparison between current models for the strength of particulate-reinforced metal matrix nanocomposites with emphasis on consideration of Hall–Petch effect. Mat. Sci. Eng. A 531 (2012) 112–1184.

5. Smallman, R.E., Ngan, A.H.W. Physical Metallurgy and Advanced Materials, 7th ed.Butterworth Einemann: Oxford, UK, 2007.

6. Yoshimasa Takahashi, Takahiro Shikama, Ryota Nakamichi, Yuji Kawata, Naoki Kasagi, Hironari Nishioka, Syuzaburo Kita, Masanori Takuma, Hiroshi Noguchi. Effect of additional magnesium on mechanical and high-cycle fatigue properties of 6061-T6 alloy. Materials Science & Engineering A 641 (2015) 263–273.

7. A.J. Knowles, X. Jiang, M. Galano, F. Audebert. Microstructure and mechanical properties of 6061 Al alloy based composites with SiC nanoparticles. Journal of Alloys and Compounds 615 (2014) 401–405.

8. H. R. Ezatpour, M. Torabi-Parizi, S. A. Sajjadi. Microstructure and mechanical properties of extruded Al/Al2O3 composites fabricated by stir-casting process. Trans. Nonferrous Met. Soc. China 23 (2013) 1262−1268.

9. Khalid Al-Dheylan, Syed Hafeez, Tensile failure micromechanisms of 6061 Aluminum reinforced with submicron Al_2O_3 metal-matrix composites. The Arabian Journal for Science and Engineering, Volume 31, Number 2C.

10. B. G. Park, A. G. Crosky, A. K. Hellier. Material characterisation and mechanical properties of Al_2O_3-Al metal matrix composites. Journal of materials science 36 (2001) 2417 – 2426

11. Meisam K. Habibi, Shailendra P. Joshi, Manoj Gupta. Hierarchical magnesium nano-composites for enhanced mechanical response. Acta Materialia 58 (2010) 6104–6114

Chapter 6. Summary

Advanced computational/numerical methods have emerged as essential tools for the assessment and the optimization of the performance of particle-reinforced metal matrix composites (PRMMCs). In the present thesis, we employed the finite-element analysis (FEA) computational technique to predict the mechanical behavior of aluminum (Al) based metal matrix composites (MMCs) reinforced by Al2O3 ceramic particles. FEA has been widely utilized for a large number of studies of PRMMCs to investigate the effect of particle volume fraction, particle size, and particle distribution on the mechanical properties of composites. Over the past decade, the computational technique has achieved a considerable improvement in the levels of accuracy and complexity.

In the current study, different from most of the previous investigations focusing on the mechanical response of the whole composites, we have taken into consideration of the stress condition of ceramic particles for a fracture condition. A representative volume element (RVE) model has been developed to predict the mechanical properties of different PRMMCs assuming that ceramic particles are fractured during the plastic deformation of the base matrix when a pre-determined fracture stress is reached on the surface of the embedded particles. Additionally, the degrees of bonding between the matrix and the particles have been changed to test their impacts on the mechanical behavior of RVE models of PRMMC.

First set of simulations have been carried out to check the reliability of the current RVE models by comparing the outcomes with experimental observations. Then, different RVE models of PRMMCs were created using the most reliable model type. Based on the results of these models,

the influence of the particle volume fraction, the particle size, and the particle distributions on Young's modulus, yield stress, and ultimate tensile stress (UTS) have been analyzed. It was found that the particle volume fraction plays a very important role in the variation of Young's modulus, yield stress, and UTS. The values of Young's modulus, yield stress, and UTS increased with increasing the volume fraction of particulate, however, the ductility of the composites drops down with increasing volume fraction. Both the particle size and the particle distributions influenced the fracture points of particles in PRMMCs. FEA results were compared with experimental results. It has been found that the results of our RVE models can reliably represent the mechanical properties (including Young's modulus, yield stress, and UTS) of real PRMMCs samples when the Al2O3 particle volume fraction is less than 10%. In the next set of computations, five models with various matrix grain sizes were created to study the influence of the matrix grain size on the yield (0.2% offset strength) strength of PRMMC. It was predicted that reducing the matrix grain size can significantly increase the yield tress when the size is under 30mm. Then, RVE models with 75% and 50% degrees of bonding were generated to compare with the 100% tied models. The results showed that the degrees of bonding have a significant effect on Young's modulus, yield stress, and UTS. Note that the RVE model is inherently limited and the development of a more sophisticated model (such as extended FEA, XFEA) would be necessary to accurately predict the strain to failure values of 6061 Al matrix composites with Al_2O_3 reinforcements.

1. Limitations

- Accurately predicting strain to failure and failure stress of PRMMCS was unable to be performed.

- The effect of Orowan strengthening, CTE and EM mismatch and dislocation densities was unable to perform in the simulations.

2. Findings

- FEA model to predict the mechanical properties in the various components of PRMMC has been developed.
- RVE models with 27 particles inside matrix show a closest stress-strain curve with the experimental result.
- Particle volume fraction plays a very important role in the variation of Young's modulus and yield stress of PRMMCs.
- RVE models with smaller particle size show relatively higher strength.
- Particle distributions have influence on the fracture points of particles in PRMMCs, result in the phenomenon that composites with different particle size and different particle distributions have different UTS and failure stress.
- Reducing matrix grain size can significantly increase the yield tress of PRMMC when the grain size is under 30μm
- Degrees of bonding has a significant effect on the young's modulus, yield stress and ultimate tensile stress of the composites.
- RVE models can best represent the mechanical properties (including yield stress, young's modulus and ultimate tensile stress) of real PRMMCs samples when the Al_2O_3 particle volume fraction is below 10%.

3. Future works

- Developing FEA analysis containing a user subroutine is required to accurately predict the strain to failure of PRMMCs.
- Refinement of model will require more accurate material properties of initial Al alloy